Finite Element Analysis to Assess the Protective Capabilities of Helmets against Mild Blast Loads

a combined numerical experimental approach using a human head surrogate

Anne Zwanenburg

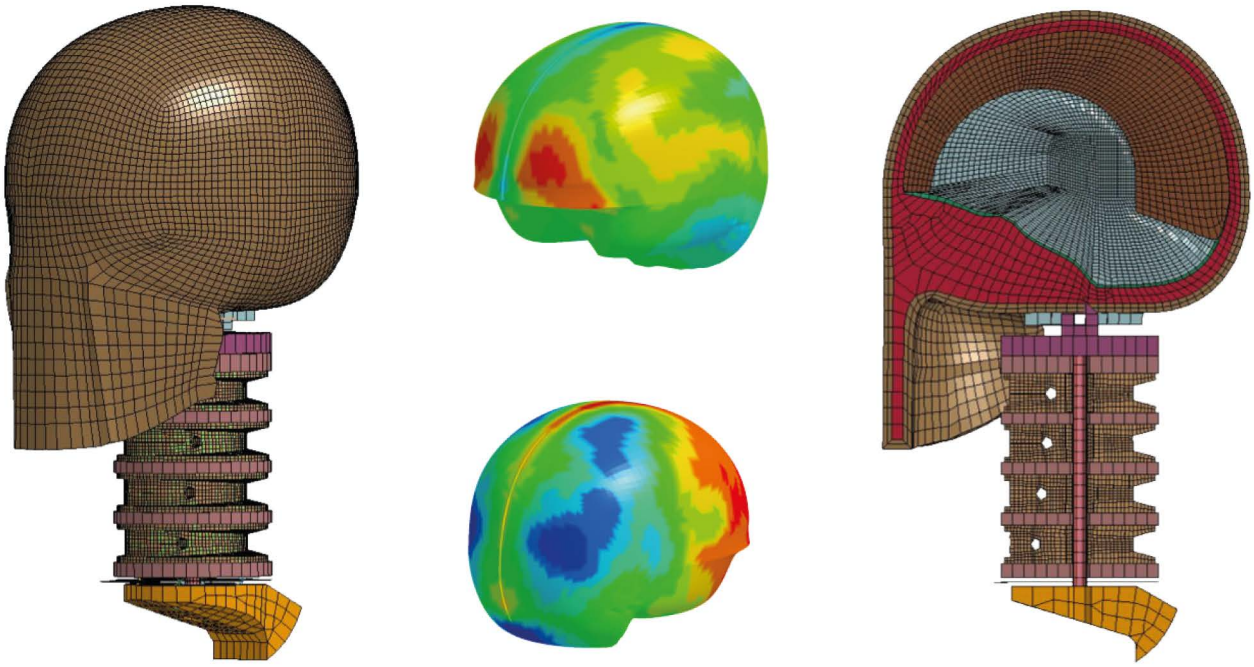

TU Delft

TNO innovation for life

Finite element analysis to asses the protective capabilities of helmets against mild blast loads

a combined numerical experimental approach using a head surrogate

by

A. Zwanenburg

to obtain the degree of Master of Science
at the Delft University of Technology,
to be defended publicly on Monday May 8, 2017 at 03:00 PM.

Student number:	1357506	
Project duration:	Augustus 1, 2015 – April 1, 2017	
Thesis committee:	Prof. dr. ir. L. J. Sluys,	TU Delft
	Ir. M. Philippens,	TNO
	Ir. Y. S. Khoe,	TNO, supervisor
	Dr. ir. J. Weerheijm,	TU Delft
	Ir. L. J. M. Houben,	TU Delft

This thesis is confidential, classification 'VERTROUWELIJK' as used at TNO, and cannot be made public until May 8, 2019.

TU Delft

Preface

This report is my final thesis written for my graduation research for the Masters' study programme Structural Mechanics at the faculty of Civil Engineering and Geosciences. It is part of TNO EBP project nr. 053.03035 and an addition to the report of Mat Philippens; Blast TBI risk reduction by military helmets: An assessment method to qualify the helmet ICP reducing performance[24]. This report contains the numerical simulations that complement the results of the experimental work for that project. A summary of the numerical work was also provided within the project deliverables as a powerpoint report[38]. This TNO study was supported by the Department for Knowledge and Innovation of the Netherlands Ministry of Defence under contract 016.12.1026.01.

My personal interests are more divers than the areas expected in the Civil Engineering industry. This is reflected in my academic record with a Bachelors' degree in Aerospace Engineering and a Minor programme Management of Industrial Production.
I would like to thank Prof. Bert Sluys for allowing me to take on what I consider to be an exotic graduation research project. Additionally I would like to thank him for his critical review of my work, communicated in such a way that I always felt better about my work after receiving feedback; an extraordinary talent.
I would like to thank Mat Philippens from the department Explosions Ballistics and Protection -TNO for the opportunity to work on my graduation project as an intern at TNO. I learned many useful things about working at a company. Things I would have missed out on working on my thesis at the university only. Similarly I would like to thank Yoeng Sin Khoe for his patient and helpful supervision during my time there. My gratitude also extends to the other committee members Jaap Weerheijm en Lambert Houben, for their interest in my work and insightful feedback.
Special thanks go out to Wim van den Heuvel and Bart de Jong from the department of Structural Dynamics -TNO. Their adoption of me and my research project in the last phase of my graduation was incredibly helpful. You made even the final phase of my project fun to work on.
Of course I would also like to thank my friends and family for listening to my ideas and work progress even when I was not making any sense. More so for supporting me and always believing in me, especially when I was struggling.
Finally and most importantly I would like to thank Arthur Scheltes for providing me among others with joy, food, comfort, and endless support during my hard work.

I have never learned more than during the time working on my graduation project. However, I never tire of learning and I am looking forward to my future adventures.

A. Zwanenburg
Pijnacker, March 2017

Summary

Soldiers that have repeated encounters with blast in the field may develop a condition known as blast-induced mTBI (**m**ild **T**raumatic **B**rain **I**njury) even when no outward physical injury is observed. The goal of this project is to contribute to the development of a method to assess the protective capabilities of helmets against the effects of the primary blast wave. The proposed approach is a combined numerical experimental method consisting of shock tube tests and Finite Element simulations of a human head surrogate. The main benefit of the simulations is that the data output is available at all positions at all times in the numerical model. The shock tube tests can provide validation of the numerical results. Therefore a combined approach is beneficial to the assessment of helmets.
In this study a simplified spherical head surrogate consisting of a Gelatin brain and Synbone skull shell is used in FE simulations to obtain a better understanding of the physics involved in the transfer of the external blast load to internal pressure distribution. A biofidelic BI2PED surrogate developed at DRDC Canada, with a life-like geometry and additional components like a skin layer and fluid skull brain interface is used to study the feasibility of a combined numerical experimental approach. Shock tube tests with a physical BI2PED supported by a Hybrid III dummy neck were done prior to this study. It included cases with three levels of protection: unprotected, standard combat helmet, full face helmet. Two loading directions were applied: face on and right lateral. Simulations with a numerical representation here named the 'BI2PED-FE' are analysed in this thesis to optimize the combined approach. All simulations are performed using the LSDYNA software in a fully Lagrangian environment, where the blast load is applied using the Load Blast Enhanced keyword that applies a pressure over time based on empirical blast profiles.

Head response to blast
A typical profile of the brain internal pressure is characterised by first a peak positive pressure after impact followed by an oscillating positive-negative sinusoidal signal. There are two dominant mechanisms that cause this pressure profile in the response of the numerical skull-brain system to blast. The first mechanism is the propagation of a blast wave due to the direct impact of the blast on the skull. The high frequent internal propagation of the pressure waves depends on the local speed of sound defined by the material properties. The second mechanism is a vibration in a superposition of Eigen modes, where the skull deformation causes a lower frequency oscillating internal pressure. This hypothesis for the second mechanism is confirmed using an alternative modal analysis, consisting of a block pulse impact test to obtain the Eigen frequencies of the model. These Eigen frequencies have been linked to the frequency content of the internal pressures and skull deformation in the response to blast. In the internal pressures additional frequencies are present compared to the skull deformation, indicating that local brain effects exist.

The BI2PED head was attached to a Hybrid III dummy neck during the shock tube tests. It is covered by a rubber-like skin layer and the brain floats in a volume of water within the skull. Influence studies were performed using the spherical head and BI2PED-FE head simulations to identify the effect of these features on the response mechanisms described.
Another hypothesis for the second mechanism was that the back and forth motion of the head on the Hybrid III dummy neck constraint present in the shock tube test is the cause of the internal pressure oscillation. This is studied by adding neck constraints to the numerical models. The BI2PED-FE head model was extended with a Hybrid III dummy neck. The simulation results show that the order of magnitude of the neck motion is two orders lower than the frequency of the internal pressure, negating this hypothesis. Additionally, the effect of the constraint on the internal pressure was negligible. Therefore it is concluded that the neck constraint is not of importance for the internal pressure distribution.
A skin layer influences the pressure transmission of the blast to the head. The initial peak pressure is reduced and the frequency of the pressure oscillation altered. The skin layer in the BI2PED-FE presented issues when combined with Load Blast Enhanced.

In general the effect of the interface on the response is expected to be limited considering literature and the simulation results with the sphere, however the specific manner in which it is modelled in the BI2PED-FE - a solid element layer with an equation of state - causes significant changes to the pressure distribution. Therefore, the results using this approach are expected to be unrealistic.

Based on the influence study results, the analysis for the optimization of the combined method was done with a reference BIPED-FE model without neck constraints, skin layer and fluid-like skull brain interface. This model was used because the influence of the HIII neck is limited and the results of the BI2PED-FE with skin and with CSF are unreliable

Combined numerical experimental approaches

In the proposed assessment method the measure of protective capabilities of helmets is based on a reduction in internal brain pressure. The combined numerical experimental assessment approaches can be subdivided into two categories.

The first category uses the experiments to determine the load that is transferred to the head underneath the helmet. This load is used as input for the simulations which determine the internal load reduction and can thus evaluate the protective capabilities of a helmet. The pressure underneath the helmet cannot be reliably measured as the results have a low reproducibility. The strain can be reliably measured but can not directly be prescribed as a load for the numerical simulations. An algorithm to translate a measured external strain field to a deformation field which can be prescribed in LSDYNA is complex to develop and likely not accurate enough due to the complex geometry of the head, large curvatures and small strains. An alternative where the deformation field is reconstructed using a superposition of skull Eigen modes scaled by strain measurements, was also found to have a low feasibility. Most importantly, it is likely not possible to describe the initial impact, local skull deformation and introduced pressure wave related to the first response mechanism according to only the skull Eigen modes. As the highest loads occur during this phase of the response this is considered critical.

The second category is proposed as an alternative strategy and uses the numerical simulations to determine the general head response, which is used to optimize the measurement of the response in the shock tube experiments. The measurements taken during the experiment are then used to determine the protective capabilities of a helmet. Two main approaches are proposed; Measuring the external skull strain, or measuring the maximum load transferred to the brain to compare the head response for different helmets. A reduction in maximum external skull strain and a reduction in the maximum load transferred to the brain are then an indication of the protective capabilities. The brain internal pressure distribution and skull external strain were analysed using different load cases of the BI2PED-FE with varying blast direction, peak incident pressure and positive phase duration. The results showed that a relation between the external skull strain and internal pressure exists. If the peak incident pressure decreases, the skull strain and brain pressure also decrease. The simulation results showed that the maximum and minimum brain pressure occur on the outside periphery of the brain. Moving further inwards reduces the pressure. A sensor in between the brain and skull could therefore measure the maximum load transferred to the brain. This last method is probably better able to measure the local effects present in the brain, which are not measured in the skull. A combination of the two methods is proposed as the best solution as the redundancy reduces the uncertainty of the assessment method. Additional sensors are proposed with respect to the current BI2PED sensor lay-out; Strain sensors on the top of the head, an internal pressure sensor in the bottom of the brain and two pressure sensors in between the skull and brain on the front and rear of the head.

Conclusions and Recommendations

The proposed combined assessment method based on the skull strains and maximum load transferred to the brain is considered feasible. The numerical BI2PED-FE however is not yet ready for validation, as the dominant frequency in the pressure response is different compared to the physical BI2PED. A third response mechanism related to a local brain effect is present in the BI2PED because the brain is not fully attached to the skull. The fluid skull-brain interface enables impact of the brain with the skull and local deformation and vibration in the brain. This third mechanism should be implemented in the numerical model, because the presence of a helmet amplifies the pressure peaks in the dominant pressure response frequency related to this mechanism. It is recommended to study this mechanism in the BI2PED and improve the skull-brain interface of the BI2PED-FE model accordingly.

After improving the validity of the numerical BI2PED-FE model, it is advised to run simulations with a simple helm model. It is recommended to study the effect of a face shield as it influences the direct impact of the blast. The purpose of the simulations with helmet are to check whether the conclusions with respect to the response and behaviour of the unprotected BI2PED head model are also valid for protected cases.
When the relation between the strain or pressure measurements during shock tube tests and internal load reduction is quantified, using a set of load cases for the simulation representative for the specific test set-up, a method to quantify the protective capabilities is available.

Contents

List of Figures

List of Tables

List of Abbreviations

mTBI	Mild Traumatic Brain Injury
BI2PED	a head surrogate developed by DRDC
BI2PED-FE	BI2PED finite element model developed by DRDC
DRDC	Defence Research and Development Canada
TNO	Dutch technical innovation company
HIII	Hybrid III crash test dummy
LAG	Lagrangian
ALE	Arbitrary Langrangian Eulerian
MMALE	Multi Material ALE
LBE	Load Blast Enhanced
CSF	Cerebral Spinal Fluid
FE or FEM	Finite Element Method
FEA	Finite Element Analysis
ICP	Intra Cranial Pressure
PMHS	Post Mortem Human Subject
FFT	Fast Fourier Transform
SSFS	Single Sided Frequency Spectrum

1

Introduction

Nowadays, soldiers in combat more often encounter blast loads due to the detonation of explosives like IEDs (improvised explosive devices), see Figure 1.1. Even when no direct physical injury is observed, these soldiers may develop a condition known as blast-induced mTBI; **m**ild **T**raumatic **B**rain **I**njury. It is a condition with long term consequences related to cognitive-learning aspects and psycho-social behaviour.[32] In order to reduce the number of injuries, ways to protect soldiers against blast loads need to be developed. The goal of this project is to contribute to the development of a method to assess the protective capabilities of helmets against blast-induced mTBI.

Figure 1.1: Soldiers close to an IED explosion (http://www.theweek.co.uk/photos/49175/us-soldiers-carry-out-controlled-ied-explosion-picture)

Existing assessment methods to study mTBI due to blast are; (Shock tube) experiments or numerical (Finite Element) simulations. An overview of both methods is presented next.
There are three options to study mTBI using a shock tube; testing animal subjects, post mortem human subjects (PMHS) or human head surrogates. Besides the ethical strict ethical guidelines and regulations, animal subjects are not suitable for the testing of helmets due to scaling effects. The material properties of human tissue quickly decay after death and PMHS are more difficult to obtain than head surrogates. There are however limitations with regard to the biofidelity of head surrogates due to production constraints.
The biofidelity of numerical simulation models can be very high in case human head scans obtained by advanced imaging techniques are used. The interaction of the air, helmet and head is however very complex to model and validation of the results is necessary. A benefit of the simulations is that response data is available everywhere in the head model. In the shock tube tests a limited number of pressure or strain sensors or accelerometers is applied.
Considering the above described advantages and disadvantages it is proposed to use a combined numerical and experimental approach to make optimal use of their respective benefits. In this combined

approach a physical human head surrogate is used in shock tube tests and a numerical model of this surrogate is used in numerical simulations. This way the simulation results can provide more detailed insight into the response and the results can be validated with the results obtained during the shock tube experiments.

In literature, both numerical Finite Element studies and experimental shock tube tests are found, with varying head model complexity. Models exist with relatively simple geometries and components, easily built and validated, that have numerical material properties based on the materials used during shock tube testing. This is similar to the approach used in this study. There are also very complex and detailed numerical models with biofedelic components. Here material properties are often based on real human tissue and the geometry based on MRI or CT scans. These models are more difficult to validate because there are limitations to the complexity that can be recreated in real life testing models. There are also Post Mortem Human Subjects that are for example tested in a shock tube. For example a human skull filled with a gel attached to a dummy neck.[31] An interesting development is the 3D printing of computational models, extending the possibilities for testing and validating more detailed models[26].

In the studies found in literature, the efficacy of helmet systems is most often measured by a reduction in peak intracranial pressure, for example in the work of Merkle et all.[18]. Occasionally a reduction in peak shear stress[29] or the displacement of the brain[36] or strains and accelerations[35] are used. One study was found that considers the effects of the helmet on the risks for actual TBI mechanisms[9]. This study also finds that pressure peaks occur at similar locations with and without the helmet and the peaks are reduced due to the presence of the helmet. The helmet is more effective for a front blast in case a faceshield is present [29], as it reduces the initial pressure peak[20]. Mitigation efficacy varies for front, side and back blast orientation.[28][35]. Multiple studies find that gaps beneath the helmets can have adverse effects which could possibly be compensated for by closing the gaps with foam.[12][29][36][35][10]

This study aims to contribute to the development of a standardised test method to compare different helmet types and indicate the helmet that is best able to protect soldiers against the effects of blast on the brain. Numerical simulations are used to obtain a better understanding of the internal pressure distribution in the brain due to blast. Additionally ways to combine the simulations with experimental data are investigated in order to propose an optimized assessment approach.

2

Problem Statement and Research Method

The project problem statement and methodology are presented in this chapter. The research questions and methods used to investigate them are discussed. At the end of the chapter a readers' guide to this thesis is included.

This work uses Finite Element (FE) analysis aimed towards a combined numerical and experimental approach to assess the efficacy of helmet systems against blast-induced mild Traumatic Brain Injury (mTBI). A physical human head surrogate is used in shock tube tests and a numerical model of this surrogate is used in FE simulations. The simulation results provide a more detailed insight into the head response and the simulation results are to be validated with the results obtained during the shock tube experiments. This leads to the following main subject of research:

Feasibility study of a combined numerical/experimental method to predict the protective capabilities of helmets against blast-induced mTBI, using a human head surrogate

This study focusses on mild Traumatic Brain Injury as primary blast injury, a result of the direct impact of the blast wave to the head. Therefore the models used in this study are limited to the head and neck of the head surrogate. The mechanical transmission of the blast into the brain is studied. The internal stresses due to the mild blast load range considered in this study (incident peak pressure 30-300MPa) remain below critical limits such that material damage and non-linearity such as plasticity and fracture do not need to be included. At this time in literature the internal pressure is most commonly used as a basis to measure the efficacy of helmets. Therefore the research in this thesis uses the reduction of internal pressure (Intra Cranial Pressure - ICP) as main parameter. As there is no consensus at present on the mTBI brain damage mechanisms and their medical implications, these are out of the scope of this work.

This research builds on previous work done at TNO. De Vries [7] showed that the response of a spherical skull-brain head surrugate measured during shock tube tests, can also be simulated numerically using the Finite Element Method. The internal pressures obtained with simulations based on an Arbitrary Lagrangian Eularian (ALE) model including the sphere and a rectangular air domain, corresponded well with the experimental results for the separate skull and brain tests. A larger difference was observed between the full skull brain experimental and numerical results. The skull-brain interface was identified as the likely cause. In the next project phase (TNO EBP project nr. 053.03035), of which this study is a part, shocktube tests were done[24] on a more biofedelic head surrogate provided by DRDC[22] called the BI2PED, supported by a Hybrid III dummy neck. These tests included cases with three levels of protection: unprotected, standard combat helmet, full face helmet, see Figure 2.1. The internal pressure signals measured showed oscillations in the internal pressure of which the origin was unknown. The internal pressures of shock tube test 22 (Appendix A) with the unprotected BI2PED head are included in Figure 2.2. Sinusoidal patterns can be distinguished in the graph. In Figure 2.3

the pressures in the front of the brain are plotted for the unprotected head, and the head with an advanced combat helmet and a full face helmet. It is seen in this graph that the sinusoidal peaks are amplified by the helmet.

Figure 2.1: Four configurations of the BI2PED during shock tube tests: unprotected, standard combat helmet, full face helmet, unprotected with skin removed[24]

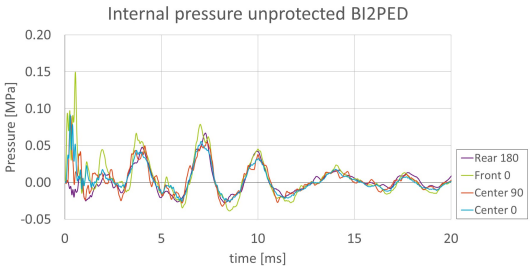

Figure 2.2: Oscillating internal pressure in the BI2PED head surrogate shock tube test 22:
No helmet [Filtered LP10kHz]

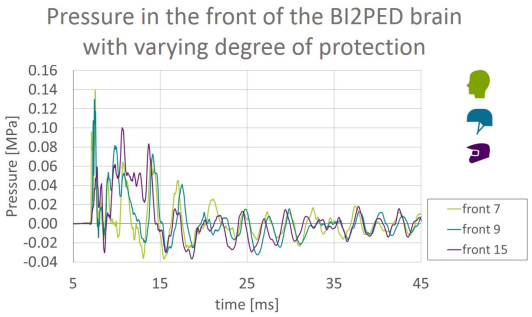

Figure 2.3: BI2PED internal pressure in the front of the brain. Test 7: No helmet, Test 9: Combat helmet, Test 15: Full face helmet. [Filtered LP10kHz]

2.1. Research Questions

The two main goals of this thesis are; Part 1. gain a better understanding of the head response mechanisms using numerical simulations. This contributes to further interpretation of the shock tube test results. Part 2. investigate ways to combine the numerical and experimental approach using the obtained knowledge.
The two parts have been divided into sub research questions which are presented next along with the methods used to investigate them. The simulation models used for each research question are summarised in Appendix G.

Part 1 - Which factors dominate the nature of the head response?

Finite Element Analysis (FEA) is used to simulate the response of the head models to blast. A spherical skull-brain based on the work of de Vries is used as a simplified first order head surrogate, Figure 2.4 a. Next the numerical equivalent of the physical BI2PED, in this work named the BI2PED-FE, is used as a more biofedelic head surrogate, Figure 2.4 b. The geometry is more similar to an actual head and a skin layer and fluid skull brain interface are included. As the BI2PED-FE provided by DRDC [3] is built for the LSDYNA software, all simulations are run using LSDYNA [1] and post processed with its companion LS-PREPOST [2]. A Lagrangian simulation environment is used that does not include fluid-structure interaction, because it has a much shorter runtime compared to the ALE option, while the main response mechanisms should be comparable.

[1] http://www.lstc.com/products/ls-dyna
[2] http://www.lstc.com/products/ls-prepost.

Part 1 is subdivided into two research questions; The first one focusses on the response of a skull-brain system. In the second one additional components are added to study their influence on the head response.

1.1 A study of the physics involved in the response of a skull brain model to blast.

The mechanical transfer of the external blast to internal brain pressures is investigated using simulations of the spherical model.
One hypothesis for the sinusoidal oscillation in the internal pressure, see Figure 2.5, is that the head vibrates in - a superposition of - its Eigen modes. The frequency content of the time response due to a blast load is determined using a Fast Fourier Transform of the the skull deformation and internal pressures. An alternative modal analysis of the head models provides the Eigen frequencies of the head models. This alternative method uses a localised block pulse to simulate a hammer impact which excites the model in its Eigen modes.

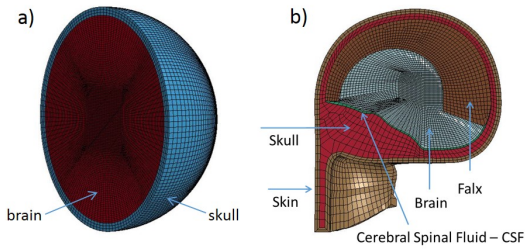

Figure 2.4: a) simplified spherical head surrogate b) more biofedelic BI2PED-FE head surrogate

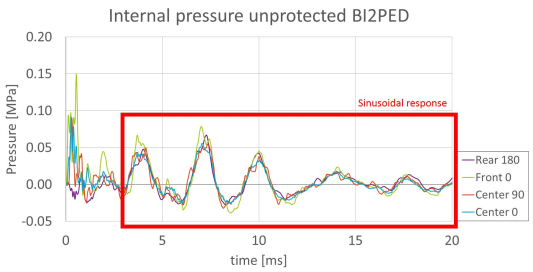

Figure 2.5: Sinusoidal part of the pressure response

1.2 What is the effect of the head geometry and other model features, properties and boundary conditions on the internal brain pressures?

The head surrogate is an approximation of a real human head. Influence studies are done to assess the effect of the components included in the BI2PED-FE model, compared to a skull-brain system. In this way, the sensitivity of the model is identified along with its most important components. This methodology is used to choose a reference model for the optimization of the numerical-experimental method in Part 2. By increasing the complexity of the model step by step and changing one main property of the model per step, the influence of this property is identified. The influence parameters are chosen based on the main differences between the spherical model and BI2PED model. The influence of a skin layer, the brain-skull interface and neck constraints are studied more extensively.

Part 2 - Can the measurement of the internal response be improved?

Different ways to combine the numerical and experimental results are investigated. Two categories of combining the two are investigated. The first focusses on using measurements of the shock tube test as input for the numerical model, such that the spatial resolution of the response is improved compared to the limited number locations of sensor output in the experiment. The second uses numerical simulations to improve the approach and the measurement locations for the shock tube experiments. Part 2 is also divided into sub questions. Based on the influence studies (see Part 1, Question 2) a reference model of the BI2PED-FE is determined which is used for the analysis of these questions.

2.1 Can the effect of a helmet be numerically evaluated without modelling the helmet?

To use numerical simulations directly to assess the protective capabilities of helmets, the load applied to the head in protected cases needs to be modelled. For an efficient combined assessment method of a series of helmets it is undesirable to have to model each helmet in full detail. For this reason it is studied whether the deformation of the head underneath the helmet observed during the experimental tests can be recreated numerically.

Multiple options are considered: Applying a strain field to the numerical model, based on measured strains during the experiments. Or ways to transform the measured strains to a deformation field, by using an algorithm that performs the transformation directly or on the basis of a superposition of modal deformation. Simulation results of the BI2PED-FE blast response and modal analysis are used to estimate the feasibility of these approaches.

2.2 What is the internal pressure distribution and can locations of maximum and minimum pressure be identified?

A set of blast loading scenarios is simulated to analyse the internal pressure distribution. Based on the results potential critical locations of maximum pressure and minimum pressure are identified. This information is used to propose an optimised measurement approach (see Part 2 Question 4).

2.3 Can a relation be defined between external skull strains and internal brain pressure?

The pressures on the skull underneath the helmet cannot be reliably measured during the experiments with the necessary repeatability of the results. Therefore it is investigated whether the skull strains could be an alternative way to measure the load applied to the head model. Using various loading scenario's applied to the BIPED-FE reference model it is studied whether a relation between the maximum external skull strain and maximum internal pressure exists. In case this relation is present, the external skull strains can be used as an indicative measure of the internal loads.

2.4 What is the optimal strain and pressure sensor layout in order to effectively combine test and FE data to determine the protective capabilities of helmets?

The answers to the previous questions are used to propose a way to optimize the helmet assessment method. From this analysis, the approach deemed most feasible is chosen and a sensor lay-out for the shock tube tests supporting this approach is analysed using the simulation results of the load cases applied to the BI2PED-FE reference model.

2.2. Thesis outline

The report is structured as follows.

- Chapter 3 contains the details of the head structure and blast load with their respective numerical modelling.
- In Chapter 4 a schematic representation of the response of a head surrogate to blast loads is presented. This break down of the response is formed using the results of the simulations and analysis in Chapters 5 and Chapter 7.
- Chapter 5 includes the verification of the spherical head model.
- In Chapter 6 the influence of added components to the skull-brain system are studied.
- In Chapter 7 the analysis of the head vibration is presented. The vibration is related to the Eigen modes.
- Chapter 8 contains the different investigated assessment approaches that combine the numerical and experimental head response results.
- In the discussion in Chapter 9, the physical BI2PED and numerical BI2PEF-FE are compared and the helmet as additional factor in the response is discussed.
- Chapter 10 includes the conclusions of the research and recommendations for future studies.

Considering the discussed research questions, the questions to Part 1 can be found in the Chapters 4, 5, 6 and Chapter 7. The answers to the questions of Part 2 are included in Chapters 7, 8 and 9.

3

Numerical Modelling

This chapter covers the physical structures and loads simulated in this study and the manner in which these are modelled numerically; From a human head to the BIPED human head surrogate to a simplified spherical head model, Section 3.1; From a physical blast to a numerical blast load, Section 3.2.

3.1. Physical and Surrogate Head Structure

This section starts with a description of human anatomy. The physical human head surrogate named the BI2PED is presented. This is the head surrogate used during the shock tube tests. It is followed by an overview of the BI2PED-FE numerical model. The section concludes with an overview of a simplified spherical head surrogate used to study the response mechanisms of head structures to blast.

3.1.1. Human head anatomy

This section is an excerpt from the literature survey of de Vries [6]. It describes the biomechanics of the human head.

The human head can be divided into two parts, the facial area and the cranial skull surrounded by the scalp [34][4]. The facial area is the front part of the head and consists of the facial cranium, skin, muscles and blood vessels. The facial cranium is the part of the skull supporting the face, the part of the skull that forms a protective vault surrounding the brain is called the neurocranium. The facial cranium consists of 14 bones, of which 13 are relatively flat (thickness 5mm), and 1 bone (the mandible) is rather thick. The mandible is the only bone that is connected to the skull by free movable joints, all other bones of the skull are fused together through complete sutures (interlocking lines). The facial cranium contains vaults, e.g. for the mouth, nose and eyes. Bones frequently have a hollow structure, and are provided with openings for vessels or nerves. The facial skull is covered with a relatively thin skin and muscles that allow for movement about the mouth, nasal and orbital openings. Soft tissues of the face are the eyes, tongue, blood vessels, nerves and cartilages and ligaments. The facial cranium is depicted in figure 1.1a, together with the neuro-cranium.

The cranial skull consists of several anatomical features, subsequently from the outer surface to the inner part: the scalp, neuro-cranium, meninges and the central nervous system (CNS), see Figure 3.1b [34][4]. These features are described below respectively:

Scalp

The scalp covers the outer surface of the neuro-cranium. This soft tissue structure (thickness 5 − 7mm) consists of 5 layers: the skin, connective tissue, aponeurosis (strong membraneous sheath preventing superficial cuts to extend), loose connective tissue, and periosteum (contacts the neuro-cranium). The first characters of these layers form the word scalp. Applying traction force to the scalp will move the outer three layers together as one. Therefore, tearing of tissue (avulsion) usually takes place at the level of loose connective tissue.

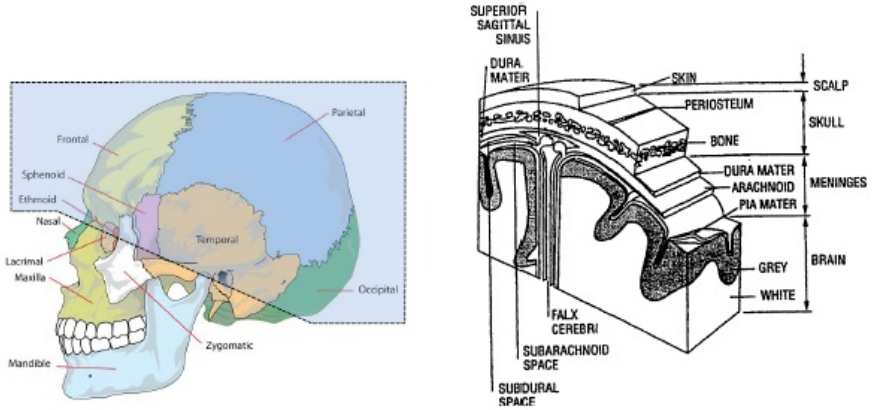

(a) The neuro-cranium consists of the bones indicated in the blue area; the facial-cranium consists of the bones that are *not* placed in the blue area

(b) The scalp, skull, meninges and brain [1]

Figure 3.1: The bone structure (a), and the anatomical features of the cranial skull (b)

Neuro-cranium

The neuro-cranium is the part of the skull that covers the brain. It is made up of 8 bones, with a thickness of 4 to 8mm: the frontal bone, two parietal and two temporal bones, the occipital bone, the sphenoid bone and the ethmoid bone, see figure 3.1a. The large cranial bones have a sandwich-like construction: dense bone at the outer and inner surface, held together by spongy bone in the middle. The base of the cranial vault is a thick and irregular plate of bone, containing small holes for arteries, veins and nerves as well as a large hole (the foramen magnum) through which the spinal cord enters into the brain, see figure 3.2a

Meninges

In between the neuro-cranium and the brain, three membranes are protecting and supporting the brain and spinal cord, called the meninges. These meninges separate the brain and spinal cord from the surrounding bones. From the outside to the inside, the following meninges are found (see figure 3.2b:

• the dura mater: a tough fibrous membrane, surrounding the brain and the spinal cord. In the skull, this membrane consists of two layers that are fused together. The inner layer covers the brain. At some places the two layers separate and form sub-structures, e.g. the falx cerebri (in between left and right cerebrum), the falx cerebelli (in between left and right cerebellum) and the tentorium (in between the cerebri and cerebelli), see figure 1.2b. These structures are thought to prevent large brain displacements.

• the arachnoid: a spider-web-like membrane, separated from the dura mater by a narrow subdural space, that is filled with a thin film of watery fluid: the cerebrospinal fluid (CSF). • the pia mater: a thin membrane of fine connective tissue invested with numerous small blood vessels. This membrane covers the surface of the brain, well into its fissures. The pia mater is separated from the arachnoid by the subarachnoid space, also filled with CSF.

The brain (and spinal cord) are surrounded by ca. 140ml of CSF. This fluid cushions the brain from mechanical shock and, during normal movement, shrinking and expansion of the brain is quickly balanced by an increase or decrease of CSF that can flow from the cranial cavity into the spinal cavity through the foramen magnum.

Brain

To the centre of the head, the brain and spinal cord are found, together forming the central nervous system. The average anterior-posterior length of the brain is about 165mm and its greatest transverse diameter is about 140mm. The average weight is 1.36kg for an adult male and a little less for a female. The brain largely is a network of neurons and supportive tissue, functionally arranged into areas that are gray or white in color and have di□erent densities. Gray matter is composed primarily of nerve cell bodies (neurons), concentrated in locations on the surface of the brain and deep within the brain. White

matter is composed of myelinated nerve cells processes (axons), that largely form tracks to connect parts of the central nervous system to each other. The brain can be divided structurally and functionally in the cerebrum (divided into right and left cerebral hemispheres), the brainstem (consisting of the midbrain, pons and medulla oblongata), and the cerebellum, which is divided into two hemispheres as well. Locations of these brain components can be found in figure 3.2a.

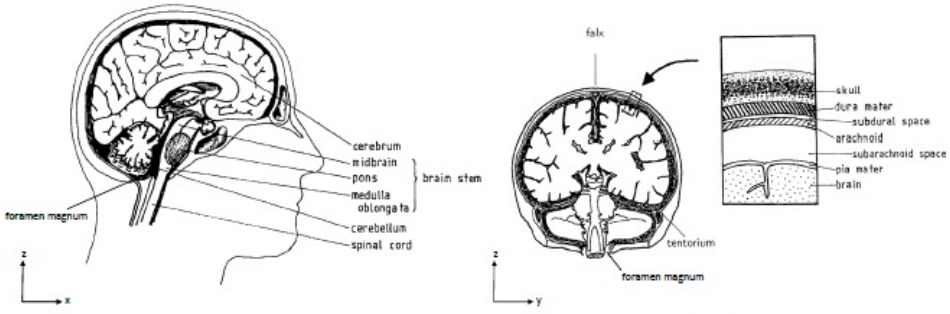

(a) The head in sagittal section: principal parts of the brain [1]

(b) The meninges of the brain [1]

Figure 3.2: Sagittal section (a), and coronal section of the human head (b)

3.1.2. Head models

Two head models are used in this research. A detailed biofidelic head surrogate; the BI2PED developed by DRDC and a simplified spherical head model. A physical BI2PED model is used for shock tube tests performed at TNO. Along with a numerical representation the BI2PED-FE, provided by DRDC, this model is the head surrogate intended for the combined numerical experimental helmet assessment method. The spherical head model is a simplified head model used to gain better understanding of the physics involved in the response to blast. It is also used to first test the methodologies proposed in this report on a simplified head model. The next two sections present an overview of the head models.

BI2PED head model

The BI2PED head model is a human head surrogate designed for blast-induced traumatic brain injury assessment[22]. BI2PED is short for Blast-Induced Brain Injury Protection Evaluation Device. The model and its components are presented in Figure 3.3. It has been validated with post mortem human subjects[23].

The BI2PED components are presented in Figure 3.4. The brain is kept in place by the Falx and Tentorium membranes. Water surrounds the brain inside the skull. This water functions as a surrogate for the cerebral spinal fluid.

Figure 3.3: Overview of the BI2PED model and its components [23]

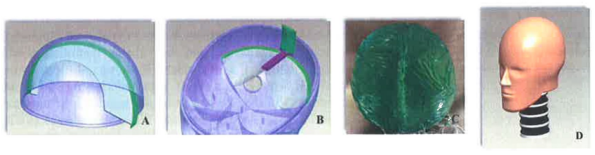

Figure 3.4: the BI2PED model: A - Falx membrane, B - Tentorium membrane, C - surrogate brain with its hemispheres, D - BI2PED including skin and attached to a neck[22]

BI2PED-FE head model

The original BI2PED finite element model provided by DRDC [3], named the BI2PED-FE in this report, is an Arbitrary Lagrangian Eulerian (ALE) model created for the numerical code LSDYNA. This model, shown in Figure 3.6 includes a mesh of the air domain through which the blast propagates and the fluid-structure interaction between the air and head. The BI2PED-FE model can be used for a Lagrangian-only simulation by using only the head mesh and removing the external air mesh. The load can in this case be applied directly to the head using the LSDYNA keyword LOAD BLAST or LOAD BLAST ENHANCED.

The head and its components and properties are presented in Figure 3.5. Note that the Falx is not connected to the other components of the head model in the original mesh provided by DRDC. Contact definitions between the Falx and head are not provided within the model files. The correct implementation of the Falx is a question posed to DRDC. An answer has not yet been received. The Tentorium membrane present in the physical model is not included in the numerical model, similar to the eye orbits, nasal cavity, nose and neck.

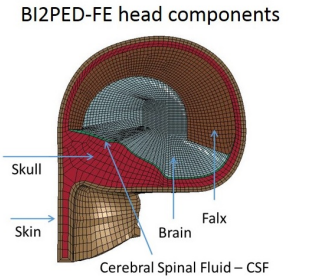

Property	Value
BI^{2}PED mass	4.5 kg
Skin thickness	5.0 mm
Skin density	1050 kg/m^3
Skull thickness	6.0 mm
Skull density	2000 kg/m^3
Skull Young's modulus	11500 MPa
Skull Poisson's ratio	0.3
Brain density	950 kg/m^3
Brain bulk modulus	1065 Mpa
CSF thickness	2 mm
CSF density	1000 kg/m^3
Falx density	1561 kg/m^3
Falx Young's modulus	7920 MPa
Falx Poisson's ration	0.379

Figure 3.5: Overview of the BI2PED-FE head model and material properties

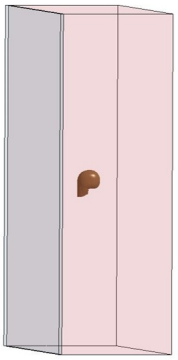

Figure 3.6: BI2PED-FE head model within the ALE air domain

In order to compare the numerical and experimental results the internal pressures need to be measured at equivalent locations. The dimensions of the BI2PED-FE model are in meters. A scan of the physical BIPED model used during the shock tube experiments has been provided by DRDC, along with a table that specifies the location of the sensors with respect to a reference point – the Nasion. This is the intersection of the frontal bone and two nasal bones of the human skull. The locations of the numerical sensors are determined using these distances with respect to an equivalent numerical reference point with the coordinates (0,-0.59797473,-0.00563155)(x,y,z). An additional 5mm is added to the distances to the numerical reference point to account for the skin thickness of the numerical model. An overview of the numerical and physical sensor locations is provided in Figure 3.7.

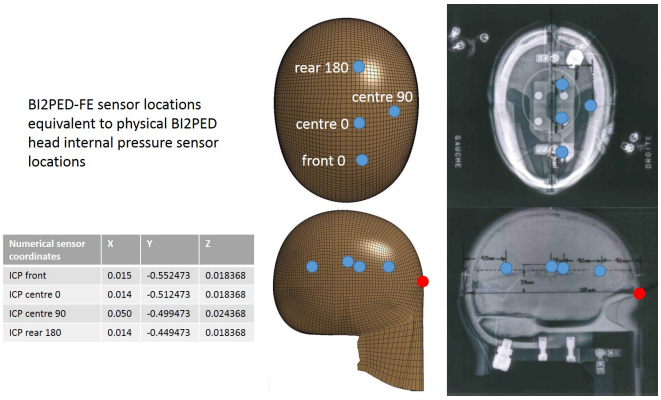

Numerical sensor coordinates	X	Y	Z
ICP front	0.015	-0.552473	0.018368
ICP centre 0	0.014	-0.512473	0.018368
ICP centre 90	0.050	-0.499473	0.024368
ICP rear 180	0.014	-0.449473	0.018368

Figure 3.7: Position of the BI2PED-FE equivalent pressure sensor locations

Spherical reference model

In order to study the physics involved in the response to blast a simplified spherical head model is used. The spherical model consists of a ballistic gelatin core as a brain simulant with an external shell constructed out of Synbone as a skull simulant. Once the basic response of the skull-brain system is known, the effect of additional, more life-like, model features and geometry can be identified. The sphere model components and its properties are presented in Figure 3.8. This material properties and dimensions are based on the spherical model of de Vries [7]. The output is studied, unless stated otherwise, at the locations shown in Figure 3.9. The dimensions of the spherical model are in millimetres.

Spherical model head components

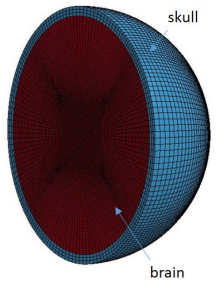

Material model:
Brain - *MAT_ELASTIC
Skull - *MAT_ELASTIC

Property	Value
Sphere radius	95.0 mm
Sphere mass	3.26 kg
Skull thickness	7.0 mm
Skull Young's modulus	1400 MPa
Skull Poisson's ratio	0.469
Skull density	700 kg/m^3
Skull speed of sound	3279 m/s
Brain Young's modulus	0.0466 MPa
Brain Poisson's ratio	0.499
Brain density	960 kg/m^3
Brain speed of sound	1478 m/s

Figure 3.8: Overview of the spherical head model and material properties

Spherical model internal sensor locations

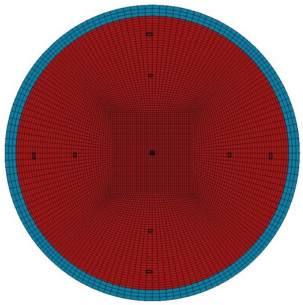

Sensor Coordinates	X	Y	Z
Front 75	0	75	0
Front 50	0	50	0
Back 75	0	-75	0
Back 50	0	50	0
Base 75	0	0	75
Base 50	0	0	50
Top 75	0	0	-75
Top 50	0	0	-50
Side 75	75	0	0
Side 50	50	0	0

Figure 3.9: Position of the spherical head model pressure sensor locations

3.2. Physical and Numerical Blast loading

A description of physical blast loading is presented in the next section. It is followed by an overview of the blast load procedure and main blast loads applied numerically in this study.

3.2.1. Blast as a result of an explosion

This section is based on the work of David de Vries [6] and an internal lecture given by A. van Erkel at TNO [33]. A blast wave is the result of an explosion, where a large amount of energy is suddenly released. The explosion can be chemical (typical rapid exothermic reaction of a solid or liquid material into gaseous reaction products), nuclear, or physical (driven by the rupture of a membrane or the bursting of a vessel). The blast wave is a combination of a shock wave and a rarefaction wave. Both wave types are shown in Figure 3.10. As the wave shape changes over time and distance they are plotted at two locations with a different distance with respect to their origin.

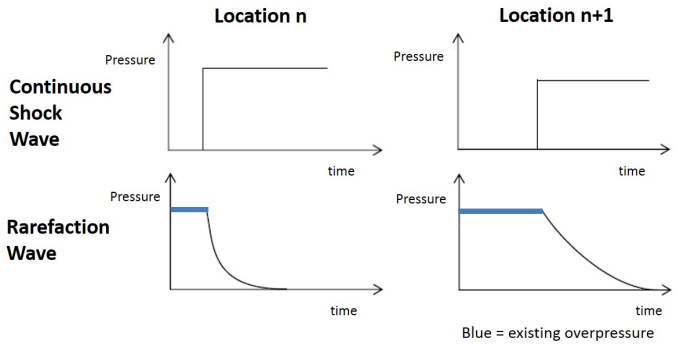

Figure 3.10: Schematic description of a shock wave and rarefaction wave plotted at two distances relative to the wave origin, where n+1 is further away

Definition: A Shock wave is a supersonic and positive discontinuity that compresses the medium and is non-isentropic. It gives an increase in particle velocity in the wave direction

Definition: A Rarefaction (expansion) wave is sonic, relieves the medium and is isentropic. It gives an increase in particle velocity in the direction opposite to the wave direction

In Figure 3.11 the explosion and resulting blast wave are depicted schematically. The detonation of a High Explosive results in a outward moving shock wave, which is ahead of the contact discontinuity. A rarefaction wave first propagates inward to the centre of the black sphere, but is reflected such that it propagates outward. Over time it overtakes the shock wave and together the two waves will form a blast wave, with a shock front and trailing rarefaction wave.

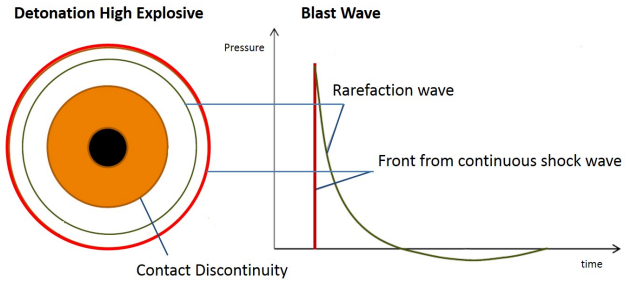

Figure 3.11: Schematic description of a detonation of a high explosive and a blast wave

Definition: A Contact discontinuity is not a wave but the front of the expanding particles of the original high pressure volume, expressed by a change in density and travelling with the local particle speed

The pressure profile of a blast wave is often described using a modified Friedlander equation. The Friedlander curve is a typical pressure-time profile of an explosion, see Figure 3.12. At the time the blast wave arrives, the pressure suddenly increases and then rapidly decreases to zero, this phase is called the positive phase. The pressure can then temporarily drop below atmospheric pressure, due to the inertia effects of the particles. This is called the negative phase.

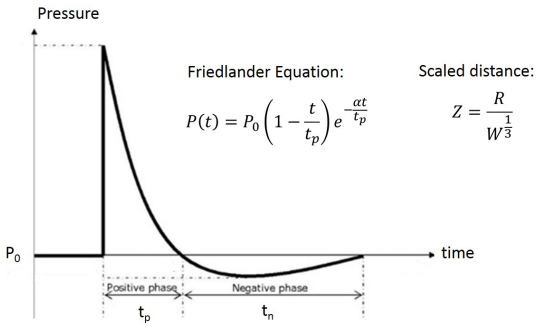

Figure 3.12: An idealised blast wave described by a Friedlander curve

At locations further away from the source, the peak pressure decreases and the phase duration elongates. The peak pressure can be related to the explosive charge weight W (equivalent TNT mass) and the distance R to the explosive charge by a scaled distance Z, see Figure 3.12.
The actual load on the structure is different than the incident pressure. The load on the structure is a result of the reflected pressure on the object surface and the airflow around the object, expansion waves and drag type effects.

3.2.2. Blast as a numerical load

This section contains a description of the blast load method and the two main numerical load cases used in this research. The LSDYNA keyword LOAD BLAST ENHANCED (LBE) is used to model the blast load on both the spherical head model and the BI2PED-FE head model. In this option a Friedlander curve is determined and applied directly to the head structure. This approach does not include fluid-structure interaction, unlike the Arbitrary Lagrangian Eulerian (ALE) option available for the BI2PED-FE head model. This means that 3D effects like flow around a structure are not included. However, simulation time is greatly reduced to hours instead of weeks using LBE instead of the ALE option. The basic response and the effect of model components on this response should be similar in both loading methods. For these two reasons LBE is preferred for the analysis in this report. Implementation and use of the ALE environment is recommended for an improved accuracy of the loading profile, to be used for validation of the models in future studies.

Load Blast Enhanced

Load Blast Enhanced (LBE) is based on CONWEP (an empirical model contained in the TM5-855 US army handbood) and the implementation of load blast is based on a report by Randers-Pehrson and Bannister 1997[25]. The user provides an equivalent TNT mass, distance and blast type as input. Then based on the initial distance, angle and outward normal of each segment designated for loading, a reflected pressure profile is constructed. A schematic representation is contained in Figure 3.13. The pressure curve is directly applied to the segments by means of nodal forces over time. The spherical air burst empirical relations are valid in the range of scaled distance: $0.147 < Z < 40 \frac{m}{kg^{\frac{1}{3}}}$

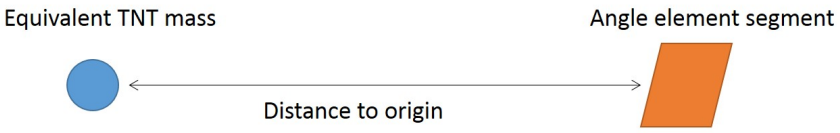

Figure 3.13: Schematic of the LSDYNA keyword Load Blast Enhanced

Numerical load cases

Two main load cases are used for the simulations contained in this report, described in terms of their peak incident pressure (Pi) and positive phase duration (tpos):
Load case 1: Pi 160kPa tpos 4ms
Load case 2: Pi 130kPa tpos 15ms

Load case 1 - LC:160kpa4ms

This blast load is the reference case used to study the behaviour of the various models to blast loading and to gain understanding of the general behaviour.
The peak incident pressure is based on the highest peak incident pressure applied during the BI2PED shock tube experiments; 160kPa. The distance of the centre of the charge to the centre of the model is 4.095m. This distance is approximately the distance between the point of detonation and start of the test section of the shock tube used in the experiment. An equivalent TNT mass of 3.85kg us supplied as model input to obtain the 160kPa incident pressure. The result is a positive phase duration of 4ms and total load duration 5ms where the negative phase is dictated by the Friedlander equation. An example of the incident pressure and reflected pressure load on a segment for load case 1 is presented in Figure 3.14. It is the load applied to a segment perpendicular to the blast direction at a distance of 100mm upstream with respect to the center of the sphere model. Note that this pressure profile does not correspond to the pressure profile of the shock tube experiments.

Load case 2 - LC:130kPa15ms

This numerical load is used to compare the behaviour of the BI2PED during the experiment with the behaviour of the BI2PED-FE during the simulations.
Measurements from the experiments were used to fit the numerical blast applied with Load Blast Enhanced to the blast in the shock tube during the BI2PED tests. During the experiments two load cases

were used; (Pi 160kPa-tpos 17ms) and (Pi 80kPa-tpos 17ms). The numerical blast load is fitted to the largest of these two cases. The procedure is contained in Appendix B. A numerical blast with an incident pressure of 130kPa and positive phase duration of 15ms was found to be the best match with the physical blast during the tests of 160kPa and 17ms. The impulse transferred by this load is overestimated numerically, however to compare the general behaviour of the physical and numerical model this is not considered problematic. The incident and reflected pressure measured at a reference segment at a distance of 150mm upstream with respect to the center of the BI2PED-FE head model is plotted in Figure 3.15.

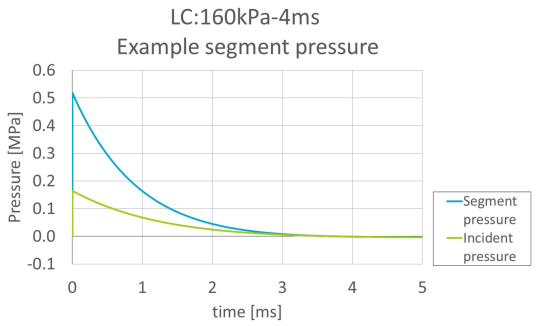

Figure 3.14: Load case 1: Incident and reflected pressure applied to a single segment 100mm upstream with respect to the model center of gravity

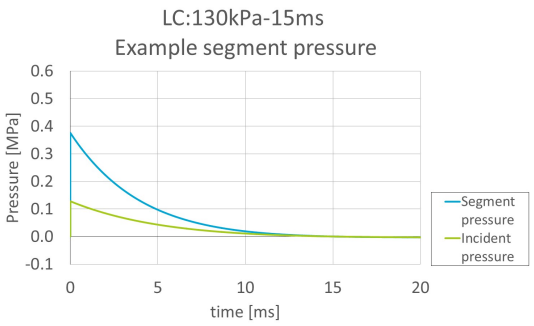

Figure 3.15: Load case 2: Incident and reflected pressure applied to a single segment 150mm upstream with respect to the model center of gravity

4

Description of the Head Model Response to Blast Loading

This chapter provides the basis for the interpretation of the response graphs and physics of the experimental and numerical results. The simulation results of Chapter 5 and 7 were used for the theoretic description provided here.

Using the simulation results of the 3D spherical model a description of the response to blast was formed. For different head models the main principles are comparable even though the reflection pattern and deformation shape might be different.
A blast load is of a very short duration, in this case about 4ms. Because the load is almost instantaneous dynamic effects are dominant. Figure 4.3 shows a schematic of the response to a highly dynamic blast load of a spherical head model. It depicts the three phases distinguished in the response; the peak, transition and vibration phase. These phases will be elucidated in the following paragraphs. Note that the deformation in the figure is exaggerated.

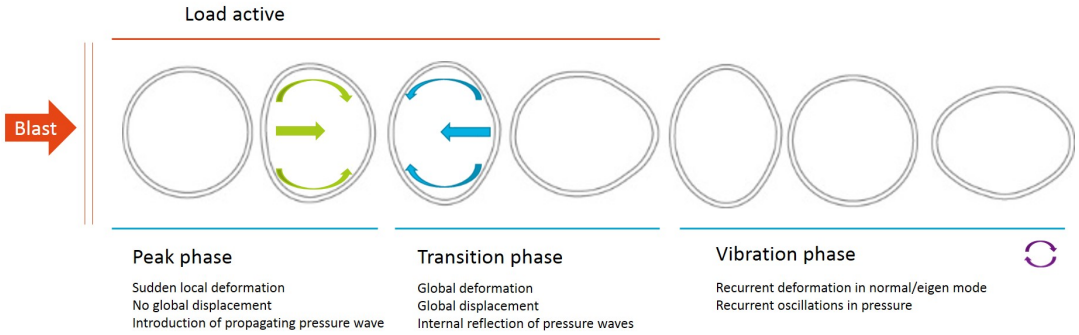

Figure 4.1: Schematic of the response of a spherical head model to a blast load

The peak phase +- 1ms
When the blast impacts the head model there is a sudden local deformation. This results in pressure waves that propagate through the structure, and a peak in the internal pressure is seen. The structure ahead of the wave is still unaffected. These pressure waves propagate with the local speed of sound of the head model materials, which is higher than the speed of the blast wave through the air. This means that the internal pressure waves travel ahead of the blast. Additionally, local bending of the skull is introduced. A ripple effect travels along the skull ahead of the blast wave. Due to inertia it takes some time for the structure to move globally.

The transition phase +-3ms
Once the pressure waves and ripple effect reach the back of the model these are reflected. Depending on the model a complicated reflection pattern will result which has an effect on the internal pressure distribution observed. At this point the whole structure deforms. The duration of the transition phase depends on the positive phase duration and head model. It is defined as the time period between the initial peak and the time at which a recurring sinusoidal pressure profile has developed. The influence of the blast positive phase duration on the transition phase can be found in Appendix D.

The vibration phase »ms
Even when the blast load is no longer present the structure will continue to vibrate. After the transition phase the model will vibrate in its normal or Eigen mode(s), this hypothesis is confirmed in Chapter 7. In the internal pressure oscillations are seen that have frequencies close to the Eigen frequencies of the model. The vibration will continue until all energy has dissipated.

Figure 4.2 shows the pressure response at different locations in the sphere model as a result of a blast load. Generally speaking the internal pressures can be described as to have a sudden compression peak that transitions to a repeated oscillation where both tensile and compressive pressures are seen. Factors that can have an influence on the internal pressure transmission are for example the impedance mismatch, viscosity of the material and geometry of the model. The temperature can have an influence on the material behaviour, but for the load considered in this project the temperature effects are negligible.

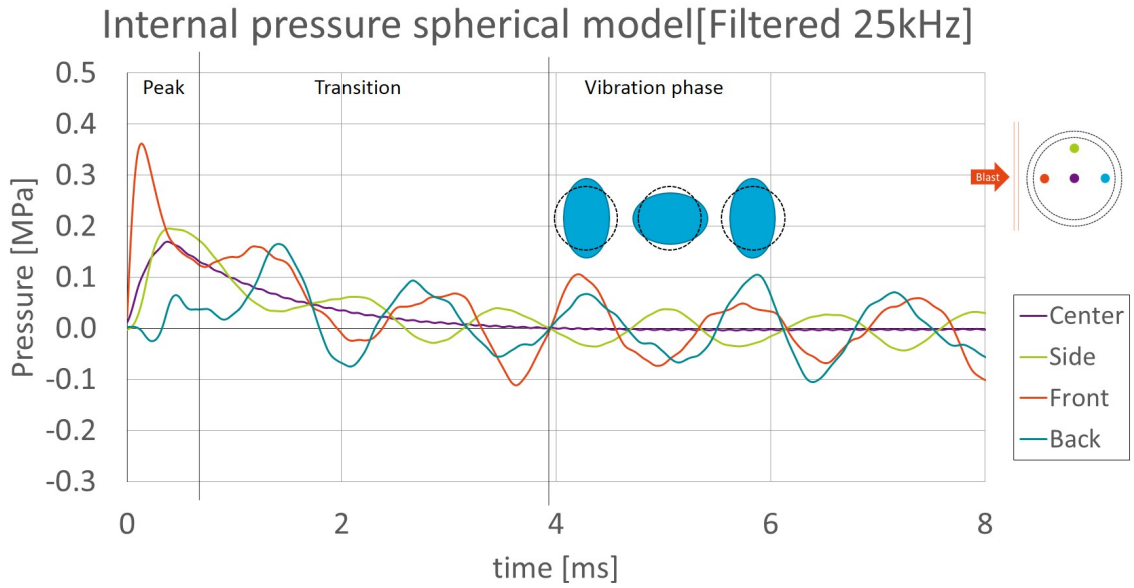

Figure 4.2: Phases in the internal pressure response of a 3D spherical head model to a mild blast load (LC:160kPa-4ms) BW filter C=25kHz

The pressure distribution of the spherical model during the different phases is presented in Figure 4.3. The peak phase shows the propagation of the pressure wave induced by the blast impact and the local deformation of the model. The vibration phase shows a deformation cycle and its pressure distribution; this cycle is recurrent. The transition phase shows moments in between the time it takes to transition from the initial impact to the vibration mode.

The blast impacts the skull at t=0.02ms. At t=0.14ms the internal pressure wave through the brain has reached the back of the model. At t=0.20ms the wave propagating through the skull has reached the back of the head. The blast has travelled to the rear of the head through the air at t=0.38ms.

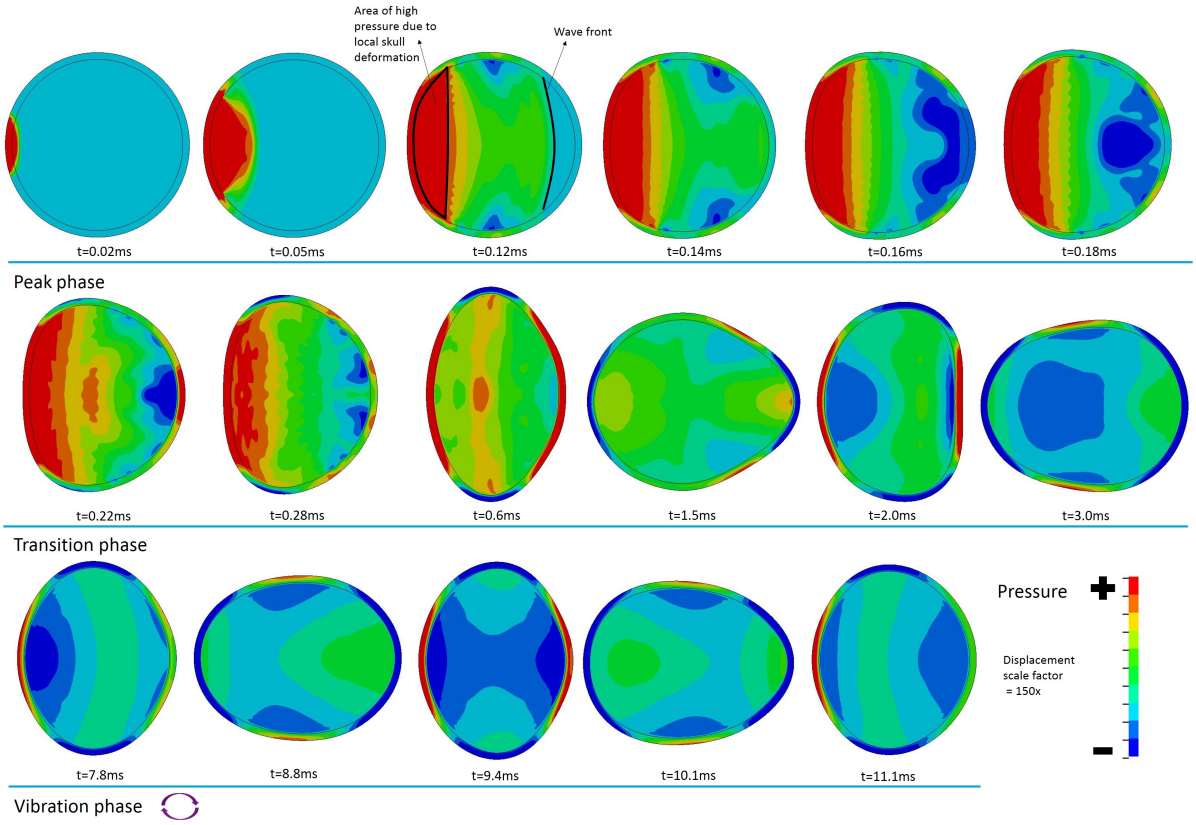

Figure 4.3: Pressure distribution in a 3D spherical head model under blast loading (LC:160kPa-4ms) Displacement scale = 150x, pressure scale: Pmin=-0.1 MPa, Pmax=0.3MPa

Response mechanisms

To summarise the above described response of the spherical model there are two dominant mechanisms in the response for a fully attached brain and skull. The impact of the blast results in local deformation and the propagation of the internal pressure wave. This is the first response mechanism and the mechanism related to the peak internal pressure. The second response mechanism is related to the oscillating internal pressure caused by a pulsating vibration of the surrogate head. In chapter 7 the hypothesis is confirmed that this is a vibration in the Eigen modes of the head, where skull deformation is dominant.

In case the brain is not fully attached to the skull local deformation and vibration in the brain is enabled. Impact of the brain relative to the skull is possible. This means that an additional third response mechanism likely exists in this case. Fluid in between the skull and brain is expected to have a significant influence on this third mechanism, as the fluid can damp the relative skull-brain impact and local brain vibration.

5

Verification of the Head Model Response to Blast

The spherical head model is used to form the description of the head response to blast presented in Chapter 4. It is also used to study the influence of the addition of head components on the internal brain pressures in Chapter 6. This spherical model is verified numerically in this Chapter to identify response characteristics and numerical artefacts.

Verification ensures correct implementation of the numerical model and reliable simulation results. A 3D model is necessary for a head model that can be loaded from different directions and that is able to include neck constraints. In order to verify the results of the 3D model, the complexity is first reduced using a 2D axi symmetric spherical model and 1D bar. Two steps are taken within the 2D verification: first the discretization of the numerical problem is studied with a mesh convergence study to identify numerical sensitivity. Then the internal pressure distribution in the brain is analysed to distinguish between numerical artefacts and physical effects. In order to reduce the complexity further and study the internal pressure wave propagation through the materials a 1D bar is used. Finally, the best element for the 3D model is identified and the results of the 3D model are compared with the 2D model for verification of the 3D results.

5.1. Verification of a 2D axi symmetrical sphere

The discretization of the 2D axi symmetric spherical model is studied with a mesh convergence study to identify numerical sensitivity. Then the internal pressure distribution is analysed to distinguish between numerical artefacts and physical effects.

Convergence study

A mesh convergence study is done for a 2D axi-symmetric spherical model using the meshes in Figure 5.1. The LSDYNA shell element formulation 15 is used, a volume weighted axi symmetric solid. It is hypothesized that the deformation of the spherical head is dominated by the Eigen mode of the model. In this case the bending of the skull should be well represented. Using solid elements generally three elements are needed over the thickness to be able to describe bending. Therefore the element sizes are varied, based on the size that results when one divides the thickness of the spherical skull by n=1,2,3,4,8 elements.

The skull external displacement of the spherical model is plotted in Figure 5.2. The displacement obtained with the 7mm element significantly deviates, and the results converge for the smaller element sizes. The same trend is observed in the internal pressures in Figure 5.3. The results are filtered using a Butterworth filter with a cut-off frequency of 25kHz, as the high frequent component in the results make it difficult to distinguish between the various curves. The element size for the sphere models used in this thesis is 2.33mm. This is equivalent to three elements over the thickness of the skull. This size is used because at the locations of interest, the pressure and displacement are well described in the 2D axi-symmetrical model.

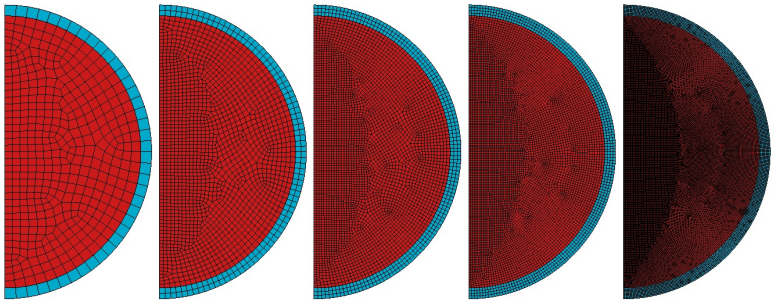

Figure 5.1: 2D axi-symmteric sphere meshes with element size: 7mm (n=1), 3.5mm (n=2), 2.33mm (n=3), 1.75mm (n=4), 0.875mm (n=8)

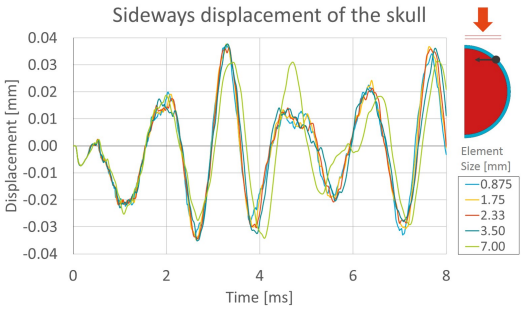

Figure 5.2: Displacement of the skull of the 2D sphere in x-direction for varying element sizes (LC:160kPa-4ms)

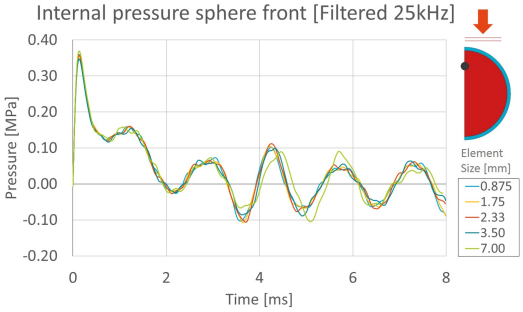

Figure 5.3: Pressure in the front of the 2D sphere for varying element sizes (LC:160kPa-4ms)

Localised pressure spots

In the finest meshes hotspots can be observed, see Figure 5.4. These are localised regions of higher stress due to localised bending of the skull, likely introduced by the large pressure jump over the shock front. The impedance mismatch of the Gelatin brain and Synbone skull is not the cause of the hot spots as a simulation with the full sphere modelled with Synbone properties showed a similar stress distribution. A simulation where only the empty skull is modelled, see Figure 5.5, shows the skull bending maxima and minima. The deformation of the skull is magnified by a factor 100x. The locations of bending maxima and minima correspond to the regions of high and low pressure 'hot spots'. A skull bending ripple travels ahead of the shockwave, due to the higher speed of sound in synbone with respect to the shock wave speed in air. It is unlikely that this ripple effect is a numerical artefact, as it is also seen in the study of Moss, where a different hydrodynamic based simulation type is used.[19]. In order to describe these hot spots accurately at least 8 elements over the skull thickness are recommended. However, the hotspots are outside of the region of internal sensor locations and therefore considered of limited importance at the moment. Additionally in reality, the skull is not fully attached to the brain. This is expected to negate these hotspots. It is therefore concluded that three elements over the skull thickness suffice.

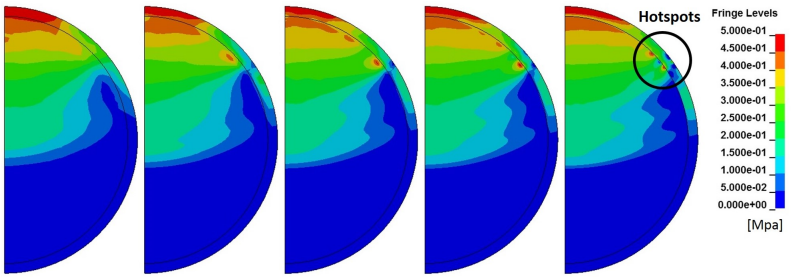

Figure 5.4: Pressure distribution with highlighted hot spots in the 2D axisymmetric sphere at time t= ms for varying element sizes: 7mm, 3.5mm, 2.33mm, 1.75mm, 0.875mm

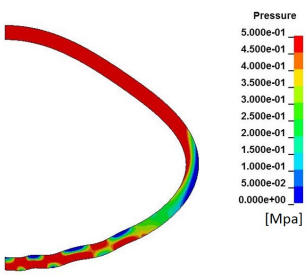

Figure 5.5: Bending ripple in a skull-only simulation (at t=0.3ms, el.size=0.4375mm, displ.scale=100x)

5.2. Pressure wave propagation through a 1D bar

The mechanical transfer of blast to internal load by inducing a pressure wave is studied in this section using a 1D bar, since for a 1D problem there are no reflected pressures from other directions. The numerical verification of the wave propagation through the bar consists of a convergence study. Parameter studies contained in Appendix E.1 show the influence of loading conditions and material properties on the internal pressure wave. A more detailed study into the response mechanisms of the 1D bar can be found in Appendix E.2. The bar used is depicted in Figure 5.6. By default the bar has the material properties of Synbone, the material of the spherical skull shell.

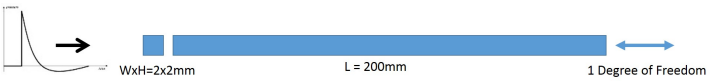

Figure 5.6: Bar with 1 Degree of Freedom

Convergence study

The influence of step size and element size on the pressure gradient over the length of a 1D bar are studied just after the initial impact of the blast. The goal is to find the element and step size that is able to accurately describe the pressure gradient through the material.

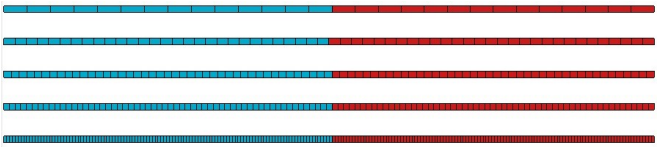

Figure 5.7: 1D bar meshes with element width 2mm and height 2mm element length: 7mm, 3.5mm, 2.33mm, 1.75mm, 0.875mm

The bars are loaded by blast load case 1: LC:160kPa-4ms. The impact of the blast with the front of the bar introduces a pressure wave through the bar. At time t=0.04ms this wave has travelled halfway through the bar. The expected pressure profile over the length of the bar is as follows: the pressure is zero in front of the pressure wave, where the bar is yet unloaded. There is a steep pressure gradient along the wave front. The pressure after the wave front is constant.
Figure 5.8 shows that smaller elements can better represent the steep pressure gradient. The elements with a length from 2.33 unto 7.00mm show pressure oscillations of numerical origin. The largest element able to describe the pressure gradient without oscillations is 1.75mm.
For the stepsize, the default LSDYNA quotient of 0.9 is varied to 0.09 and 0.009 for the bar with the element size of the spherical model of 2.33mm. LSDYNA uses the transient time of an acoustic wave through an element using the shortest characteristic distance to determine the minimum step size for an element. By looping over the elements the minimum step size for the mesh is determined and scaled with the quotient[13]. Figure 5.9 shows negligible differences in the pressure gradient for the different steps size quotients. It is concluded that the default step size suffices.

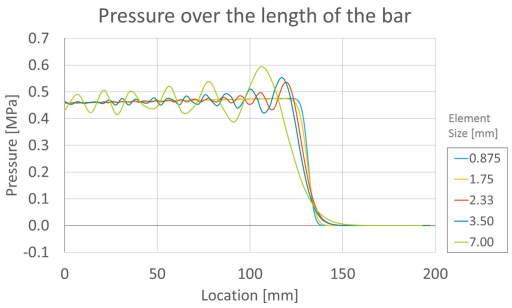

Figure 5.8: Pressure over the length of the bar at t=0.04ms. Blast impact at 0mm. (LC:160kPa-4ms)

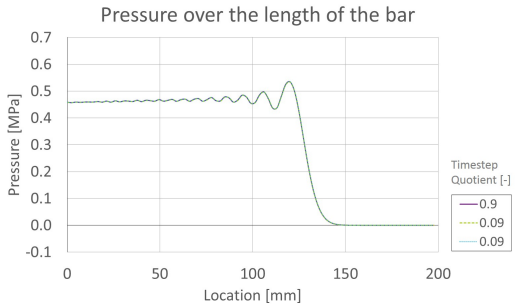

Figure 5.9: Pressure over the length of the bar at t=0.04ms. Blast impact at 0mm. (LC:160kPa-4ms)

5.3. Verification of a 3D plane symmetric sphere

Different element types are compared for the 3D model, then the results are compared with the results of the 2D axi symmetric sphere. The high and low frequent components in the internal pressure signals are next discussed. Finally recommendations are provided regarding the element size.

Element type formulation

For the 3D plane symmetric sphere model, various element types are compared, in order to find the most appropriate element to use. The elements are listed in table 5.1. The details of the element formulations can be found in the LSDYNA theory manual.[15] The results are verified by comparing them to the results of the 2D axi symmetric sphere.

Tetrahedron elements allow for easy meshing of complex shapes. However, pressure locking occurs with tetrahedron element 3. Element 13 is a special pressure tetrahedron designed to avoid this problem. The element gives good pressure results, but becomes unstable after a time when using small elements, which are needed for accuracy. Unrealistically large deformations develop and as a result the program terminates with a fatal error due to a negative element volume. Because of the issues with the tetrahedon elements the use of hexahedron elements is preferred.

The default 1 integration point hexahedron constant stress element develops hourglass modes, mainly on the exterior shell, see figure 5.10. Element 3 is not suitable because of the nearly incompressible gel material that is incompatible with its element formulation. Because the external strains need to be coupled to internal pressure for the combined assessment method proposed in Section 8.2, element equation 2 - a fully integrated formulation - is used for the skull elements. For the gelatin brain the default element type 1 with reduced integration is considered to be appropriate, as hourglass modes are negligible. The same element size of 2.33mm is used for the 3D plane symmetric sphere as for the 2D axi symmetric model because the internal pressure in this case corresponds well to the 2D results, see Figure 5.11.

LSDYNA Element Formulation	Description
Equation 1	8 node constant stress solid
Equation 2	8 node fully integrated S/R solid
Equation 3	8 node fully integrated quadratic with nodal rotation
Equation -2	8 node fully integrated S/R for bad aspect ratio
Equation 10	4 node 1 IP tetrahedon
Equation 13	4 node 1 IP pressure tetrahedon

Table 5.1: Overview of the compared 3D element types; the black box contains the elements used in the final 3D spherical model

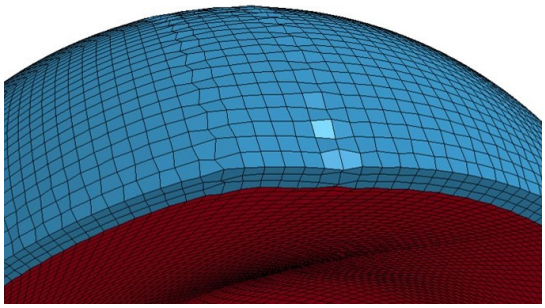

Figure 5.10: Hourglass modes in the 3D spherical model fixed at the bottom using element type 1, displacement scale = 5x

Figure 5.11: Internal pressure in the front of the 2D and 3D sphere model, unfiltered (LC:160kPa-4ms)

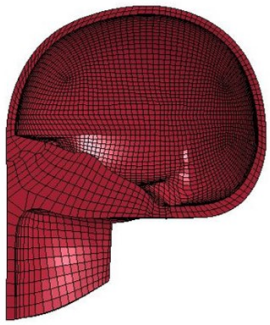

Figure 5.12: Crossection of the BI2PED-FE skull with 2 elements over the skull thickness

Remark:
The BI2PED-FE skull is modelled with 2 reduced integration elements over the thickness. It is generally recommended to use at least three elements over the thickness if bending is a significant deformation mode. This is confirmed considering the above-mentioned convergence study of the 2D axi-symmetrical sphere. For non linear material behaviour, as is included in the BI2PED-FE, even more elements are recommended. This should be taken into account when one reviews the BI2PED-FE simulation results.

Conclusion regarding the discretization of the spherical model
In case the sphere is fixed at the bottom element type 2 is advised in order to prevent hourglass modes in the skull. If the sphere is unconstrained the default element type 1 suffices.
The maximum element size able to describe the bending deformation in the spherical model is 2.33mm. For an accurate description of the pressure gradient of the pressure waves induced by impact a maximum element size of 1.75mm is advised. To well describe the localised pressure hot spots along the skull due to localised bending of the skull an element size of 0.875mm is recommended. In the BI2PED head model non-linearity such as visco elasticity is included for which elements smaller than 2.33mm are advised.
Because this study is interested in the global response mechanisms and overall pressure distribution the element size of 2.33mm can be used in the spherical model. If the brain geometry is more biofedelic, the material properties are non homogeneous or isotropic and one is interested in local pressure and damage effects this element size is not considered sufficient. Similarly if a quantitative study of the internal pressure is applied to compare the results with exposure limits smaller elements are advised. For a Lagrange simulation more detailed elements can be implemented. However, the gained benefit by increased accuracy is limited, because the load applied using load blast enhanced is a very coarse estimation of the actual load, see Appendix B. For a more accurate loading profile the ALE simulation type should be used, see Section 3.1.2.

High and low frequent components in the internal pressures
In the internal pressures of the sphere both a low and high frequent component exist, see Figure 5.13. The results are filtered by specifying a cut-off frequency for the Butterworth filter incorporated in the post-processor LSPREPOST in order to remove noise from the graphs and present clearer results, see Figure 5.14. As a result of the filter, peak pressures are reduced. It is necessary to identify the origin of the high frequent component to assess if it can be neglected in the response. It is hypothesized that the origin of the high frequent component lies in internally reflecting and propagating pressure waves. This hypothesis is tested using a 1D bar in Section 5.2. There it is shown that pressure waves resulting from impact indeed propagate through the bar. The origin of the lower frequent component is assumed to be related to vibration of the model in its Eigen modes. This is tested using a 1D bar in Appendix E.2. As the results of this study are not conclusive the hypothesis is tested on the spherical model in Chapter 7. There it is proven that the low frequent component is indeed related to vibration in the models Eigen modes.
In reality the high frequent pressure waves are damped due to material properties such as visco-elasticity and attenuate due to energy dissipation. Both visco-elasticity and energy disspation are are included in the BI2PED-FE model and damp the high frequent component, see Section 6.1. Therefore it is concluded that the results of the spherical model can be filtered. The maximum pressure is slightly higher in case the results are unfiltered. Therefore the cut-off frequency for the filter and the amount of damping in the model should be taken into consideration when actual damage mechanisms or exposure limits are concerned. These are however out of the scope of this project.

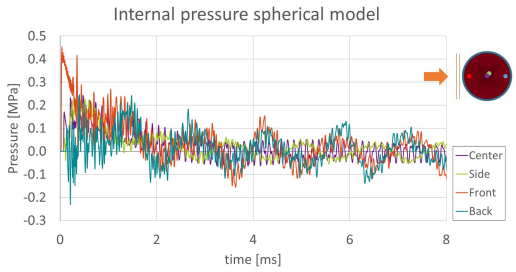

Figure 5.13: Internal pressure in the 3D spherical model (LC:160kPa-4ms) unfiltered

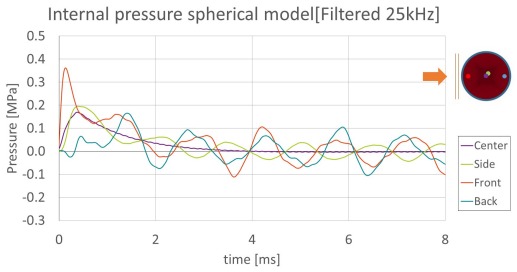

Figure 5.14: Internal pressure in the 3D spherical model (LC:160kPa-4ms) BW filter C=25kHz

6

Influence study of head model components

In Section 6.1 the BI2PED-FE is compared with the 3D spherical model first to indicate which properties have a large influence on the response. The presence of a skin layer - Section 6.2 - and the brain-skull interface - Section 6.4 - are studied further separately due to their large impact on the results. The addition of neck constraints is covered in Section 6.3.

The sphere model is a simplified representation of a head used to better understand the mechanics of blast load transfer through a brain-skull system. The BI2PED model is a more biofedelic head surrogate with a more complex geometry and additional components like a skin layer and fluid-like skull-brain interface. The BI2PED is positioned inside a shock tube during the experiments and attached to a Hybrid III neck. The purpose of the influence studies presented in this Section is to provide insight into how these described features influence the head response.

6.1. Comparison between the spherical and BI2PED-FE head model

It is checked whether the response mechanisms of the spherical model also apply to the BI2PED-FE model by comparing both models. The B2IPED-FE is first reduced such that the only main difference between the 3D sphere and BI2PED-FE is the shape of the sphere. This is done by removing the skin and jaw. The BI2PED-FE skull is given the material properties of the sphere's skull synbone. The Cerebral Spinal Fluid (CSF) and brain material of the BI2PED-FE are both given the properties of the sphere's gelatin. From this reduced sphere-like BI2PED-FE, the BI2PED-FE model is reconstructed by increasing the complexity step by step, as shown in Figure 6.1. The influence of each step is visualised by plotting the internal pressures at points in the BI2PED-FE similar to points in the original sphere. All models are loaded with the reference load case with peak incident pressure 160kPa and positive phase duration 4ms, using Load Blast Enhanced (Section 3.2.2). The pressures for each model 1-6 are plotted in Figures 6.2-6.7. The most significant differences are discussed.

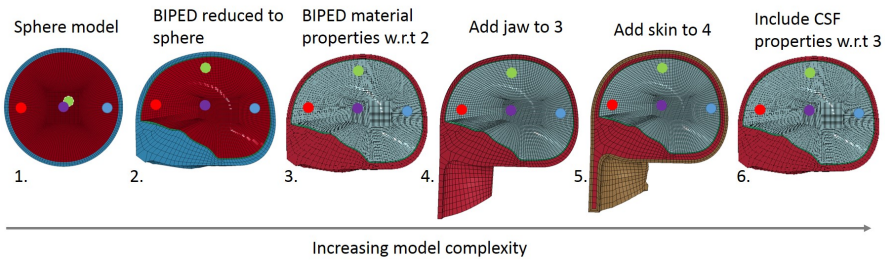

Figure 6.1: Comparing the BI2PED-FE model with the spherical model, step by step. Coloured dots represent output locations

- Models 1-2, Figures 6.2-6.3: The pressure profile is similar. An initial peak, transition and oscillation are seen in both pressure graphs. Energy dissipation and damping is not included in the sphere - model 1, but is included in the BI2PED-FE - model 2. The high frequent oscillations that are filtered from the sphere results, dissipate over time in the BI2PED-FE without filtering due to the included Rayleigh energy dissipation.
- Models 2-3, Figures 6.3-6.4: The brain material is modelled visco-elastic in the BI2PED-FE - model 3. This removes the high frequent oscillations seen in the first milliseconds compared to the BI2PED-FE with shpere-gelatin properties - model 2.
- Models 3-4, Figures 6.4-6.5: Adding the jaw - model 4 - does not greatly influence the pressure results.
- Models 4-5, Figures 6.5-6.32: Adding skin - model 5, results in significant negative pressures that are unexpected. Further inspection of the simulation results, Section 6.2 indicates this model shows an unrealistic response.
- Models 3-6, Figures 6.32-6.7: The CSF layer has a significant influence on the pressure distribution. Negative pressures are reduced and the sinusoidal shape of the response has a lower frequency in model 6 compared to model 3. The interface is studied in more detail in Section 6.4.

It can be concluded that the response of the BI2PED-FE is similar to the response of the sphere, except when skin or CSF is included.

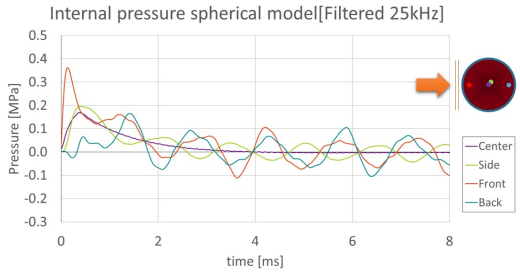

Figure 6.2: Internal pressure model 1 (LC:160kPa-4ms)

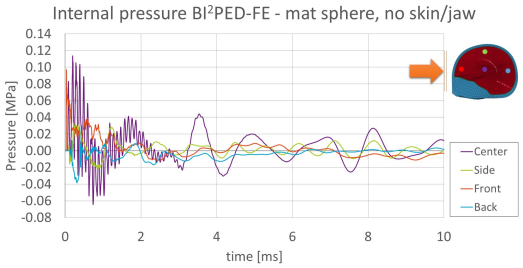

Figure 6.3: Internal pressure model 2 (LC:160kPa-4ms)

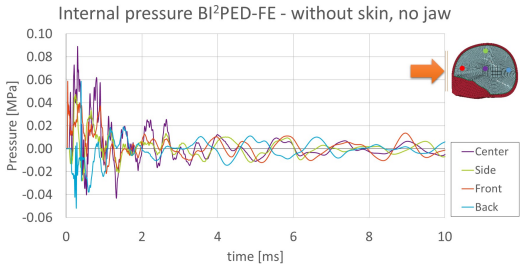

Figure 6.4: Internal pressure model 3 (LC:160kPa-4ms)

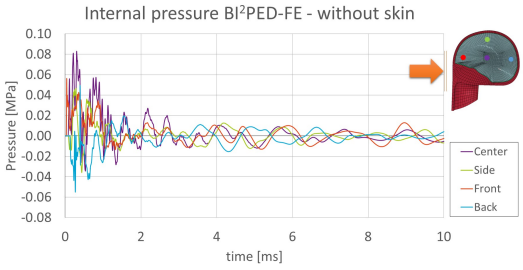

Figure 6.5: Internal pressure model 4 (LC:160kPa-4ms)

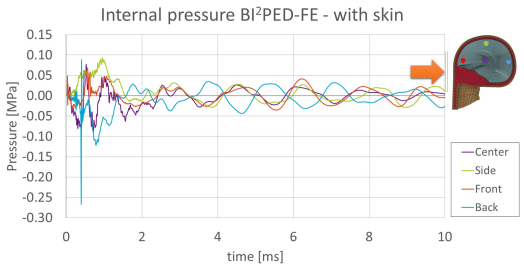

Figure 6.6: Internal pressure model 5 (LC:160kPa-4ms)

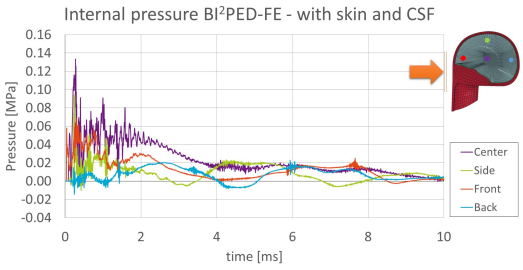

Figure 6.7: Internal Pressure model 6 (LC:160kPa-4ms)

6.2. The presence of a skin layer

In Section 6.1 it is shown that the presence of a skin layer has a large influence on the internal pressure distribution of the BI2PED-FE brain. The skin of the BI2PED physical model is a rubber-like mask. It is modelled numerically using the LSDYNA material model MAT SIMPLIFIED RUBBER/FOAM.[14] It uses a family of uni-axial load curves at discrete strain rates. In order to provide a statement on the reliability of the BI2PED-FE with skin, the skin layer is studied further in this section.

Influence skin on global displacements

Figure 6.8 shows that the BI2PED-FE with skin exhibits large global displacements downwards (z-direction) compared to the BI2PED-FE without skin. These large displacements are not seen when a sphere with and without an external skin layer are compared, Figure 6.9. Note that the orientation of the positive y direction is opposite between the two models, as a consequence of the head model orientation within the global coordinate system. For the sphere the displacements with skin are smaller than in the case without skin. This could be explained by the added mass of the skin.

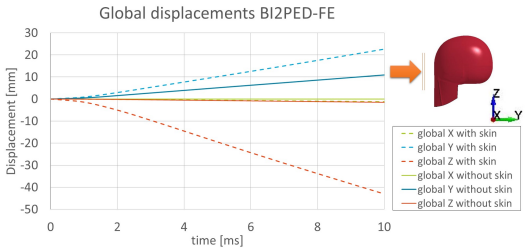

Figure 6.8: Global displacements of the BI2PED-FE with and without a skin layer (LC:160kPa-4ms)
note: in the BI2PED model the frontal blast originates upstream of the head in the **negative y direction**

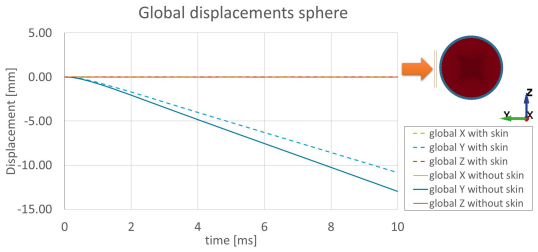

Figure 6.9: Global displacements of the 3D spherical model with and without a skin layer (LC:160kPa-4ms)
note: in the spherical model the frontal blast originates upstream of the head in the **positive y direction**

Comparing the displacement in Figures 6.15 and 6.14 of the physical BI2PED without and with skin visually measured during the shock tube tests and processed using the software package Aramis, it is seen that the difference in displacement is negligible compared to the difference seen in the BI2PED-FE. In both shock tube test cases the y (backwards) displacement of the head is around 30mm. Correcting for the difference in time before impact, both cases reach this maximum displacement after about 50ms. The reference points used to plot the graphs are slightly different in the two cases due to the visual measurement approach of the Aramis software package, however the effect is negligible.

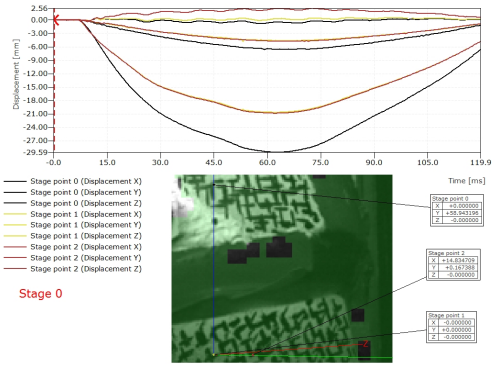

Figure 6.10: Displacement of the BI2PED head measured during shock tube test nr22 - without skin

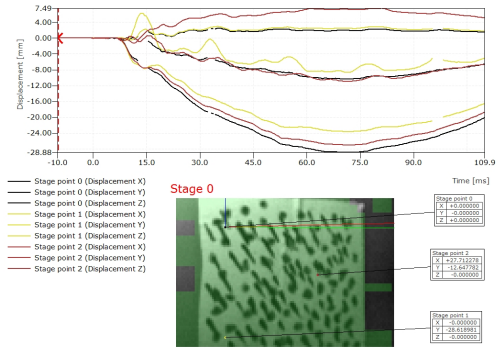

Figure 6.11: Displacement of the BI2PED head measured during shock tube test nr8 - with skin

Influence skin on internal pressure distribution

Looking at the internal pressures of the sphere with - Figure 6.13 - and without skin - Figure 6.12 - two main differences can be seen. The first is that the initial peak is reduced by the presence of the skin. The second is that the frequency content is changed. Both a lower and higher frequency component are observed.

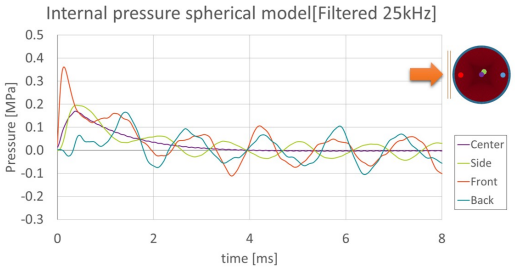

Figure 6.12: Internal pressure in the 3D spherical model without a skin layer [BW filter C=50kHz] (LC:160kPa-4ms)

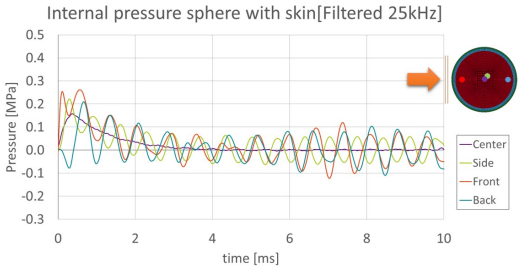

Figure 6.13: Internal pressure in the 3D spherical model with a skin layer [BW filter C=50kHz] (LC:160kPa-4ms)

Figure 6.14 and 6.15 show the internal pressures of the physical BI2PED during the shock tube tests with and without skin. Similar to the results of the spherical model it is seen that the initial peak is damped by the skin and that the frequency of the periodic pressure is slightly affected. One of the peaks around t=7ms, is amplified in the case with skin. The cause of the amplification is unknown at this time.

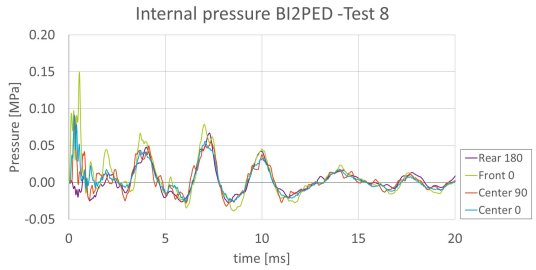

Figure 6.14: Internal pressure BI2PED measured during shock tube test nr8 - with skin

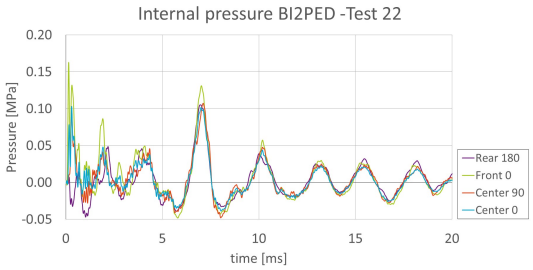

Figure 6.15: Internal pressure BI2PED measured during shock tube test nr22 - without skin

A 1D model that represents a cubical slice from the sphere is used to investigate the wave propagation into the model with skin, Figure 6.16. It is similar to the bar used for the parameter studies in Section 5.2. The internal pressure in the bar, Figure 6.18 and 6.17, shows an added low frequent component in the case with skin, similar to the one in the full sphere. Each material boundary provides a frequency component which depends on the impedance mismatch, that defines which part of the wave is transmitted or reflected. The pressure in the gel is significantly lower than the other pressures in the 1D sphere. It is not explicitly stated in the LSDYNA material model manual provided by LSTC[14], but the material model is probably compressible. This explains the reduction in pressure on the edge of the bar in the skin layer.

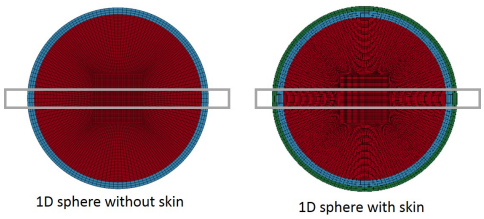

Figure 6.16: Creating a 1D sphere by taking a cubical slice from the spherical model

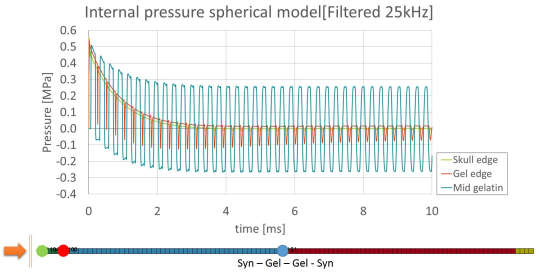

Figure 6.17: Pressure in the 1D sphere without a skin layer (LC:160kPa-4ms)

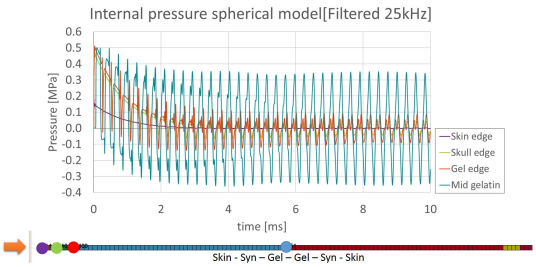

Figure 6.18: Pressure in the 1D sphere with a skin layer (LC:160kPa-4ms)

Influence skin on BI2PED-FE

An investigation into the influence of the skin on the head model response is done to estimate the reliability of the BI2PED-FE response including skin. Large negative pressures are seen in the case with skin compared to the case without skin, see Figure 6.19 and 6.20. The skin also results in an unexpected increase in head motion of the BI2PED-FE, see Figure 6.8. The investigation above shows that no unexpected material behaviour is present in the sphere model and it's 1D representation. No unrealistic motions are seen in the sphere model. Negligible differences in displacement of the head are seen in the BI2PED shock tube tests. Additionally, the unrealistic motions are not seen in the ALE model. Therefore it is concluded that the results of the BI2PED-FE response - with skin and loaded using Load Blast Enhanced are unrealistic and the problem is BI2PED-FE specific. The pressures seen in Figure 6.19 for the BI2PED-FE are therefore likely also unrealistic.

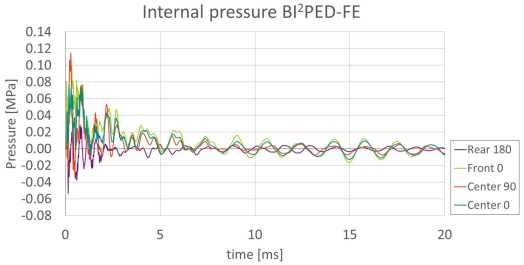

Figure 6.19: Internal pressure BI2PED-FE without a skin layer (LC:130kPa-15ms)

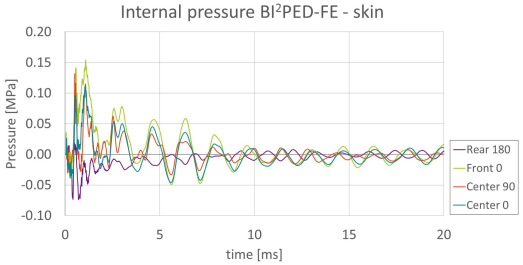

Figure 6.20: Internal pressure BI2PED-FE with a skin layer (LC:130kPa-15ms)

6.3. The addition of neck constraints

During the experiments the BI2PED-FE head model was attached to a Hybrid III dummy neck, whereas in the numerical model no neck constraint is present. The neck could have an influence on the results in multiple ways. There is an additional area with which the airflow interacts. The blast could be reflected by the neck causing an additional load at the bottom of the head. The neck adds mass to the total system influencing inertia. The constraint prohibits free movement of the model, influencing the deformation shape of the model. Additionally the kinetic energy of the prohibited movement dissipates internally. One hypothesis is that the back and forth motion of the head-neck system could be the cause of the periodicity of the internal pressure signals. The addition of the neck constraint is investigated in this Section by reviewing literature, simulations of the spherical model and simulations of the BI2PED-FE.

Literature review

In literature several studies can be found that cover the influence of the neck on the blast response. The human head-neck computational model of Roberts[26], like the BI2PED, also consists of a skull, skin, brain and HybridIII neck and it has been validated with shock tube tests. Moreover, the influence of neck kinematics have been studied numerically in a seperate study[27], by comparing the

H3N(HybridIII) with a detailed high fidelic parametric probabilistic human FEM neck, HHFEM. The simulated blast overpressures (BOP) were 517, 690 and 862kPa. It is concluded in the study that the first 5ms are not influenced by the presence of the neck, since the time necessary to transmit the stress waves have not coupled the neck to the head within this interval. It states that "the high-pressure dynamic waves that account for peak pressures have dissipated before the neck moves significantly". Moreover, according to the writers, the peak intra-cranial pressure (ICP) is not influenced at all. It is mentioned that the peak shear stress is in fact influenced by the attachment of the neck, however this event occurs later in time, as of 20ms, since the shear is coupled to the rotational motion of the head. The study concludes that the type of neck influences the strains in the brain but not the pressures. However, a difference in ICP between the two necks is seen at 0,5ms after the initial peak. The author thinks this is likely due to difference in attachments between head and neck.
Salimi has also studied the influence of the neck boundary conditions, by comparing a free, completely fixed neck and a neck attached to a body[28]. It is a detailed numerical model including also dura and pia mater, CSF, falx and tentorium and helmet and padding system, with a simulated BOP of $\pm$430kPa. This study concludes that the neck boundary condition has no influence on the ICP, even after 5ms. The boundary conditions influence the shear stress and strain most in case of a back blast. If the neck is completely fixed, a second peak in shear stress is observed around 28ms.

Sphere model with neck constraint

The maximum influence the neck constraint can have on the sphere internal pressure distribution is identified by comparing a free floating sphere with a fully fixed sphere, representing an infinitely stiff neck. The 3D spherical model is used, because if a neck is attached to the 2D axi symmetric model the sphere can not be loaded face on due to the symmetry in the model.
Looking at the internal pressures of the clamped sphere, an additional low frequent component is seen, see Figure 6.21. The origin of is likely the back and forth movement of the head model. The Fast Fourier Transform of the pressure signal shows an additional peak at 60Hz in case the model is fixed. This frequency is equal to the frequency of the back and forth mode of the fixed sphere, obtained by a Modal Analysis. The maxima and minima of the red and blue striped trend lines represent the maximum deformation before the head reverses direction. The green trend line reaches its maximum when the head passes its neutral central configuration.
Comparing the pressure in the back of the sphere in the peak and transition phase for the fixed and free sphere, the difference is minimal, see Figure 6.22. The difference is negligible at the other output locations in the sphere.
Because the clamp is representative of an infinitely stiff neck, it is expected that a less stiff HIII neck has a bigger excitation and longer period. Therefore it is concluded that the time scale of neck movement is large enough that the influence on the sphere response occurs outside of the peak and transition phase, where the largest internal pressures occur. This conclusion agrees with the findings in literature presented above.

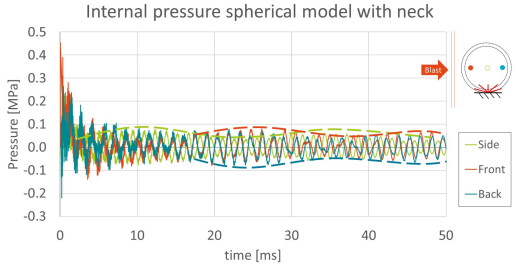

Figure 6.21: Additional low frequent component in the response of the fixed 3D sphere

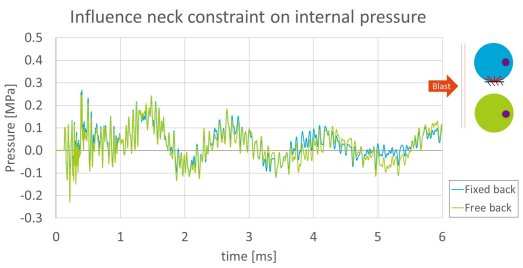

Figure 6.22: Comparing pressure in the back of the 3D sphere model: fixed vs free floating

BI2PED-FE including neck constraints

The main question is whether the physical BI2PED head response is influenced by the presence of a flexible neck. The DRDC BI2PED-FE head model is extended with an existing Hybrid III neck from a LSTC Hybrid III dummy[1] and the response of the total head-neck model is evaluated. The neck of the open source HIII dummy model is isolated and rotated to fit the the BI2PED-FE head model. The proper working of the head-neck model in the existing ALE simulation model (ALE = Arbitrary Lagrangian Eulerian) is verified upon request of DRDC. The results of a test simulation are included in Appendix C. A detailed report of the coupling of the head-neck is found in [37]. Figure 6.23 shows a cross section of the dummy neck attached to the BI2PED.

Because of the unrealistic displacements that are seen when the skin is present, a test simulation of the head neck coupling is shown in Figure 6.24 of the BI2PED-FE without skin, attached to the Hybrid III dummy neck. It is a simulation with a duration of two seconds (2s) with the load case Pi 130kPa tpos 15ms using Load Blast Enhanced as described in Section 3.2.2.

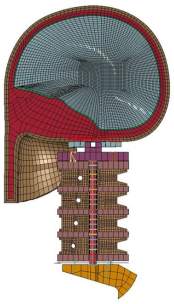

Figure 6.23: Cross section of the LSTC HIII neck attached to the DRDC BI2PED

Figure 6.24: Test case: the LSTC HIII neck with DRDC BI2PED without a skin layer and CSF

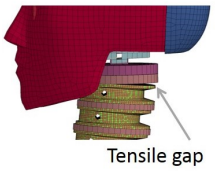

Figure 6.25: Tensile gap in the original LSTC HIII dummy neck due to a lack of a tensile contact definition

Analysis of the HIII-FE neck motion

The frequency of the neck motion is around 3Hz, whilst the frequency content of the pressure in the brain is around 500-2500Hz. That means that the frequency of the neck motion is 2 orders lower than the frequency of the internal pressure response of the BI2PED-FE model. This corresponds to the previous findings with the fixed sphere model. It is concluded that the neck motion is not the origin of the dominant frequency present in the pressure response.

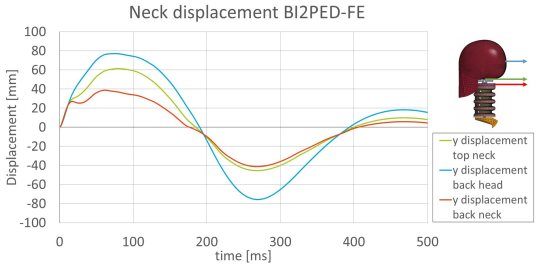

Figure 6.26: Displacement of the BI2PED-FE without skin and CSF attached to the HIII neck, large timescale (LC:130kPa-15ms)

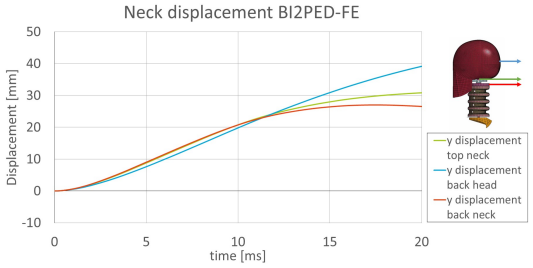

Figure 6.27: Displacement of the BI2PED-FE without skin and CSF attached to the HIII neck, small timescale (LC:130kPa-15ms)

Remark on the test simulation result:

The LSTC HIII dummy neck is less stiff compared to the HIII neck attached to the BI2PED during the shocktube tests. In Figure 6.26 it is seen that the maximum displacement of the head is 80mm. The displacement of the head of the physical BI2PED was determined using the visually recorded displacement of a random visual pattern stuck to the side of the BI2PED head. This data was processed using the Aramis software. Figure 6.28 shows that the displacement of the side of the BI2PED head has a maximum of 30mm. The difference could be caused by the lack of tensile contact between the rubber and the disks in the original numerical dummy neck, Figure 6.25. Adding tensile contact is expected

to increase the stiffness of the neck. However, the effect of the above-mentioned is not expected to change the order of magnitude of the neck motion frequency. The frequency of the neck motion in the experiment is around 5Hz, compared to 3Hz in the simulation. Using the comparison with a simple mass-spring system, shown in Figure 6.29, the difference in neck stiffness can be estimated. In order to obtain an equal neck motion frequency, the numerical neck should be 2-3 times more stiff. In this case the order of magnitude of the neck motion remains two orders lower than the dominant frequency of the internal pressure.

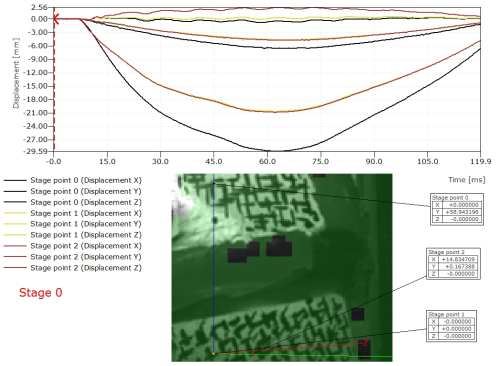

Figure 6.28: Displacement of the BI2PED head measured during shock tube test nr22 - without skin

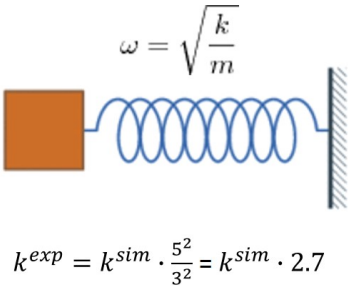

Figure 6.29: Estimation of the necessary increase in numerical neck stiffness

Influence neck constraint on BI2PED-FE internal pressure

The influence of the neck constraint on the internal pressures in the peak and transition phase is determined by comparing three cases of the BI2PED-FE without skin and CSF: unconstrained, attached to a HIII neck and fully fixed. The fully clamped neck base is representative of an infinitely stiff neck. This way the upper bound of the neck influence is determined.

Figures 6.30 - 6.32 show the internal pressures at the sensor locations for the BI2PED under the shock tube blast load case. The case where the model is attached to the HIII neck shows an additional high frequent component in the internal pressure around t=10ms. The displacements shown in Figure 6.27 show that around that time a rotation of the head with respect to the neck is introduced.

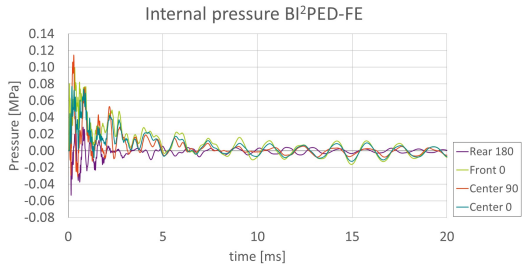

Figure 6.30: Internal pressure of the BI2PED-FE without skin and CSF, without neck constraint (LC:130kPa-15ms)

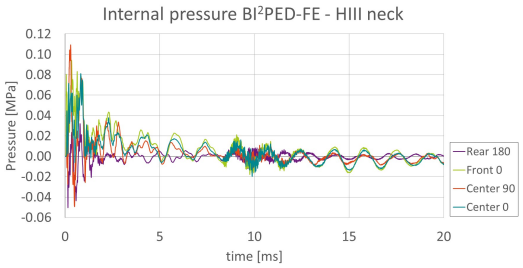

Figure 6.31: Internal pressure of the BI2PED-FE without skin and CSF, constrained by HIII neck (LC:130kPa-15ms)

The pressure at the frontal sensor location is plotted for the three cases in Figure 6.33. From the four sensor locations this is the location where the results are most pronounced. There is a significant difference between the clamped case versus the free and HIII attached case. This is unlike the results of the fixed sphere, where the effect on the internal pressure was minimal compared to the free case. Unlike the sphere, the BI2PED is not symmetric. The impact of the blast on the jaw area results in a rotation of the unconstrained BI2PED-FE. This motion is resisted where the model is fixed which results in a different pressure distribution. The inertia of the head is reflected by the constraint and adds to the internal pressure moving through the brain. This effect is more pronounced because the BI2PED brain is unsymmetrical. The HIII neck does to some extent allow rotation and motion of the head. The effect of the neck constraint on the internal pressure is negligible unless the neck is extremely stiff, which is unrealistic. Therefore it is concluded that the neck does not need to be included in the simulations.

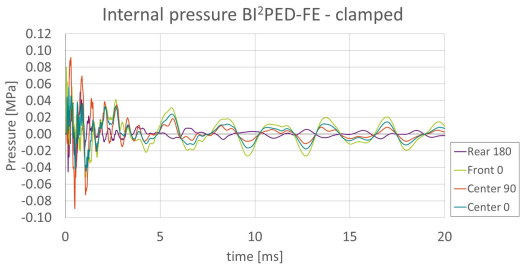

Figure 6.32: Internal pressure of the BI2PED-FE without skin and CSF, fixed at the connection with the HIII neck (LC:130kPa-15ms)

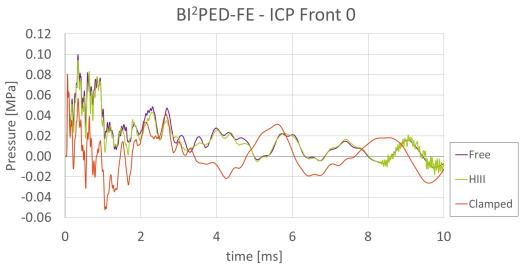

Figure 6.33: Internal Pressure of BI2PED-FE without skin and CSF at ICP Front 0: unconstrained, constrained by HIII neck, fully fixed (LC:130kPa-15ms)

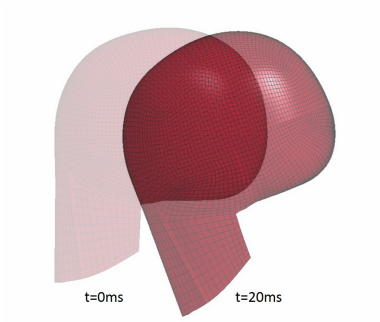

Figure 6.34: Displacement of the unconstrained BI2PED-FE (LC:130kPa-15ms)

6.4. The brain-skull interface

In a human the brain floats in a water like substance, the Cerebral Spinal Fluid. In the BI2PED model, the brain floats in water, although the enclosed volume is not fully filled with water. In the top region an air bubble is present. In the BI2PED-FE model, the interface is modelled as a fluid solid interface layer. The interface of the BI2PED-FE has a significant influence on the brain internal pressures (Intra Cranial Pressures - ICP), as is shown in Section 6.1. In this Section, various ways to model the interface are investigated and their influence on the head response presented in order to be able to assess the reliability of the BI2PED-FE simulation results including CSF. It includes a short overview of results found in Literature and a comparison of different interface types applied to the spherical model. It concludes with a short discussion of the interface layer contained in the BI2PED-FE.

Literature review

In literature mainly three types of methods to model fluid between the skull and brain are found, of decreasing computational complexity:
- An ALE approach where the fluid consists of Eulerian elements
- A friction based contact model
- A soft solid element layer
Chafi has studied the effects of CSF during sudden impact loads[5]. Note that these impact loads are modelled as sudden linear and angular accelerations applied to the skull. Three options for a soft solid element layer were studied, visco-elastic, elastic with fluid like properties and nearly incompressible elastic with a low shear and high bulk modulus. The best fit with the findings from experiments was found to be the fluid like elastic case, where there was little difference between sliding or tied contact interface. The study concludes that effect of CSF properties like bulk modulus on the pressure response is limited, but can be significant in the shear strains. It also significantly influences the brain local relative motion.
A study by Gu includes the influence of meninges on the response to blast load[11]. It compares numerical models of the head without layers between skull and brain, with only CSF in between and with the full layers of CSF and pia mater and dura mater. In this case the CSF is build out of Eularian

elements. It shows that both the case with no meninges and the case with only CSF have very similar results. The peak ICP is almost equal and the pressure response is very similar later on. In case of the full model both the peak and pressure later on are reduced. In the shear stress, a difference can be seen between all models. Adding CSF reduces the peak shear and delays its occurrence. Adding the meninges enlarges this effect.
Zhang finds that a Lagrangian description is more suitable for modelling the CSF than an ALE approach, because the latter underestimated the load transferred from the skull to CSF[36]. The report states that a Lagrangian description is valid in case the deformation of the CSF is small.
The studies indicate that the peak ICP is not notably influenced by the fluid and the influence on the pressure after the peak is limited.

Comparison of interfaces for the spherical model
The skull-brain interface in the BI2PED-FE is either fully attached or with a Lagrangian solid element layer. To study the influence of the interface type on the load transfer between the skull and brain the simplified 2D axi symmetrical model is used with the following three different interfaces:
- Fully attached = Reference case
- Interspersed solid fluid layer
- Penalty based contact

In the fully attached case the two parts share nodes, therefore both compressive and tensile forces are transferred. The penalty based contact algorithm only transfers compressive loads by creating an artificial contact stiffness where the parts are prohibited from intruding on each other. This means that a gap can develop in regions where tensile forces would be present otherwise. In the last option fluid is modelled as a solid element layer that is fully attached to both parts.

Fluid layer
The internal sphere pressures in the back of the model are presented in Figure 6.35 and 6.36 for the reference sphere and the model with a fluid layer. The solid fluid layer is modelled using the LSDYNA ELASTIC FLUID material model, based on the Bulk modulus. The results are similar to the the case where the interface is fully attached. Although the high frequent signal has a larger amplitude, which is damped over time.

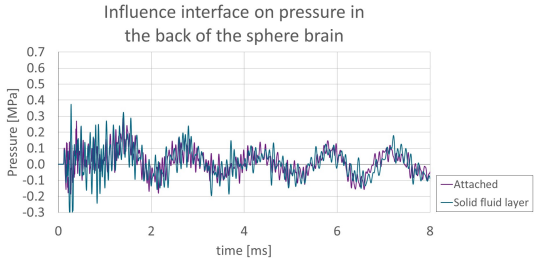

Figure 6.35: Internal pressure in the back of the 2D spherical model brain with a fully attached interface and a solid fluid layer interface (LC:160kPa-4ms)

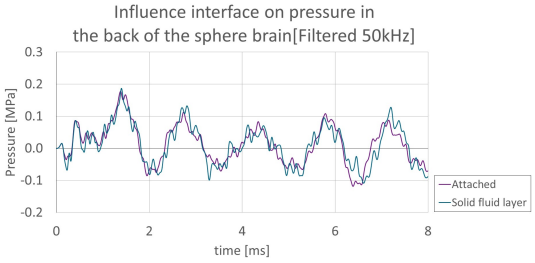

Figure 6.36: Internal pressure in the back of the 2D spherical model brain with a fully attached interface and a solid fluid layer interface [BW filter C=50kHz] (LC:160kPa-4ms)

Penalty contact
Figures 6.37 and 6.38 are plots of the pressure at the back of the sphere for the reference case and the model with penalty contact between the skull and brain. High frequent large peaks are seen in the penalty based case. Closer investigation shows that there are multiple impacts at the rear of the skull against brain, and similar smaller impacts at the front.

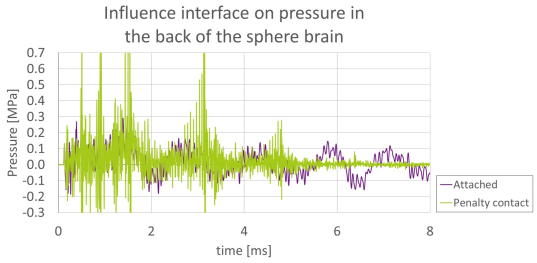

Figure 6.37: Internal pressure in the back of the 2D spherical model brain with a fully attached interface and a penalty contact based interface (LC:160kPa-4ms)

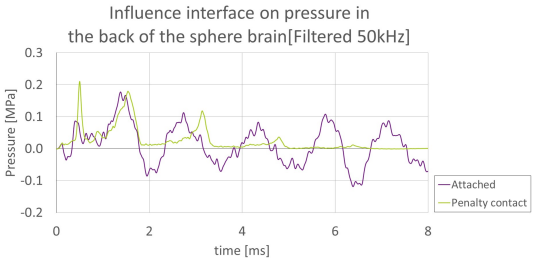

Figure 6.38: Internal pressure in the back of the 2D spherical model brain with a fully attached interface and a penalty contact based interface BW filter C=50kHz (LC:160kPa-4ms)

Localised impact of the skull to the brain

Figure 6.39 shows the impact of the skull against the brain at the back of the head and the resulting high amplitude pressure wave for the sphere with a penalty contact interface. Because the skull is not attached to the brain, the localised bending in the skull (explained in Section 5.1) is more prominent. The skull introduces pressure waves into the brain each time the skull impacts the brain locally. If the pressure signal is filtered, the impacts are no longer visible. If the results are filtered no negative pressures remain. This is not unexpected because there are no tensile forces transferred by the skull-brain interface. Then the pulsating deformation of the skull does not stretch the brain.

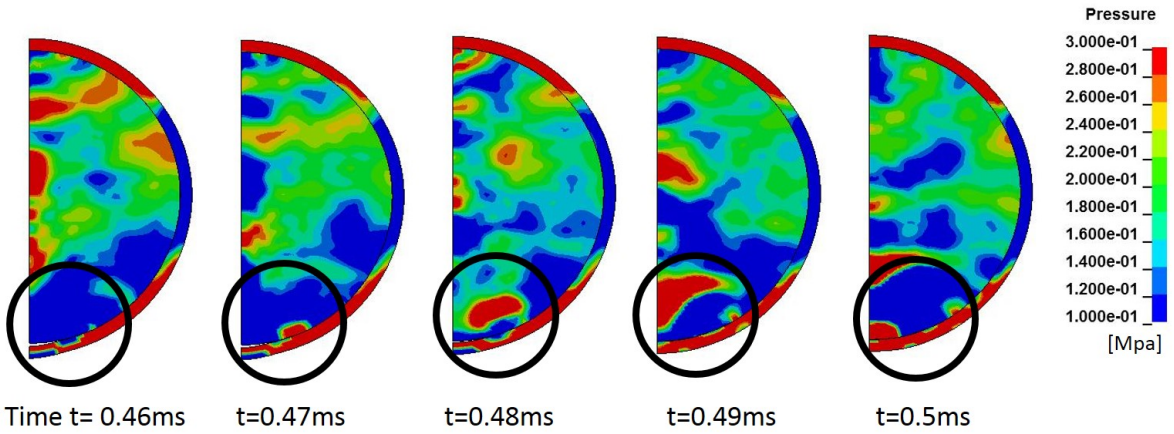

Figure 6.39: In case of penalty contact for the 2D sphere model, impact of the skull against the brain introduces high amplitude pressure waves in the brain (LC:160kPa-4ms)

Combination of penalty contact and neck constraint

In order to assess the maximum influence of the penalty based contact, the penalty based contact is combined with a fully fixed neck constraint using the 3D sphere model. The internal pressures are compared for the free floating and fixed cases, with fully attached and penalty based interfaces.

From the pressures presented in Figure 6.40 it is seen that no low frequent negative pressures are present in the gel, similar to the 2D case described above, in the case of penalty based contact. This is explained by the lack of tensile forces that can not be transmitted by the interface. It is also seen that when there is no neck constraint the vibration is quickly dampened, after which the model continuous to move as a rigid body.

It can be observed that the first positive pressure peaks are larger at the back of the head, in case of penalty contact with a neck constraint, Figure 6.41. The skull bending stiffness resists deformation of the highly deformable gel if they are attached. When there is no attachment of the gel to the much stiffer skull, the inertia of the gel builds up additional pressure when the displacement at the back is prohibited by the neck constraint. Large deformations of the gel are expected in case the gel is not nearly incompressible and constrained within an enclosed volume. In a simulation where the Poisson's ratio is modified, these large deformations in the gel are confirmed.

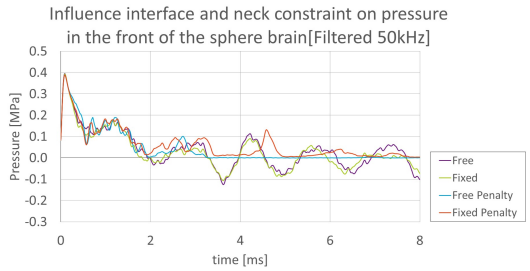

Figure 6.40: Internal pressure in the front of the 3D spherical model brain for varying neck constraint and interface type [BW filter C=50kHz] (LC:160kPa-4ms)

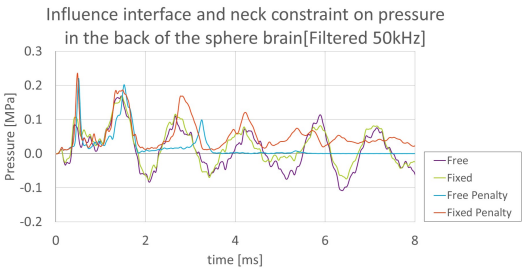

Figure 6.41: Internal pressure in the back of the 3D spherical model brain for varying neck constraint and interface type [BW filter C=50kHz] (LC:160kPa-4ms)

BI2PED-FE interface study

In the BI2PED-FE model an option to include CSF is available. A fully attached solid element layer is present between the brain and skull, sharing nodes. For this layer an equation of state is defined. Comparing the internal pressure in the BI2PED-FE without CSF, Figure 6.42, and with CSF, Figure 6.43 it is seen that both the frequency and amplitude of the internal pressures is influenced. Based on the findings from literature and the study of the fluid layer using the spherical model, this is unexpected. Likely the specific manner in which the interface is modelled using an Equation of state causes this effect. Both the BI2PED-FE with and without skin show a different internal pressure distribution than the one observed in the physical BI2PED shock tube test results. Additionally using an approach where the brain is attached to the skull has the consequence that if during the experiments internal impact occurs at the rear of the head, this is not captured by the BI2PED numerical model. Effects like cavitation [16] are also not included. It is concluded that the modelling of the interface in the BI2PED-FE is not sufficient.

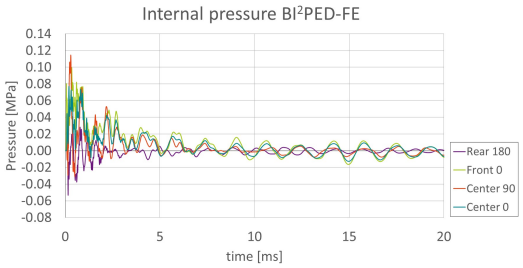

Figure 6.42: Internal pressure of the BI2PED-FE without skin and CSF (LC:130kPa-15ms)

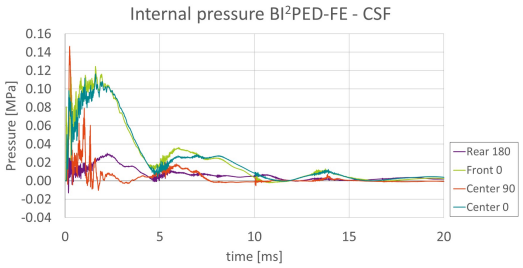

Figure 6.43: Internal pressure of the BI2PED-FE without skin and with CSF layer (LC:130kPa-15ms)

7

Numerical Analysis Regarding the Head Vibration and Modal Deformation

In this chapter the head vibration is linked to skull deformation based on the model Eigen modes. Section 7.1 contains a description of the method used and the method is applied to the spherical head model as a proof of principle in Section 7.2. It is applied to the more complex BI2PED-FE model in Section 7.3. A sensitivity study of the developed method is contained in Section 7.4. The modal deformation of the BI2PED-FE is compared with the modal deformation observed in the BI2PED in the shock tube experiments in Section 7.5

A periodic pressure response is seen in the shock tube test measurements and the numerical simulations. In Chapter 4 this is the part of the signal contained in the vibration phase. To better understand the response the origin of the periodic pressure is investigated. One hypothesis is that the back and forth movement of the neck is responsible for the oscillations. Section 6.3 showed that this is not the case. The other hypothesis is that modal deformation is responsible for the characteristic periodic pressure. If the response of the model can be described using modal superposition this creates possibilities for the combined numerical and experimental assessment method described in Section 8.1.2.
The purpose of this chapter is to investigate whether modal deformation is dominant in the head vibration and responsible for the periodic internal pressure. By relating the frequencies contained in frequency spectrum of the blast response to the Eigen frequencies of the model this hypothesis is tested.

7.1. A block pulse impact as an alternative for an implicit modal analysis

The goal is to relate the modal deformation of the skull to the head vibration and oscillating internal pressure. This can not be done directly because a model analysis of the full head model provides only a few low frequent local brain modes and many spurious modes. The origin of this issue probably lies in the fact that the brain has a stiffness ten times lower than the skull and therefore a lower modal vibration. Starting from zero the numerical modal analysis searches for Eigen frequencies and finds an infinite number of higher order local brain Eigen modes. The higher frequent modes involving the skull deformation are never reached using this procedure. An alternative method to find the modes for the skull-brain system is therefore needed. It is however possible to find the Eigenmodes and frequencies using a modal analysis for an empty skull.

The method explained in this section is inspired by hammer impact modal analysis experiments [2]. It uses the non-problematic modal analysis of the empty skull to calibrate a block pulse load (hammer impact) that excites the skull in Eigen modes that can be recognized in the blast response. This calibrated load can then be used to analyse the full skull-brain model. The basis of this method is a Fast Fourier Transform (FFT) of the time response that provides the frequency content that can be compared

with Eigen frequencies. The Fourier analysis transforms the displacement or pressure signal from the time domain into the frequency domain. Next the two steps of the block pulse method - calibration and analysis - are explained.

Figure 7.1 is a graphic representation of the first step; calibrating the block pulse load using the empty skull.
(a) Determine the frequency content of the time response of the empty skull to blast using a FFT
(b) Find the corresponding Eigen modes with a modal analysis by comparing the Eigen frequencies to the frequency content of the blast response
(c) Determine a block pulse load that returns vibrations of the model in these Eigen modes using an FFT of the block pulse time response

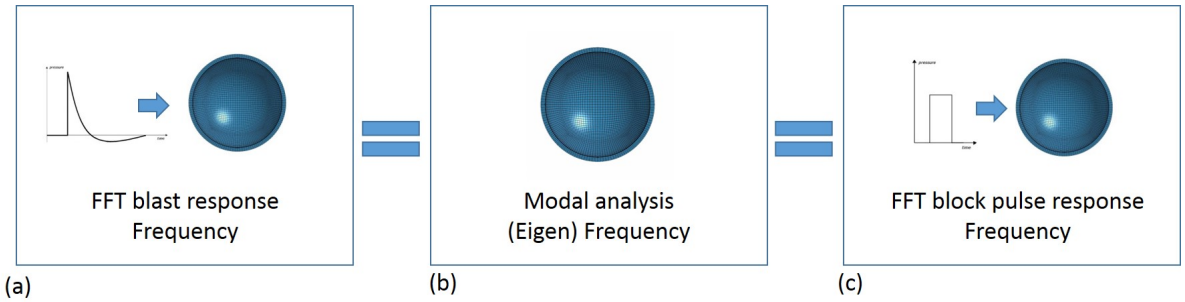

Figure 7.1: Calibration of the block pulse load using a modal analysis and the frequency content of the blast response of the empty skull

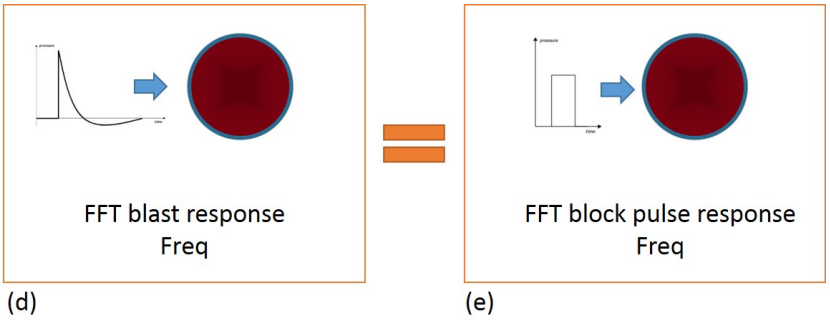

Figure 7.2: The calibrated block pulse load as an alternative for the brain-skull modal analysis

Figure 7.2 is a graphic representation of the second step; Analysing the skull-brain model with the calibrated block pulse.
(d) Determine the frequency content of the time response of the skull-brain model to blast using a FFT
(e) Apply the calibrated block pulse to the spherical skull-brain model

By comparing the frequency content of the block pulse induced modal response with the frequency content of the blast response modal deformation can be recognized in the blast response. An alternative for a modal analysis of the brain-skull system is provided. This alternative method is applicable to the skull-brain structure specifically because the skull deformation is dominant in the vibration. Therefore, after the link between the skull vibration, skull Eigen mode and block pulse response modes is established, the filled skull can be analysed. It is expected that this method is only applicable to such structures where the deformation of the stiffer dominant part is imposed on the more flexible part.
The spherical model is used to provide a proof of principle for the approach in Section 7.2. A displacement signal is used to relate the deformation due to blast to modal deformation. Then the relation between modal deformation and internal pressures is tested. Finally, an identical approach is applied to the more complex BI2PED-FE model in Section 7.3. The influence of the pulse duration and amplitude and output location is checked in a sensitivity analysis in Section 7.4.

For the blast load on the sphere the reference blast load case is used: LC:160kPa-4ms. The block pulse has an amplitude of 518kPa. The amplitude is based on the peak reflected pressure applied to the spherical model in case of the reference blast load. The frequency content of a pulse depends on the length and amplitude of the pulse. A dirac delta function with infinite amplitude contains the full frequency spectrum. As a first estimate, the pulse peak is chosen at least as high as blast load peak pressure, in order to provide a similar frequency content. The duration of the pulse is 0.1ms, because the blast signal quickly decays after the initial peak. The block pulse load cases are referred to as P:amplitude-duration. For the reference block pulse case this is P:518kPa-0.1ms.

7.2. Proof of principle with the 3D spherical model

The above described approach is first applied to the simplified spherical head model. First the deformation of the skull during vibration is related to the modal deformation of the sphere. Then the relation between the modal deformation of the skull and the internal pressures is further investigated.

7.2.1. Empty spherical skull

Investigation of the spherical skull response shows a pulsating deformation of the sphere, with maxima and minima at the front-back and sides of the sphere, anti-phase. Therefore the node on the side of the sphere is taken to inspect the frequency content. An off-center displacement output location is tested in the sensitivity analysis in Section 7.4. Figure 7.3 shows the frequency spectrum of the empty skull under the reference blast load. Three distinct peaks are identified in the spectrum. The modal analysis of the empty skull is checked for corresponding frequencies. The deformation seen in the modes with matching frequencies can be recognized in the response of the skull to blast. The three modes from the modal analysis are depicted in Figure 7.4. The first two modes with frequencies 1.74kHz and 2.44kHz can be excited by a localised block pulse depicted in Figure 7.6. The third mode with frequency 4.87kHz is excited by the uniform block pulse presented in Figure 7.7. This shows that the block pulse load is able to excite the model in the Eigen modes needed.

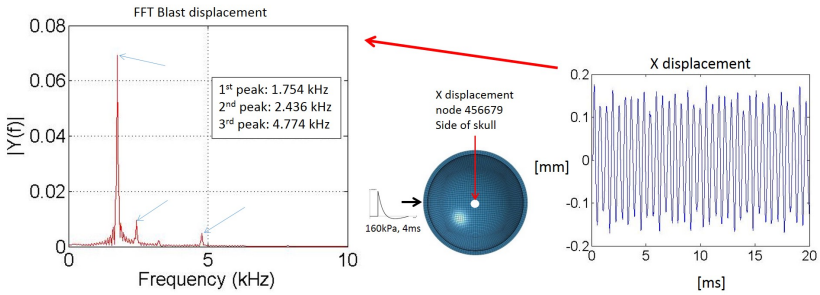

Figure 7.3: Single sided frequency spectrum of the sideways displacement X of the skull exterior (LC:160kPa-4ms)

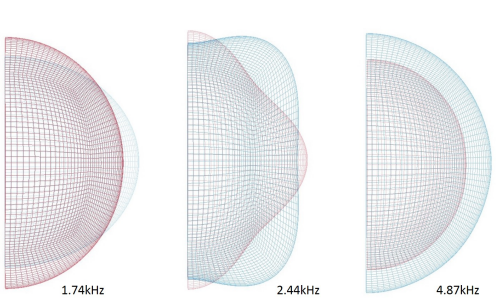

Figure 7.4: Skull Eigen Modes with frequencies matching the three frequencies in the blast response spectrum, left to right freq=7.74kHz, 2.44kHz and 4.78kHz

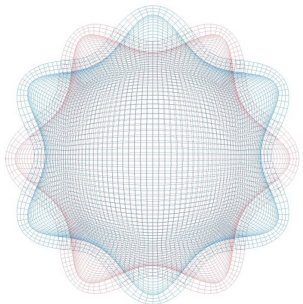

Figure 7.5: Additional skull Eigen mode type excited by the localised block pulse load, shown 2.495Hz

In the spectrum of the localised block pulse, Figure 7.6, additional peaks are seen with frequencies not present in the blast response spectrum. These frequencies correspond to multiple modes of the type shown in Figure 7.5, with an increasing amount of maxima-minima for higher frequencies. This can be explained by the fact that the block pulse is applied locally, whereas the blast load is applied along the entire exterior. It is likely that the localised nature of the block pulse is responsible for the bending of the skull edge. These additional peaks can therefore be disregarded from the results for both the empty skull and the skull filled with gelatin in Section 7.2.2.
The analysis is continued with only the localised block pulse, since the contribution of the third mode excited by the uniform block pulse is small. In the case where the skull is filled with brain matter it is expected that this uniform compression and expansion is negligible, because of the near incompressibility of the brain material.

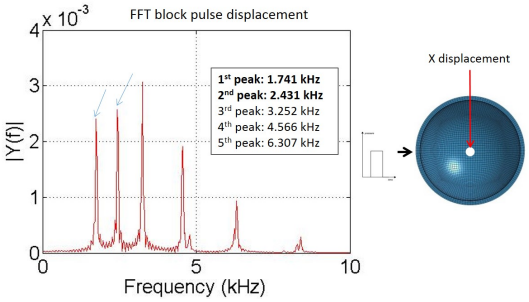

Figure 7.6: Single sided frequency spectrum of the sideways displacement X of the skull exterior due to a localised block pulse (P:518kPa-0.1ms)

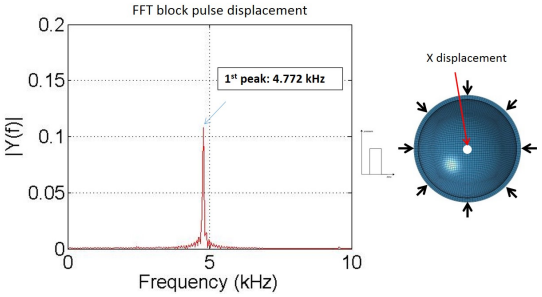

Figure 7.7: Single sided frequency spectrum of the sideways displacement X of the skull exterior due to a uniform block pulse (P:518kPa-0.1ms)

7.2.2. Gelatin-filled spherical skull

The localised block pulse is now applied to the full skull-brain spherical head model. First the displacements of the skull exterior are related to the modal deformation, then the internal pressures.

Sideways displacement skull exterior

The frequency spectrum of the sideways displacement of the skull exterior is determined under both the blast load and the localised block pulse which was determined in the previous section. Inspection of Figures 7.8 and 7.9 shows that the two main peaks found in the blast response spectrum are also represented in the spectrum of the block pulse. The additional peaks seen in the block pulse spectrum can be disregarded as previously explained. It can be concluded that the deformation of the skull of the full skull-brain spherical model under blast loading is related to its Eigen modes.

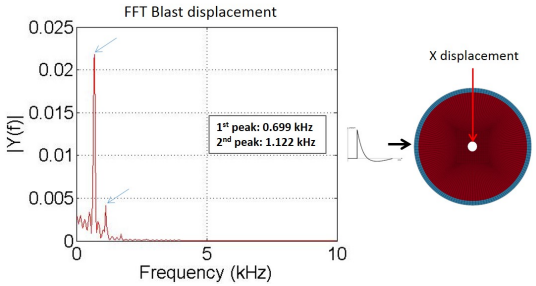

Figure 7.8: Single sided frequency spectrum of the sideways displacement X of the filled skull exterior under blast loading (LC:160kPa-4ms)

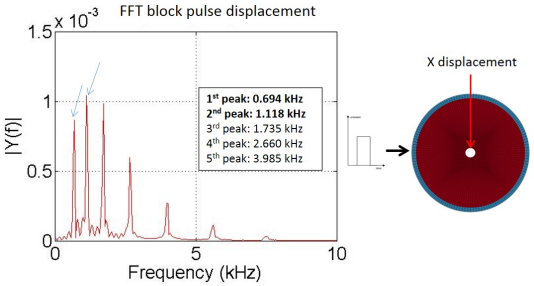

Figure 7.9: Single sided frequency spectrum of the sideways displacement X of the filled skull exterior under localised block pulse (P:518kPa-0.1ms)

Internal pressure

Next the internal pressures are related to the modal deformation of the skull. Figures 7.10 and 7.11 show the single sided frequency spectrum (SSFS) of the sphere internal pressures at respectively the middle and back of the sphere. Comparing them with the frequency content of the displacement in 7.12, additional higher frequency peaks are observed in the pressure spectrum. Additionally, the frequency spectra of the internal pressures differ between locations. The additional peaks are further investigated in the sensitivity study in Section 7.4. The spectra of the different locations are next compared.

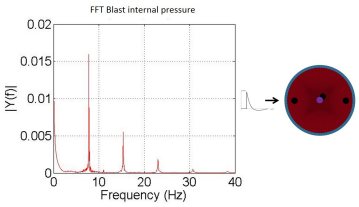

Figure 7.10: SSFS of the pressure in the middle of the sphere under blast (LC:160kPa-4ms)

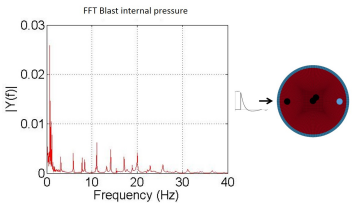

Figure 7.11: SSFS of the pressure at the back of the sphere under blast (LC:160kPa-4ms)

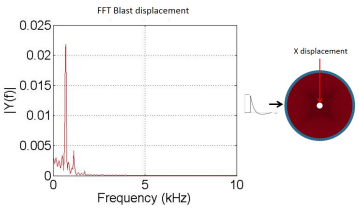

Figure 7.12: SSFS of the side displacemen under blast (LC:160kPa-4ms)

Figures 7.13 - 7.16 show the lower frequent part of the SSFS of the sphere internal pressures. The spectra of the front and back locations share the maximum frequency, which is similar to the maximum in the spectrum of the side of the sphere. The maximum frequency in the middle of the sphere is one order higher. The bold face frequencies are also present in the spectrum of the skull displacement. The italic face frequencies are shared between pressure output locations. It is concluded that the internal pressure is related to the modal deformation. However, additional effects are seen in the internal pressures that might not be accounted for if one only considers the external skull deformation. This has consequences for the strain based indirect measurement method in Section 8.1. Most peaks are shared between some locations, but differ in amplitude. This suggests that not all modes contribute equally to the pressure per location. The middle of the sphere is a special case, as the center is compressed by the relative skull contraction in all directions.

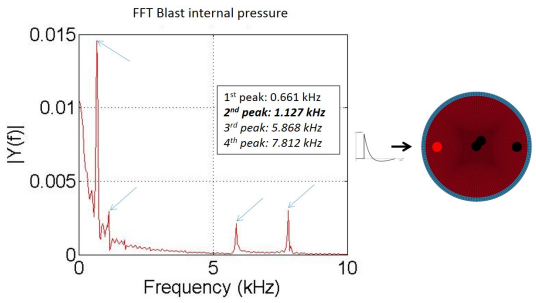

Figure 7.13: SSFS of the pressure in the front of the sphere under blast loading (LC:160kPa-4ms)

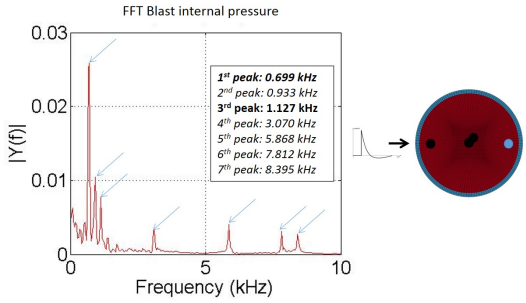

Figure 7.14: SSFS of the pressure at the back of the sphere under blast loading (LC:160kPa-4ms)

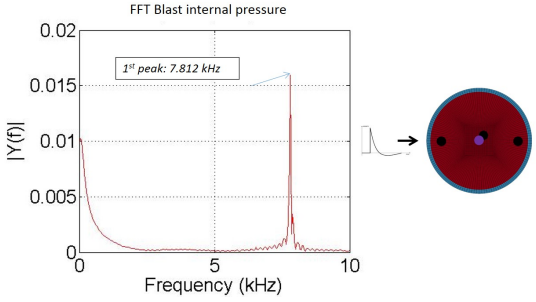

Figure 7.15: SSFS of the pressure in the middle of the sphere under blast loading (LC:160kPa-4ms)

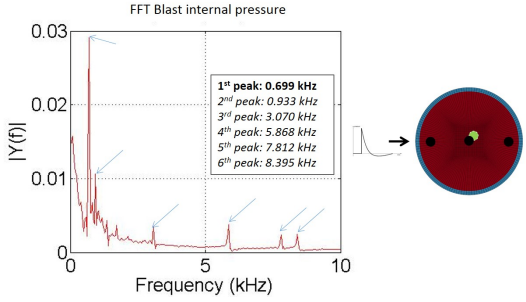

Figure 7.16: SSFS of the pressure at the side of the sphere under blast loading (LC:160kPa-4ms)

7.3. BI2PED-FE vibration analysis results

The same procedure described above for the spherical model is applied to the BI2PED-FE, without skin and without CSF. For brevity, only the results for the full skull-brain BI2PED are presented in this section. Both the displacement analysis and the internal pressure analysis are included. The calibration of the block pulse using the BI2PED-FE empty skull is summarised.

7.3.1. BI2PED-FE skull-brain model

The empty biped skull is used to calibrate the block pulse such that the same modes are excited by the block pulse as by the blast. A block pulse applied at the front of the head does excite the empty skull in modal deformation seen in the modal analysis. However, these are different modes than found in the blast response. A block pulse applied at the top of the BI2PED-FE head excites the model in the modes that are present in the blast response. This block pulse is used to first relate the displacement of the skull exterior of the full skull-brain BI2PED-FE model. Then the relation between the internal pressures and modal deformation is checked. For the BI2PED-FE the load case LC:130kPa-15ms is presented to be able to compare the frequency content of the BI2PED-FE with the frequency content of the BI2PED response during the shock tube tests in Section 7.5. The load case LC:160kPa-4ms returned a similar frequency spectrum, as the positive phase duration does not alter the vibration modes excited.

Sideways displacement skull exterior

Figures 7.17 and 7.18 show the single sided frequency spectrum of the BIPED skull filled with brain material under the application of a blast load and a block pulse applied at the top. The two largest peaks have a matching frequency. It can be concluded that under blast loading the skull deforms according to its Eigen modes.

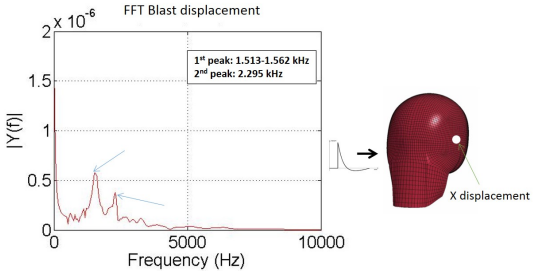

Figure 7.17: Single sided frequency spectrum of the sideways displacement X of the filled skull exterior (LC:130kpa-15ms)

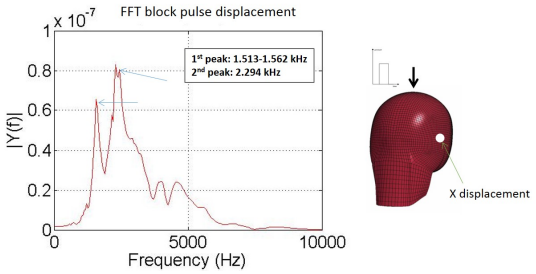

Figure 7.18: Single sided frequency spectrum of the sideways displacement X of the filled skull exterior under localised block pulse (P:518kPa-0.1ms) applied at the top

Internal pressure

Figures 7.20 - 7.22 show the single sided frequency spectrum of the pressure at the internal BI2PED-FE sensor locations. The main frequencies are indicated in the graphs. The bold face frequencies are also found in the displacement spectrum. The italic face frequencies are shared between Intra Cranial Pressure (ICP) sensor locations. More frequencies are shared between the spectra than are labelled in the figure, but these peaks are small in amplitude. Additional frequencies are present in the pressure spectrum compared to displacement spectrum, similar to the results found for the spherical model, and the contribution of frequencies varies per sensor location.

It is concluded that the skull deforms in its Eigen modes during the vibration phase of the response to blast. Not all modes contribute equally to each location in the head and additional frequencies, both higher and lower, are seen in the pressure spectra compared to the skull deformation. This suggests that local effects are present in the brain.

It is hypothesized that the higher frequencies in the pressure spectra belong to higher order modes. The lower frequencies are thought to be related to local brain motion which does not influence the skull deformation. This is further analysed in the next Section, where the sensitivity of the alternative modal analysis method is studied.

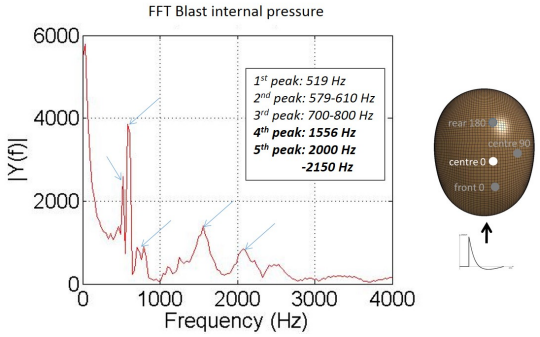

Figure 7.19: Single sided frequency spectrum of pressure at ICP Center 0 (LC:130kpa-15ms). Largest peak frequency = 30.5 and 579Hz

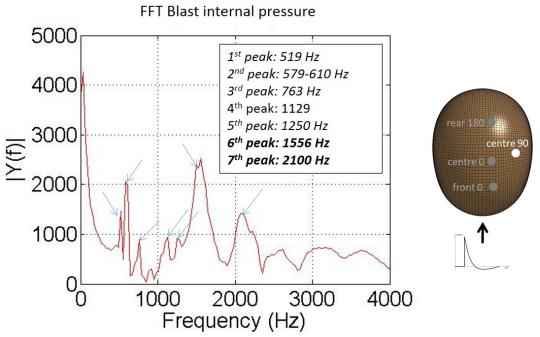

Figure 7.20: Single sided frequency spectrum of pressure at ICP Center 90 (LC:130kpa-15ms). Largest peak frequency = 30.5 and 1556Hz

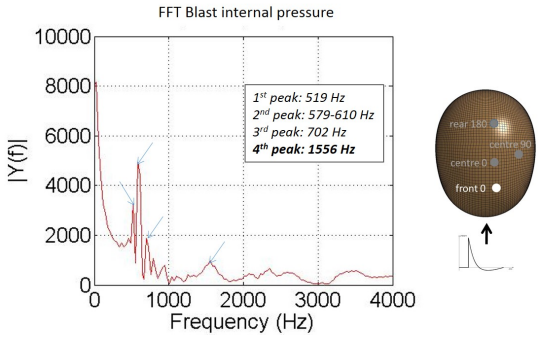

Figure 7.21: Single sided frequency spectrum of pressure at ICP Front 0 (LC:130kpa-15ms). Largest peak frequency = 579Hz

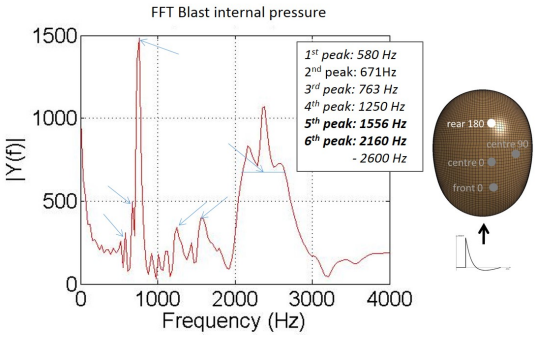

Figure 7.22: Single sided frequency spectrum of pressure at ICP Rear 180 (LC:130kpa-15ms). Largest peak frequency = 763Hz

7.4. Sensitivity of the modal analysis method

The sensitivity of the modal analysis method is studied in this Section. The influence of the displacement output location is investigated. The influence of the block pulse length and amplitude is also studied, along with the influence of the signal length used for the FFT.

Influence of the displacement output location

Additional frequencies are seen in the internal pressure spectra compared to the displacement spectrum in Section 7.2.2. The hypothesis is that higher order modes might be present, but are not distinguishable at the location of the displacement point output as it is located at a deformation maxima. The output spectrum of two different displacement output locations are compared in Figure 7.23 and 7.24. It is seen that an additional peak is present at the location halfway along the sphere skull arc, compared to the one at the side of the skull. This indicates that an additional mode contributes to the displacement of this point. Additionally, small peaks are seen in the higher frequency region. These orange labelled frequencies match with the additional peaks from the internal pressure spectra in Figures 7.13 - 7.16. This indicates that the additional frequencies in the pressure signals are induced by higher order modes. Figures 7.25 and 7.26 show that for the block pulse also additional peaks - modes - are found with a displacement output point halfway along the skull exterior arc. These higher order modes are likely difficult to measure with external strain sensors as their contribution is small.

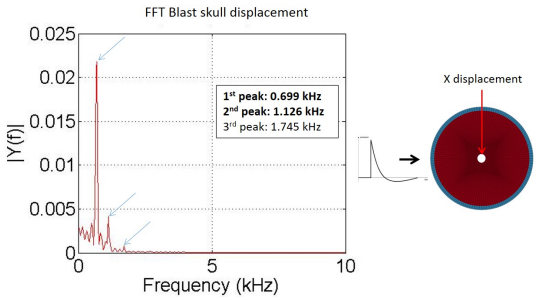

Figure 7.23: Single sided frequency spectrum full sphere model, reference case blast: blast (LC:160kPa-4ms) displacement side skull

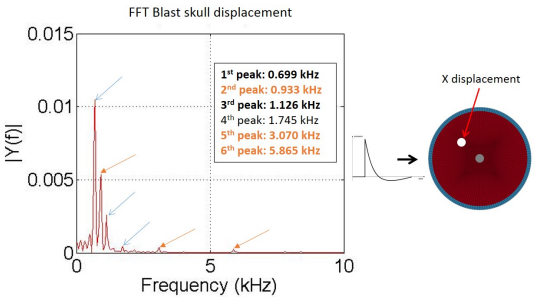

Figure 7.24: Single sided frequency spectrum full sphere model: blast (LC:160kPa-4ms) displacement location mid arc

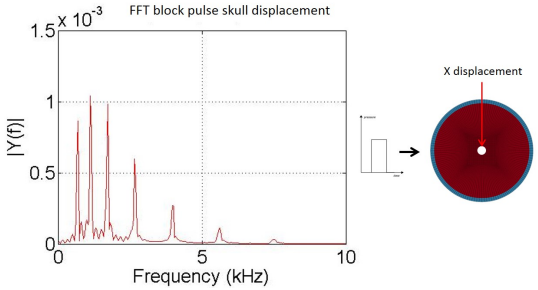

Figure 7.25: Single sided frequency spectrum full sphere model, reference case pulse: pulse (P:518kPa-0.1ms) displacement side skull

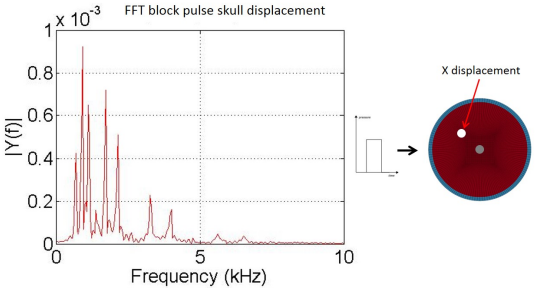

Figure 7.26: Single sided frequency spectrum full sphere model: pulse (P:518kPa-0.1ms) displacement location mid arc

Influence of the block pulse shape

The influence of the block pulse amplitude is checked by applying half and double the amplitude compared to the reference case. It is assumed that both cases should fall within the range of reasonable loads. From Figure 7.27 and E.4 it can be seen that the amplitude of the pulse within this specific range has a negligible influence on the modes found. Therefore it is safe to assume a block pulse in the vibration analysis with the amplitude of the applied pressure due to the blast considered.

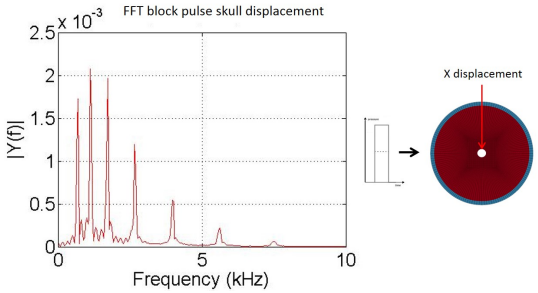

Figure 7.27: Single sided frequency spectrum full sphere model: pulse (P:1036kPa-0.1ms) pulse double amplitude

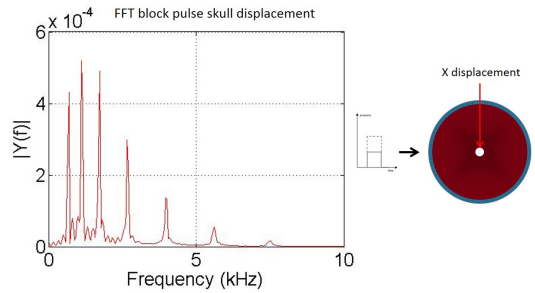

Figure 7.28: Single sided frequency spectrum full sphere model: pulse (P:259kPa-0.1ms) pulse half amplitude

The influence of the block pulse duration is studied by dividing the pulse length of the reference case by a factor ten and by multiplying the pulse length by ten. From the results presented in Figure 7.29 and Figure 7.30 one can conclude that the pulse length is of influence for the modes found. The difference between a pulse load of 0.01ms - Figure 7.29 and 0.1ms Figure 7.23 is minimal. The result of a shorter pulse is that higher order modes are slightly amplified. However, these modes correspond to the mode shapes that are not present in the blast response and are neglected in the analysis. Therefore the block pulse of 0.1ms duration is sufficient.

In case of a relatively long pulse of 1ms, see Figure 7.30, the frequency spectrum is different in shape. It takes 0.14ms for the pulse to travel from impact to the back of the head. The pulse duration of 1ms is therefore too long to measure the response of an unloaded sphere. Therefore it is recommended to use a block pulse with a duration that is shorter than the time needed for the pulse to traverse the model.

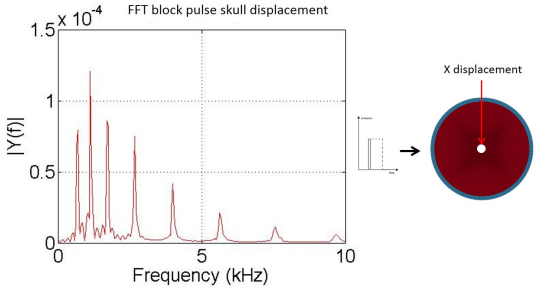

Figure 7.29: Single sided frequency spectrum full sphere model: pulse (P:518kPa-0.01ms)
pulse duration /10

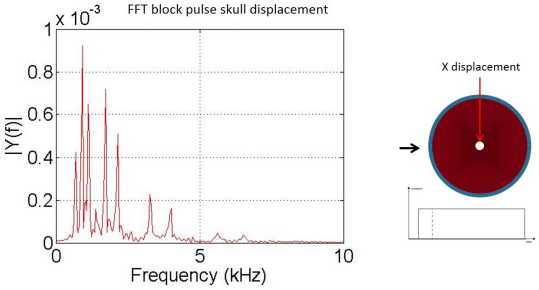

Figure 7.30: Single sided frequency spectrum full sphere model: pulse (P:518kPa-1ms)
pulse duration x10

Influence of the sample size for the Fast Fourier Transform

The response to blast can be divided into three phases. The peak, transition and vibration phase. In the peak phase the mechanism of load transfer by means of a pressure wave and local skull deformation is dominant. In the vibration phase the mechanism of a superposition of Eigen modes is dominant. In order to find the Eigen modes excited by the blast in the vibration phase, a sample with enough cycli is needed. In Figures 7.31-7.33 the frequency spectra of the pressure in the side of the sphere is plotted for different sample sizes.

Figure 7.31 shows the spectrum for the full sample size of 20ms in which all three phases are represented. If the peak and transition phase are excluded from the sample, the result is as in Figure 7.32. The very low frequent peaks are removed and the subsequent peaks are sharper. This low frequent contribution is seen in Figure 7.33 where only the peak and vibration phase are included in the signal. It is concluded that for a longer sample size, the match with modal frequencies increases. The low frequent contribution is likely related to local brain deformation, not measured at the skull exterior.

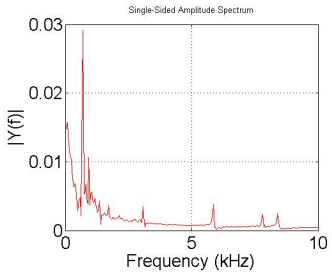

Figure 7.31: Single sided frequency spectrum of the pressure in the side of the full sphere model: FFT sample size 0-20ms

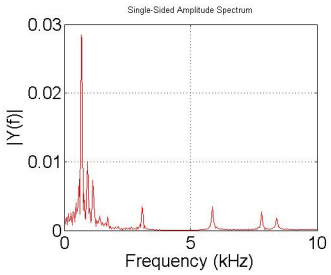

Figure 7.32: Single sided frequency spectrum of the pressure in the side of the full sphere model: FFT sample size 4-20ms

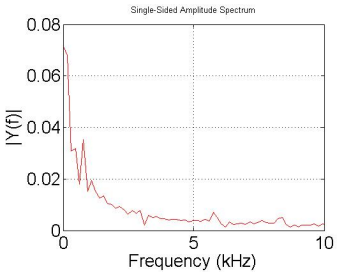

Figure 7.33: Single sided frequency spectrum of the pressure in the side of the full sphere model: FFT sample size 0-4ms

7.5. Modal deformation in the BI2PED vs the BI2PED-FE

In this section the frequency content of the BI2PED response is compared to the BI2PED-FE. The external skull strains were recorded for the face on shock tube tests of the BI2PED without skin on the front and side of the BI2PED head model.[24] The results of test 22, the 21 gram test with incident pressure 160kPa and positive phases 17ms are included in this section. See Appendix A for an overview of the shock tube test matrix. The external sensor locations of the BI2PED can be seen in Figure 7.34. Note that for the Fast Fourier Transform of the sensor signals the complete length of the measurements of the experiments are used; this is around 100ms. For the simulations a signal length of 20ms is used. The expected result is, as argued in the sensitivity study above, that the contribution of the peak and transition phase is less pronounced in these BI2PED results compared to the BI2PED-FE.

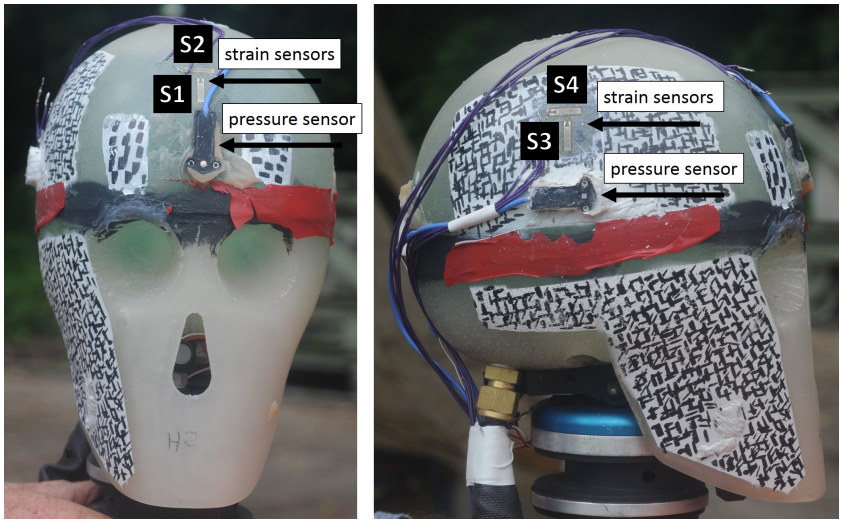

Figure 7.34: Position of the BI2PED external strain and pressure sensors

Similar to the BI2PED-FE the spectra of the BI2PED are location specific. Not all frequencies contribute equally per location. The different peak frequencies are summarised in Table 7.1. The peaks in the spectra of the BI2PED-FE are summarised in Table 7.2. Comparing the frequencies for the different locations of the BI2PED and the BI2PED-FE, is is noticed that the order of magnitude of the frequencies matches. In both models frequencies of around 1000-1500Hz and 600-700Hz are seen. In the physical BI2PED model a frequency of around 300-400Hz is dominantly present that is not found in any of the sensor data of the BI2PED-FE. Another difference between the BI2PED and BI2PED-FE spectra is the higher frequency of around 2200Hz. This frequency is not significantly present in the spectra of the BI2PED while it is the second largest component at the numerical BI2PED-FE ICP rear 180 location. In Figure 9.2 the spectra of the strain sensor on the front of the skull and the internal pressure at sensor ICP Front zero is plotted. They were scaled to fit to the same axis. Frequencies higher than 1500Hz can be neglected for these spectra.[24] It shows that similar to the BI2PED-FE there is a match between the frequency of the skull deformation and internal pressures.

It can be concluded that the modal deformation is present in the BI2PED. However, the in the BI2PED dominant frequency component of 300-400 Hz is not represented in the BI2PED-FE model. It is unknown whether this frequency is the result of a mode shape not present in the numerical model, or of a different origin. This frequency is the main component that results in a different pressure profile for the BI2PED and BI2PED-FE and likely caused by a third response mechanism related to the skull-brain interface. This is further discussed in the discussion in Chapter 9. The higher frequent component of 2200Hz is considered of less interest, as the lower frequencies are more dominant in the internal pressure distribution.

BI2PED sensors

Sensor	Peak freq [Hz]
S1	600-700 1200
S2	300-400 600-700 1000
S3	1200
S4	200-300 1000 1200
ICP Front 0	300-400 600-700 1200
ICP Center 0	300-400 600-700 1200
ICP Center 90	300-400 600-700 1000
ICP Rear 180	300-400 600-700

Table 7.1: Overview of the peak frequencies in the spectra of the BI2PED sensors

BI2PED-FE sensors

Sensor	Peak freq [Hz]
Side x displacement	1513-1561 2295
ICP Front 0	519 579-610 702 1556
ICP Center 0	519 579-610 700-800 1556 2000-2150
ICP Center 90	519 579-610 763 1129 1250 1556 2100
ICP Rear 180	580 671 763 1250 1556 2160-2600

Table 7.2: Overview of the peak frequencies in the spectra of the BI2PED-FE sensors

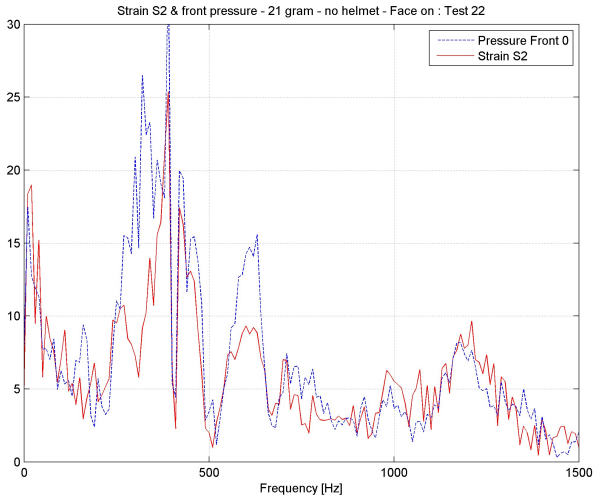

Figure 7.35: Scaled frequency spectra for strain S2 and ICP Front 0 of the BI2PED during shock tube test 22.[24]

8

Optimizing the Experimental Numerical Helmet Assessment Method

Different ways to combine numerical Finite Element (FE) simulations and shock tube experiments are investigated in this chapter. First the different approaches are discussed in Section 8.1 and 8.2. Their feasibility is estimated on the basis of numerical simulation with the BI2PED-FE in Section 8.2.1.

The proposed combined numerical experimental assessment approaches can be subdivided into two categories:
The first category, contained in Section 8.1, contains methods that use the experiments to determine the load that is transferred to the head. This load is used as input for the simulations which determine the internal load reduction and can thus evaluate the protective capabilities of a helmet. As is discussed in Section 8.1 the feasibility of this approach is low. Therefore an alternative strategy is proposed with the second category of assessment methods.
The second category, contained in Section 8.2 uses the numerical simulations to determine the general head response, which is used to optimize the measurement of the response in the shock tube experiments. The measurements taken during the experiment are then used to determine the protective capabilities of a helmet. Multiple options that are considered feasible are discussed.

8.1. Applying the load to the head numerically on the basis of external skull strains

In the numerical simulations the spatial resolution of measurement output is higher compared to the experiment. Response data is available everywhere in FE models, whereas in experiments only a limited number of sensors is used. Therefore it is investigated whether the FE simulations can be used to determine the effect of a helmet on the internal loads.
For a standardised and efficient assessment method it is undesirable to model every tested helmet in detail. Mainly because the helmet itself, the airflow around it and the interaction of it with the head are complex and too time intensive to model and validate. An alternative would be to measure the load transferred by the helmet to the head during experiments and applying this directly to the head numerically, without modelling the helmet itself.
The limited reliability and repeatability of the pressure measurement underneath the helmets means it can not be used as a source for the numerical load to the head. Therefore the external skull strains as a basis for the head load measurement are investigated.
Figure 8.1 shows a schematic of the skull exterior and strain measurement. The strain is measured parallel to the skull exterior. A parallel strain field can not be applied directly as a load in LSDYNA or similar packages, and this approach of questionable feasibility is too time intensive to research and develop for this project. For the FE simulation either a load or displacement field perpendicular to the skull exterior is needed.
Two approaches to recreate the skull deformation as a displacement field from measured strains are next discussed.

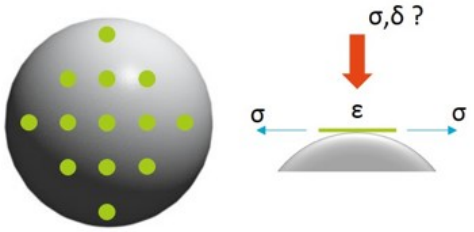

Figure 8.1: Schematic of the eternal skull strains as a basis for a numerically applied load

8.1.1. Recreating a displacement field from a measured strain field

Ideally, the strain field measured during the experiment with a net of sensors would be directly applied as a load for the numerical model. However, such a method is not available at this time. Current FEM formulations available for this type of problem are load or displacement controlled. The strain measurements taken during the experiments can provide stresses in plane of the skull. To calculate the response numerically, loads perpendicular to the skull are needed, see Figure 8.1.
Eppinger has developed a method where a band of strain sensors provide curvatures of a closed loop.[8] An algorithm then calculates the shape of the contour. This way a displacement field can be reconstructed. However, for the head model a 3D field instead of a 2D contour is needed. This would considerably complicate the algorithm needed to compute the head shape from the strain field. Additionally, the head form has relatively large curvatures. The precision of Eppingers method is dependent on the distance between sensors and the local curvature. It is expected that there is not enough space on the head surface to obtain the accuracy needed. Addtionally, the displacements as a result of the blast load are smaller then the thoracic deformation seen in car crash tests, for which Eppingers method has been effectively used.[30].
Because the method needs considerable work to be made suitable for 3D applications, and it is probably not accurate enough for the desired application, it is not deemed a feasible option at this time.

8.1.2. Using modal deformation to recreate the skull displacement field from the measured skull strains

Assuming the head deforms in its normal modes, the strain can be measured at surface locations on the skull exterior that are representative of these modes. If the normal mode according to which the model deforms is known, this mode can be scaled using the experimental measurements. A displacement field based on this mode, or a superposition of modes can then be constructed and applied as a load to the numerical model. An example of the procedure for a single node is illustrated in Figure 8.2.

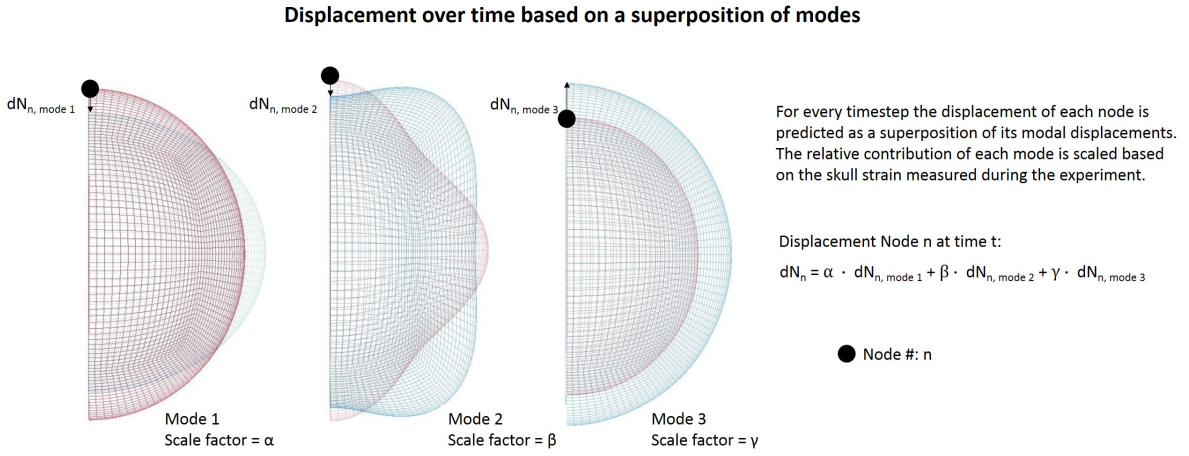

Figure 8.2: The displacement of a single node as a superposition of modal deformation

The internal pressures as a result of this displacement field can be validated with the internal pressure sensors of shock tube experiments. The numerical model can then be used to look at all other locations in the head to check where the highest load occurs and its amplitude.

For the vibration phase the frequencies of the skull deformation modes are found by applying a Fast Fourier Transform to the blast time response. The alternative modal analysis described in Chapter 7 can identify the corresponding skull modes. If the response frequencies and deformation shapes agree with the identified Eigen modes the next step is to recreate the displacement field and and apply this as a numerical load.
In Chapter 7 it was shown that there are additional frequencies present in the blast response pressure signals compared to the deformation of the skull. These local effects are likely not represented in the superposition of skull modes. In order to recreate the internal response it is then necessary to apply the exact deformation of the skull over time for the entire duration of the response. It is however unclear if the deformation of the skull during the peak and transition phase can be described using a superposition of modes. This is critical as the highest loads occur during these phases. A frequency analysis using the Fast Fourier Transform can not reliably analyse the response in these phases as there are not enough repeated cycles.
The proposed method is only suitable when the response in all three response phases can be described according to modal shapes and when these modes can be superimposed to recreate a displacement field. At this point there are considerable doubts with respect to the feasibility of this approach. The options presented in the next section are considered a better alternative.

8.2. Optimizing the measurement approach used for shock tube experiments

During the shock tube tests a limited number of sensors is used to measure the response of the head model. It is therefore useful to predict measurement locations of interest, such that the assessment of the effect of the helmet on the response is optimized. The corresponding sensor lay-out depends on the assessment approach used. Three approaches are proposed:

- Measuring the maximum load that occurs in the brain
- Measuring the maximum load applied to the skull
- Measuring the maximum load transferred to the brain

The manner in which the BI2PED-FE simulations can be used to optimize these measurement methods for the physical BI2PED shock tube tests are now discussed.

Measuring the maximum load that occurs in the brain
By analysing the numerical simulations, locations of highest and lowest pressure can be identified. These results can then be used to optimize the internal pressure measurement locations during the experiment, such that the probability of measuring the highest load is increased. Helmet efficacy is then measured as the reduction of the maximum pressure in the brain.

Measuring the maximum load applied to the skull
The numerical results are analysed to identify if a relation between the external strains and internal pressures exist. If a relation exists, skull strains measured in an experiment may be used to estimate pressures in the brain. It is likely that smaller skull strains correspond to lower internal brain pressures. Helmet efficacy is then measured as the reduction of external skull strain.

Measuring the maximum load transferred to the brain
The numerical results are analysed to identify the location of largest load transfer between the skull and brain. The pressure at this location then indicates the maximum load applied to the brain. In this case the distribution of the load over the brain and the critical locations where damage occurs is not leading. Helmet efficacy is measured as the reduction in the pressure load transferred to the brain.

8.2.1. Numerical analysis in order to optimize the BI2PED pressure sensor layout

The head response is analysed with respect to the pressure distribution of the brain and skull and the maximum skull strain. The results are used to predict the feasibility of the proposed assessment approaches. Different load cases are applied to a reduced numerical BI2PED-FE model.[1] The peak incident pressure of Load case 2 (LC:130kPa-15ms) is varied with four amplitudes; 32.5kPa, 65kPa, 130kPa and 260kPa. Load case 1 (LC:160kPa-4ms) is included to study the influence of the positive phase duration. Because of directionality in the head response to blast three load directions are applied: face on loading, right lateral loading and rear loading.

Figures 8.4 and 8.5 show maximum and minimum pressures and maximum strain locations of BI2PED-FE for the different load cases. The strain consists of a hydrostatic part, related to pressure and a deviatoric part. To include both hydrostatic and deviatoric components of the strain the principal strain is reported. Maximum strains in the skull appear in the jaw, but as this part is not relevant for this study it is not displayed in the pictures of the strain results, see Figure 8.3.

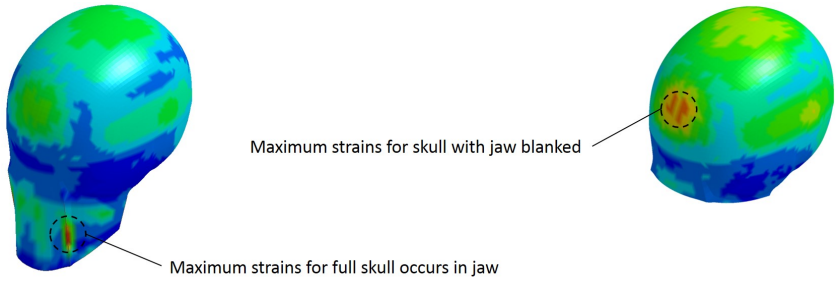

Figure 8.3: Skull strain with jaw unblanked (left) and blanked (right).

Maximum and minimum internal brain pressure

Considering the locations of maximum pressure in the brain in Figures 8.4 and 8.5 the following can be concluded. In general, the maximum pressure occurs on the outer periphery of the brain at the location where the blast first impacts the skull. This holds for face on, lateral and rear blast impact. In the face on case the location is at a slight offset to the side of the brain. If the incident pressure is reduced, the locations of maximum pressure shift to other locations in the brain. In Figures 8.4 and 8.5 this is seen for the load cases of incident pressure of face on 65kPa and 32.5kPa face on and rear facing blast.
Generally speaking the minimum pressure occurs at the location opposite to the first blast impact. A shift in minimum pressure is also seen in case of reduced peak incident pressure of 65kPa or 32.5kPa for both the face on and rear facing load .

Maximum skull strain and pressure

The location of highest strain occurs at the position of highest pressure on the skull, where the blast first impacts the head. The maximum pressure in the skull is located in the middle of the front of the skull slightly above where the eye sockets would be. The maximum pressure in the brain does not occur directly behind this point on the skull. Similar to the brain internal pressure a shift in maximum skull strain is seen for decreasing incident pressure. Large strains are observed at the locations of maximum deformation of the skull when it deforms in its Eigen modes. As the skull strains decrease, the internal pressures also decrease.

[1] This is the BI2PED-FE without a skin layer, neck and fluid layer. In Chapter 6 it was shown that the simulation results with skin and fluid layer are unreliable and that the neck has negligible influence on the internal pressure distribution.

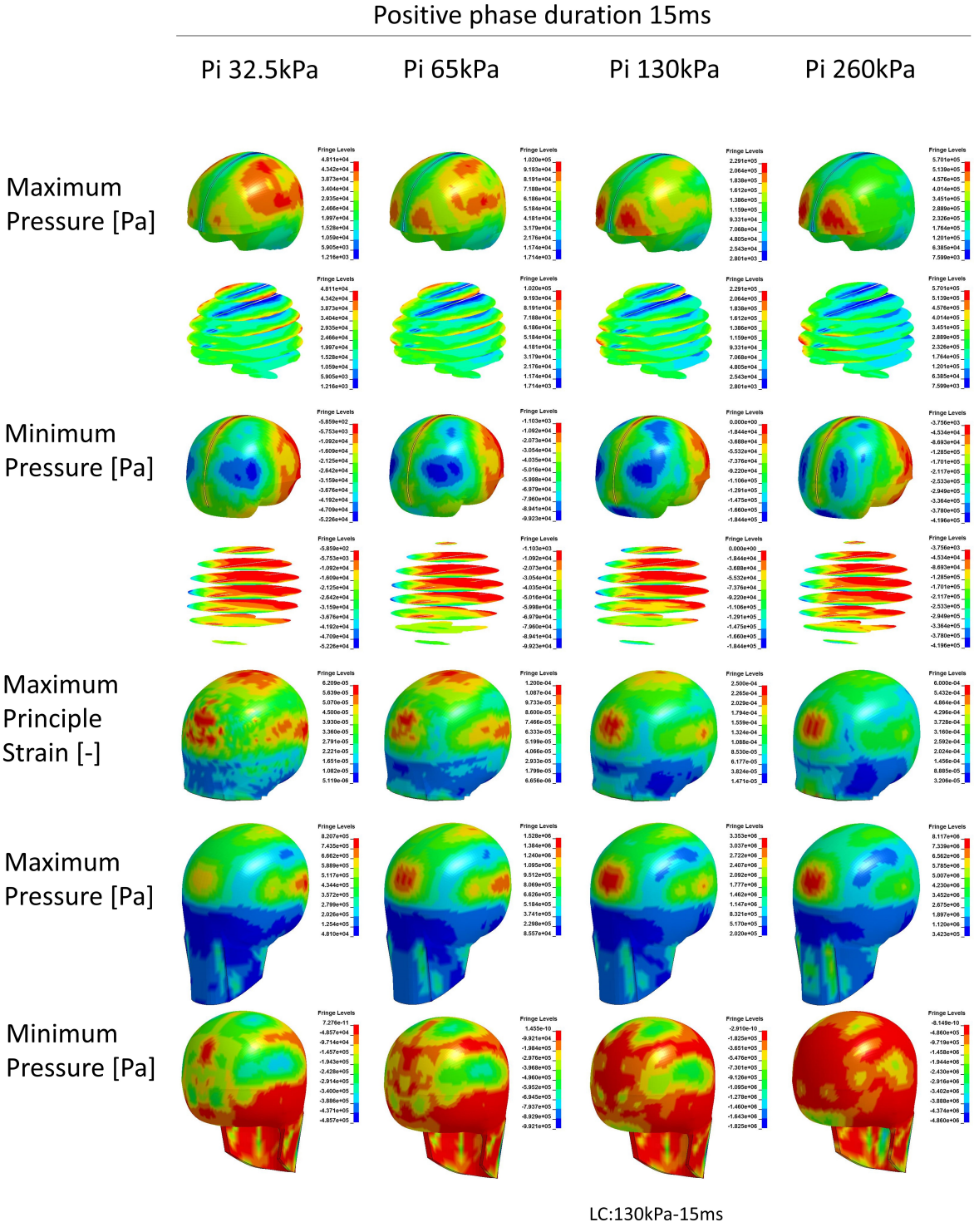

Figure 8.4: Pressure and strain distribution of the BI2PED-FE for load cases with varying peak pressure

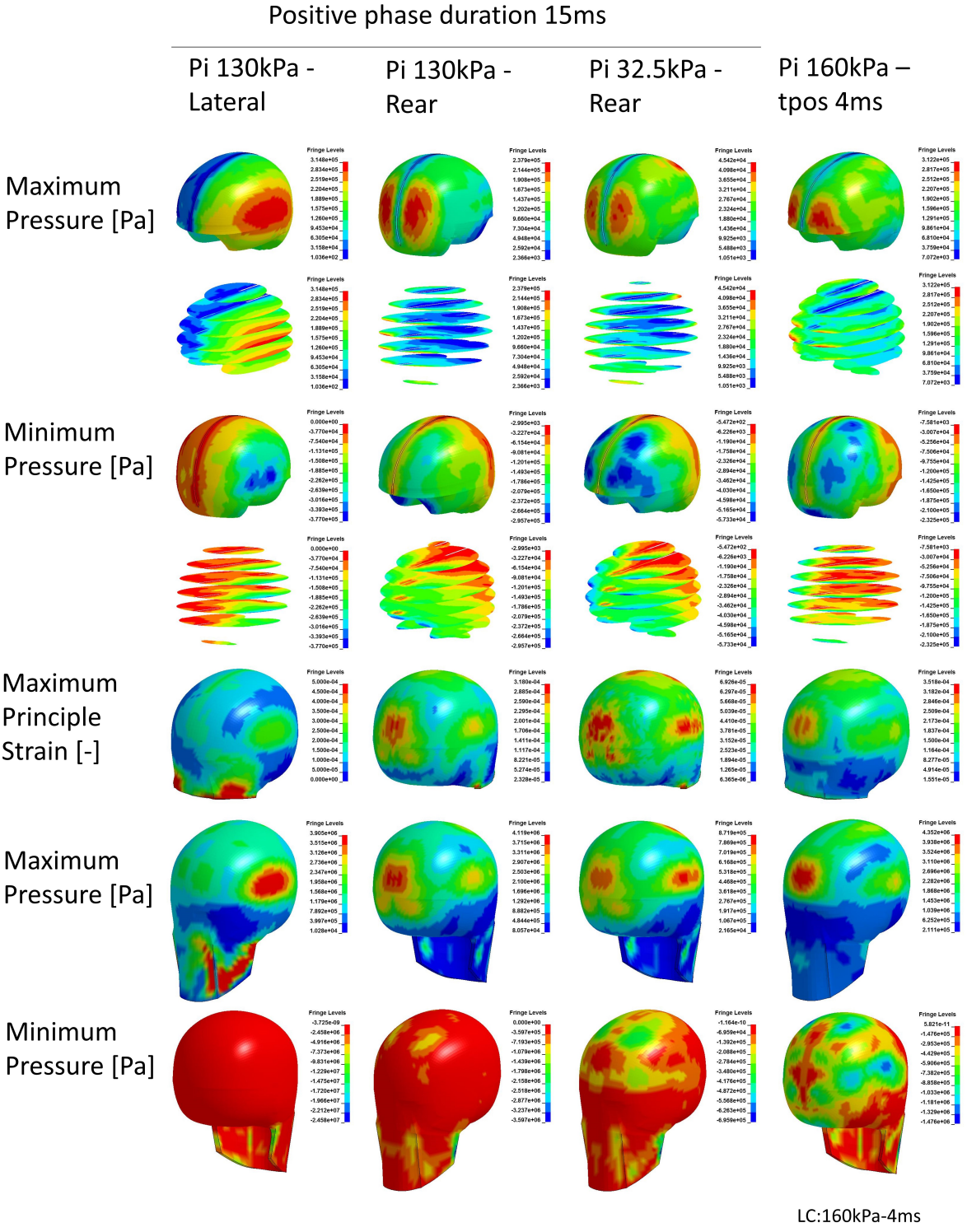

Figure 8.5: Pressure and strain distribution of the BI2PED-FE for different load directions and for a different positive phase duration

The locations of maximum and minimum pressure are summarised in Table 8.6. The maximum strains occur at the locations illustrated in Figure 8.7.

Load Case Pi - tpos	Direction	Max ICP [MPa]	Time [ms]	Location	Min ICP [MPa]	time	Location
32.5kPa – 15ms	Face on	0.043	0.36	C	-0.052	0.61	F
65kPa - 15ms	Face on	0.10	0.66	D	-0.10	0.65	F
130kPa - 15ms	Face on	0.23	0.04	A	-0.18	0.45	E
260kPa - 15ms	Face on	0.57	0.04	A	-4.20	0.41	E
130kPa – 15ms	Lateral	0.31	0.04	B	-0.38	0.30	G
130kPa - 15ms	Rear	0.24	0.03	F	-0.30	0.18	H
32.5kPa – 15ms	Rear	0.045	0.50	C	-0.057	0.51	C
160kPa – **4ms**	Face on	0.31	0.03	A	-0.23	0.40	E

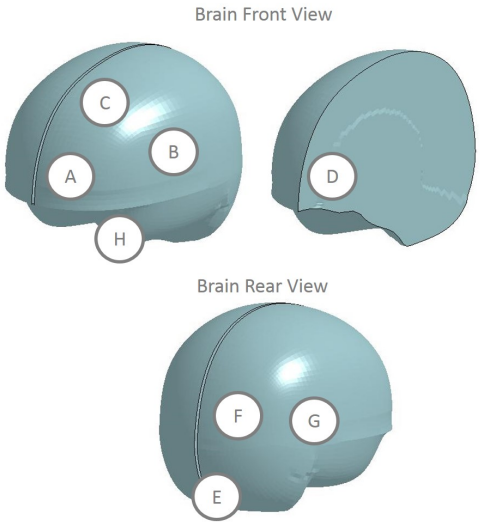

Figure 8.6: Overview of the locations of maximum pressure and minimum pressure in the brain

Figure 8.7: Overview of the locations of high skull strains

Because of the directionality in the head response to blast, it can be concluded that the positions of sensors need to be optimized for every load direction tested during the experiments. Additionally, as the location of maximum and minimum pressure in the brain is sensitive to the peak incident pressure, the sensor lay-out is optimised for a specific load range. During the BI2PED shock tube experiments two incident pressures were used; 160kPa and 80kPa. The numerical load case of 130kPa was fitted to be qualitatively comparable with the 160kPa load case, Appendix B, such that the simulation results can be compared with the shock tube test results. The 65kPa case can be considered qualitatively comparable with the 80kPa load case. In the numerical simulations the location of maximum and minimum pressure shifts between these two cases. Therefore it can be concluded that the optimal sensor lay-out might be different for the two shock tube experiment load cases.

The feasibility of the three assessment approaches is now discussed using the results of the numerical simulations.

Measuring the maximum load that occurs in the brain
Both maximum and minimum pressure occur on the outside periphery of the brain, moving further inwards reduces the pressure. If the sensors are located in the gel near the edge of the brain the gel could tear or be damaged during production or curing of the gel. Additionally a sufficient body of gel needs to be present between the sensor and the skull edge for the full pressure transfer between the skull and brain. This distance likely depends on the type of instrumentation used.
Neuro-pathological expertise is necessary to identify internal brain damage mechanisms. The BI2PED brain is a simplified surrogate, where the material is homogeneous and it does not include the local

detailed brain structures, therefore it is not able to accurately represent these internal damage mechanisms without modifications to the head surrogate. Additionally the location of maximum internal pressures could be different in case a helmet is present.
Given the current level of detail of the model, it is concluded that measuring the internal loads is not an accurate prediction of the damage in the brain and the location of maximum local internal pressure. The internal loads can however be used to validate the numerical results and to identify a trend of decreasing internal loads.

Measuring the maximum load applied to the skull
A relation between the external skull strain and internal pressure is identified using the above presented numerical simulations. Locations of maximum strain are predicted using numerical results for a specific load case. It is proposed to locate the sensors at the blast impact location and the locations of maximum modal skull deformation. This method is considered promising. It should be investigated whether the relation between external strain and internal pressure is valid for protected cases, and whether additional strain sensors are needed in these cases.
The main benefit of this approach is that external measurements suffice, making it practical in use during testing.

Measuring the maximum load transferred to the brain
Because both maximum and minimum pressure in the brain occur on the outside periphery, it is suggested to measure the load transferred to the brain using a sensor between the skull and brain. It should then be checked whether the presence of the physical sensor influences the load transfer to the brain, as the sensor material properties are different from the head materials, and whether the load transfer is similar in protected cases. Expertise on the necessary instrumentation is needed to assess the feasibility of this approach.
The main benefit of this approach is that it is able to measure internal effects.

Three methods have been proposed. The last two methods are considered most promising for a standardised assessment method at this time. However, the internal pressure sensors can be very useful for validation of the numerical simulation results and should be included in the model. It is recommended to add a pressure sensor in the bottom part of the brain where minimum pressures occur. It is suggested to further develop the strain based skull load measurement. The existing locations of the strain sensors on the BI2PED correspond to the locations of high strain. However strain sensors on the top of the head are recommended to be included in the future. It is also recommende to further study the method that measures the load transferred to the brain. The latter is probably better able to measure the local effects in the brain discussed in Chapter 7. For example effects due to the relative internal motion of the brain with respect to the skull. A sensor between the brain and skull is not included in the current BI2PED head. If both methods can be implemented it is advised to use the redundancy to lower the uncertainty of the helmet assessment test results. The current sensor lay-out and proposed additional sensors are presented in Figure 8.8 In this case if both the internal brain load and external skull load are reduced when protective gear is included this is a strong indication that the helmet is effective in protecting the brain against blast.

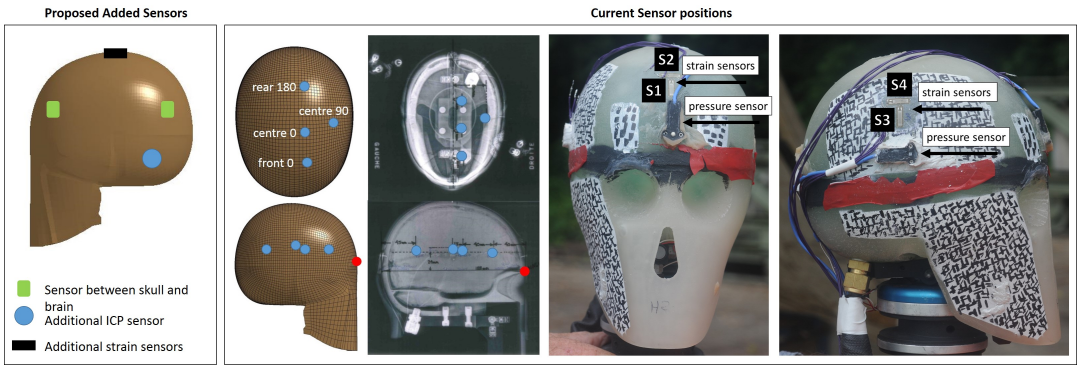

Figure 8.8: Current sensor positions and proposed additional sensors

9

Discussion

In this chapter a comparison is made between the physical and numerical BI2PED. There is a difference in internal pressure response of the two models. The response is compared and characteristics of the models are discussed to indicate the likely origin of the difference in response. Then a helmet as additional factor in the response is discussed.

Comparison of the BI2PED and BI2PED-FE

There are various differences between the physical head model (BI2PED) and numerical head model (BI2PED-FE), see Section 3.1.2. Currently the Falx, a thin membrane structure in between the two brain hemispheres, is not connected to the head in the numerical model. Eye sockets are present in the physical model that do not exist in the numerical model. Additionally the physical BI2PED is attached to a Hybrid III dummy neck and positioned inside a shock tube during the experimental tests. The reflections of blast on the shock tube walls are not included in the numerical model. Finally, the BI2PED brain floats in water inside the skull. In the numerical model water is not able to flow, it is modelled as a solid fluid layer fully attached to both the brain and skull.

Difference in internal pressure response of the BI2PED vs BI2PED-FE

The response of the BI2PED shows a dominant lower frequency in the internal pressure of 300-400Hz. The pressure peaks in this lower frequency are amplified in the transition phase in protected cases in the physical BI2PED model, see Figure 9.4. However, in the numerical BI2PED-FE model the frequency of 500-700Hz is dominant. The pressure signals of both models are plotted in Figure 9.1. Additionally in the physical BI2PED all sensors register pressures that are in phase between sensor locations, whilst in the BI2PED-FE this is not the case. As the BI2PED low frequency is more dominant in the internal pressure compared to the external strains, shown in Figure 9.2, it is assumed that this is a local brain effect and less related to a difference in skull stiffness between the physical and numerical model.

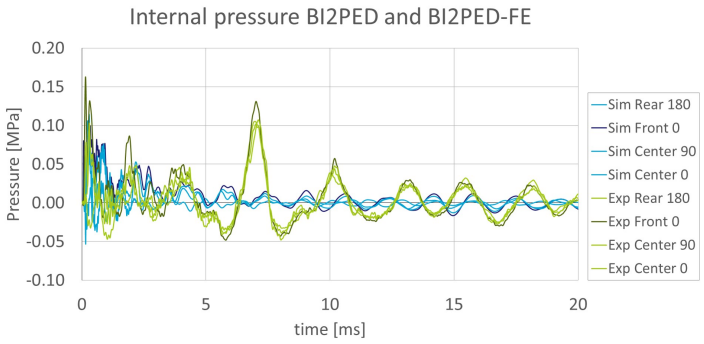

Figure 9.1: Internal pressures of the BI2PED shock tube experiment test 22 [Filtered LP10kHz] and the BI2PED-FE (LC:130kPa-15ms)

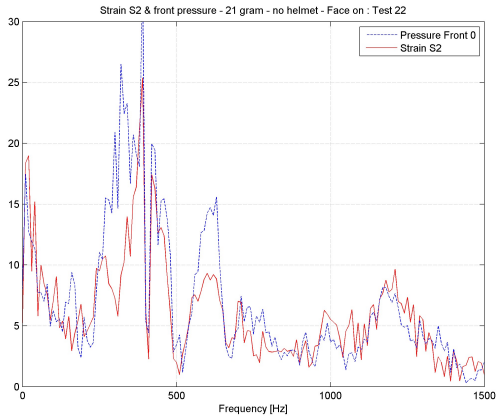

Figure 9.2: Scaled frequency spectra for strain S2 and ICP Front 0 - Test 22[24] This location showed the best match between external strain and internal pressure

Recap:
In Chapter 7 it is shown that the vibration of the head consists of a superposition of Eigen Modes, and that not every mode contributes equally per location in the head. A relation exists between the skull deformation and internal pressure as they both vibrate in similar frequencies. However in the internal pressures, frequencies are present that are not present in the frequency spectrum of the skull displacements. This indicates that local brain effects exist.

The previously described differences between the numerical and physical model are now discussed one by one to indicate which one is most likely the cause of the difference in the dominant frequency of the internal pressure.
The Falx membrane is expected to increase the stiffness of the head when the membrane is stretched. It is previously posed that a local brain effect is present which is not fully dependent on the skull stiffness. Therefore the Falx is not expected to be the main cause of the low frequent component in the pressure response.
The physical model has eye sockets through which the frontal impact of the blast could be transmitted. This locally reduces the stiffness of the skull, which could decrease the modal response frequencies. But again it is not expected that this is the cause of the difference in the lower frequency region between the two models.
The numerical blast load overestimates the impulse transferred to the model, but the influence of the positive phase on the frequency of the pressure response and skull deformation is not significant, as is shown in Appendix D. The peak pressure is lower in the numerical blast, but the simulation results in Section E.1 and Chapter 7 show that the peak pressure does not significantly alter the vibration frequencies. Lastly, the presence of shock tube walls in the experiments is expected to alter the load transferred to the head due to shock reflection. A preliminary study of an unprotected sphere model showed that the effect of the walls is expected to be limited, Appendix F.
The stiffness of the HIII neck is different between the simulations and experiments, but Section 6.3 showed that this is not related to the dominant frequency in the pressure response as the frequency of the neck motion is 2 orders lower than the frequency in the pressure response. Therefore the effect of the neck is outside the time period of interest and not related to the dominant sinusoidal frequency of 300-400Hz in the BI2PED internal pressure.

The difference between the models that is most likely responsible for the difference in pressure distribution is the brain-skull interface. In the physical model water is present with a bubble of air at the top. In the numerical model the fluid interface is modelled as a solid fluid layer. Zhang [36] states that the solid element layer approach is valid in case deformation of the CSF is small. But the bubble of air in the physical model allows for movement of the water. Additionally S. Ouellet, one of the developers of the physical BI2PED headform[1] observed during tests of the model that the low frequent component pressure peaks increase in case the water level in the head form is lowered. This suggests that an additional third response mechanism damped by the water level is present in the physical model.

[1]The development of the BI2PED model is described in the following report[22]

A third response mechanism

Different theories regarding the origin of the third mechanism are now discussed.

One hypothesis is that the brain moves as a whole inside the skull resulting in alternating internal impact with the back and front of the skull. This could explain the fact that all pressures are in phase. The water in this case would damp the brain motion. Penalty contact simulations, where the brain is free to move with respect to the skull, with the spherical model show that in this case the neck can amplify the pressures. However in the BI2PED tensile pressures are present in the brain, that are not present in the simulations of the spherical model with penalty contact. This means that in the BI2PED tensile forces in the brain are present that are not caused by the bending of the skull pulling on the brain. Some tension in water can be transferred until cavitation occurs. However, a bubble of compressible air is present, making tensile pressure in the water very unlikely.

A second hypothesis is that the brain comes into contact with the skull during blast impact and starts to vibrate in its own local modal frequencies. Reducing the water level would in this case lower the damping of this impact, increasing the pressure peaks. A simulation of only the BI2PED-FE brain, where the front of the brain is hit with a pulse, shows that frequencies between 200Hz and 500Hz are present in the brains vibration response, see Figure 9.3. These frequencies are not present in the BI2PED-FE model where the brain is fully attached to the skull. This indicates that the type of interface is related to the frequency content of the brain internal pressures.

The true mechanism is likely a combination of effects similar to the hypotheses described above.

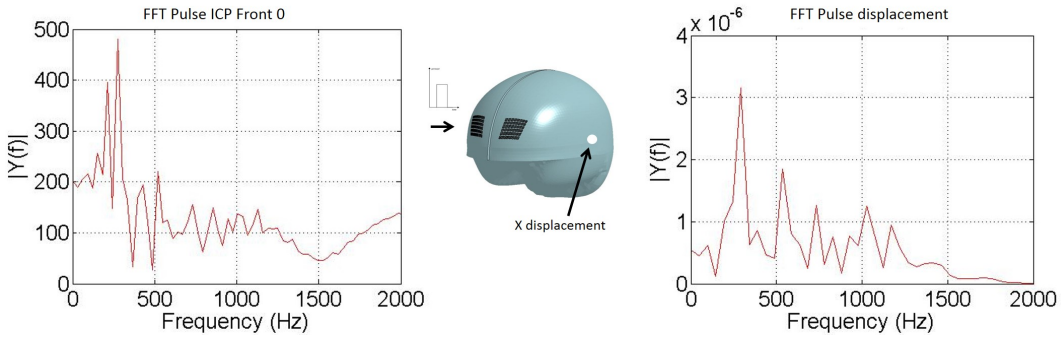

Figure 9.3: Single sided frequency spectrum of the BI2PED-FE brain internal sensor ICP Front 0 and sideways brain displacement due to a pulse load (P:259kPa-0.01ms)

The effect of a helmet on the head response

As previously described, the presence of a helmet amplifies the pressure peaks for the dominant frequency in the BI2PED model. Additionally, the transfer of the blast load into the head is altered influencing the amplitude of the first peak pressure, see Figure 9.4. Both these effects are now discussed consecutively.

One explanation for the amplification of the sinusoidal pressure peaks is that the blast load surface area is increased in the case of a helmet. The total load transferred is then increased, resulting in a higher acceleration of the head model. The relative impact of the skull to the brain, as described in the third mechanisms hypotheses would then increase and amplify the pressure response.

A different cause could be the concentration of air pressure in the space in between the helmet and head, called underwash. As the blast pushes air in between this spaces, and there is no outflow of air, the load can be amplified. Multiple studies find that gaps beneath the helmets can have adverse effects which could possibly be compensated for by closing the gaps with foam.[12][29][36][35][10]. The presence of the shock tube walls and the too small diameter of the tube used, see Appendix F, is expected to magnify the effect of air concentration underneath the helmet at the bottom.

Besides the amplification of the transition phase, the helmet also influences the load transfer via direct blast impact. In the case of the full face helmet the initial peak is reduced as the direct impact of the blast to the front of the head is reduced, see Figure 9.4. From the discussed it is concluded that the pressure and strain distribution of the unprotected head in Chapter 8 cannot be directly transposed to the protected head without additional simulations. The simulation results do indicate a trend and can be used to estimate the feasibility of the respected proposed approaches.

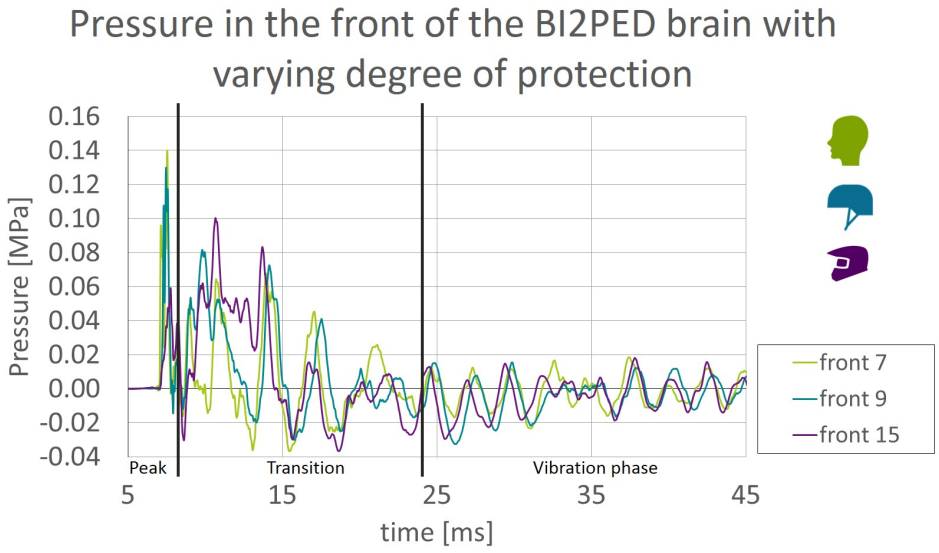

Figure 9.4: BI2PED internal pressure divided in phases in the front of the brain. Experiment; frontal blast (160kPa, 17ms) Test 7: No helmet - Test 9: Combat helmet - Test 15: Full face helmet. [Filtered LP10kHz]

10

Conclusions and Recommendations

This thesis aims to investigate options for a combined numerical experimental assessment method to assess the efficacy of helmet systems in protecting against Mild Traumatic Brain Injury - mTBI. The research objective is studied using a set of research questions. The answers to these are discussed here. The chapter ends with recommendations for future development of the combined assessment method.

Part 1: Which factors dominate the nature of the head response?

1.1 A study of the physics involved in the response of head models to blast. Chapters 4, 5, 7

In the internal pressure response of the spherical and BI2PED-FE head model to blast there are two dominant mechanisms. The first mechanism is the propagation of a blast wave due to the direct impact of the blast on the skull. The second mechanism is a vibration in a superposition of Eigen modes, where the skull deformation causes an oscillating internal pressure. In the physical BI2PED head an additional third mechanism is present involving the brain and fluid. This third mechanism is not represented in the numerical simulation results of the BI2PED-FE. This means that the numerical BI2PED-FE model is not ready for validation. The skull-brain interface type is identified as the origin of the lack of the third mechanism. In the physical BI2PED relative brain motion with respect to the skull is possible due to the fluid interface. This motion is not allowed in the numerical model where they are fully attached.

1.2 What is the effect of the head geometry and other model features, properties and boundary conditions on the internal brain pressures? Chapter 6

The effect of the presence of a skin layer, neck constraint and fluid interface on the brain internal pressure distribution, studied using the spherical and BI2PED-FE model, is now discussed.

The Influence of A Skin Layer
A rubber-like skin layer is present in the physical BI2PED head. Simulations with the spherical and BI2PED-FE model show that the effect of the skin layer is significant.
In the spherical model the addition of a rubber-like skin layer caused a damping of the peak pressure in the front of the brain with 20 percent. The pressures in the back of the brain are amplified. The frequency of the internal pressures is increased fromt 600Hz to 4000Hz with an additional low frequent component of 150Hz.
The reduction of the initial frontal peak pressure and increase of the frequency of periodic pressures is also observed comparing the shock tube experiment data of the BI2PED with and without skin.
Numerically the skin layer, combined with loading of the type LOAD BLAST ENHANCED leads to unrealistic head motion of the BI2PED-FE and therefore likely unrealistic pressure distribution. In the ALE environment, which includes fluid structure interaction, these unrealistic head motions are not seen. The cause of this issue was not identified in a preliminary study into the skin.
From the simulation results with the sphere and BI2PED-FE it is concluded that the influence of the

skin layer is significant; The peak pressure is damped and the frequency of vibration phase changed due to the presence of the skin.

The Influence of Neck Constraints
During the shock tube tests the BI2PED head was supported by a HIII dummy neck. Simulations with the spherical and BI2PED-FE model show that the influence of the neck on the internal pressure distribution is negligible.
The spherical model was simulated free floating and fixed at the bottom and showed negligible influence of the constraint on the peak pressure in the peak and transition phase. These results agree with the results found by Salimi [28]. The only significant influence of the constraint is that a low frequent signal of 30Hz is added to the internal pressure in the vibration phase where the frequency of 600Hz is dominant. As the effect of the neck constraint is related to the free motion of the unconstrained head the influence occurs much later in time when the initial peak pressures due to the blast have dissipated. This means that the influence of the neck occurs out of the time domain of interest.
The BI2PED-FE dummy was extended with a freely available HIII dummy neck model[1]. Similar to the spherical model the HIII neck has little influence on the peak pressure and internal pressure response. This corresponds to the conclusions of Roberts [27][26]. The frequency of the neck motion in the numerical model is 3Hz, but in the shock tube experiments this frequency is 5Hz. This means that the numerical neck should be an estimated 2-3 times more stiff to obtain similar neck motion. The neck stiffness can be improved by adding tensile contact between the rubber and neck disks.
It was hypothesized that the neck back and forth motion was responsible for the oscillating internal brain pressure. However, the frequency of the neck motion is 2 orders lower than the frequency of the internal BI2PED-FE pressures of 500-2000Hz. This means the neck is not responsible for the oscillating pressure phenomena.
In the extreme case that the BI2PED-FE was fully fixed a significant deviation in internal pressures is seen, most pronounced in the sensor data from the front of the brain. Here, the clamp case shows otherwise unseen negative pressure after the initial peak and the frequency of the oscillations is lowered. This is different for the spherical model where a fully clamped neck constraint did not significantly influence the results. This difference can be explained by the difference in geometry and the fact that the unconstrained BI2PED-FE shows a rotational chin-in motion in the unconstrained case.
Based on the simulations results of both the spherical model and the BI2PED-FE, it is concluded that the influence of neck constraints on the internal pressures is not significant in the time response domain of interest (+-30ms), unless the neck is extremely stiff, an unrealistic case.

The Influence of the Skull-Brain Interface
In the physical BI2PED head the brain floats in an enclosed volume of water. The modelling of the numerical skull-brain interface such that it can include the effects of this volume of water is not found in Literature or in the interface types modelled in the spherical and BI2PED-FE head.
Three main approaches to model the cerebral spinal fluid (CSF) brain-skull interface are: Eulerian fluid elements, Lagrangian soft solid elements and contact/friction based interface. Summarizing the conclusions of the studies by Zhang [36](Eulerian and Lagrangian), Chafi [5] (Lagrangian), Gu [11] (Lagrangian) literature shows that the influence of the CSF on the peak pressure is limited and if the pressure response is influenced it is slightly damped over time for different types of modelling. Using the spherical model an elastic solid element layer was compared with a fully attached skull-brain interface and penalty contact. The elastic fluid layer showed a slight damping of the internal pressure over time. Using penalty contact no negative pressures occur in the brain and the periodic pressure signal damps out within 6ms. In the case of penalty contact combined with the neck clamp the pressure peaks at the back region of the head are amplified.
In the BI2PED-FE the fluid is modelled as a solid elastic layer with an equation of state. The peak pressures are amplified in the brain, the negative pressures almost entirely removed and the periodic signal is damped out after 20 ms. The frequency of the pressure signal is changed to 200Hz.
In general the effect of the interface on the response is expected to be limited considering literature and the simulation results with the sphere, however the specific manner in which it is modelled in the BI2PED-FE causes significant changes to the pressure distribution. Therefore, the results using this approach are expected to be unrealistic.
It is concluded that the fluid present in the physical BI2PED head model is not adequately modelled

using the approach provided in the BI2PED-FE. The alternative options used in the spherical model test simulations are not expected to directly solve this issue. The sharing of nodes prohibits relative motion of the brain with respect to the skull. Penalty contact does not provide the resistance of the water to this motion. An Eularian approach might be necessary to adequately model the fluid behaviour.

Based on the influence study results, the analysis in Part 2 regarding the measurement of the internal response was done with a reference BIPED-FE model without neck constraints, skin layer and CSF. This model is chosen because the influence of the HIII neck is limited and the results of the BI2PED-FE with skin and with CSF are unreliable.

Part 2: Can the measurement of the internal response be optimized?

2.1 Can the effect of a helmet be numerically evaluated without modelling the helmet? Chapter 8

Multiple options that use the external skull strain as a basis to measure the load applied to the head underneath the helmet are investigated. At this time it is not possible to apply a strain field as a function of time directly to the numerical model in LSDYNA. In general the application of a strain field as a load is problematic. An algorithm that calculates the deformation of the head based on the strain field is complex to develop and probably not accurate enough due to the complex geometry, large curvatures and small strains of the BI2PED head.
An alternative approach is to recreate the skull deformation using the superposition of Eigen modes. In this case the external skull strains are used as a way to scale the modes. This method shows multiple challenges at the moment. One of which is that a direct numerical modal analysis is not able to provide the most important modes. An alternative method using a block pulse impact is able to predict the Eigen modes of the spherical model, but this method is more difficult to apply to the more complex BI2PED-FE head. The modal deformation of the different Eigen frequencies could be determined experimentally, but the frequencies of the numerical and physical BI2PED response differ, suggesting the modes might be different. Additionally, it is uncertain whether the initial peak pressure can be captured with modes. If this is possible it is expected that an impractically large number of higher order modes is needed. Besides that, it is possible that underneath the helmet different modes are excited than in the case without a helmet. Lastly, in the internal pressures additional frequencies are seen compared to the external skull displacements. This could indicate that during the response there are internal effects present, that are not measured when one considers the external skull strains. This means that a method based only on the external strains is likely not able to fully describe the internal effects in the brain.
Considering the challenges described above it is concluded that at this time it is not feasible to numerically apply the load underneath the helmet without modelling the helmet. Therefore an alternative strategy is considered where the numerical results are used to optimize the measurement of the response and effect of a helmet in shock tube tests.

2.2 What is the internal pressure distribution and can locations of maximum and minimum pressure be identified? Chapter 8

A pattern in the areas of maximum and minimum pressure was investigated using different load cases; varying blast direction, peak incident pressure and positive phase duration.
In general it can be posed that the maximum internal pressures occur at the location where the blast first impacts the head and pressure waves into the brain are initiated (Pi > 130kPa). This holds for the loading directions face on, right lateral and rear blast impact. For mild load cases additional locations of critical pressure are present throughout the brain(Pi < 65kPa). In the case of a mild blast (Pi = 32.5kPa) to the back of the head the maximum pressure occurs at the front of the brain.
The minimum pressures generally occur at locations opposite the first impact region of the blast. This is seen for face on, right lateral and rear impact. Similar to the regions of maximum pressure the regions of minimum pressure change when the peak incident pressure is reduced (Pi < 32.5kPa).
During the BI2PED shock tube tests two load cases were used (Pi 160kPa - tpos 17ms and Pi 80kPa - tpos 17ms). Considering the above it is possible that the locations where the maximum and minimum pressures occur are not identical for the two load cases.

If one wants to measure the maximum and minimum pressure inside the brain, it can be concluded that the optimal internal pressure-sensor lay-out depends on the load case and load configuration. Depending on the shock tube test set-up a specific optimisation for the test series is necessary.

Load Case Pi - tpos	Direction	Max ICP [MPa]	Time [ms]	Location	Min ICP [MPa]	time	Location
32.5kPa – 15ms	Face on	0.043	0.36	C	-0.052	0.61	F
65kPa - 15ms	Face on	0.10	0.66	D	-0.10	0.65	F
130kPa - 15ms	Face on	0.23	0.04	A	-0.18	0.45	E
260kPa - 15ms	Face on	0.57	0.04	A	-4.20	0.41	E
130kPa – 15ms	Lateral	0.31	0.04	B	-0.38	0.30	G
130kPa - 15ms	Rear	0.24	0.03	F	-0.30	0.18	H
32.5kPa – 15ms	Rear	0.045	0.50	C	-0.057	0.51	C
160kPa – **4ms**	Face on	0.31	0.03	A	-0.23	0.40	E

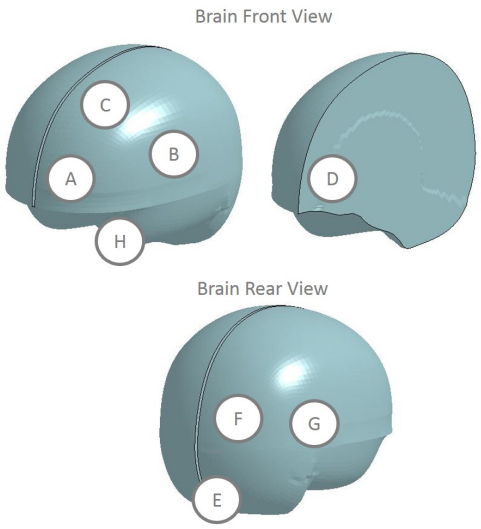

Figure 10.1: Overview of the locations of maximum pressure and minimum pressure in the brain

2.3 Can a relation be defined between external skull strains and internal brain pressure? Chapter 8

A reduction in the external skull strains in protected cases could indicate the ability of the helmet to reduce the internal brain load. Various load cases have been compared and the results suggest that a relation exists between the maximum strain observed at the skull exterior and the maximum internal pressure. If the peak incident pressure decreases both the maximum external skull strain and internal pressure decrease. The maximum strains occur at the location of blast impact and at the locations of maximum deformation of the dominant mode shapes.

2.4 What is the optimal strain and pressure sensor layout in order to effectively combine test and FE data to determine the protective capabilities of helmets? Chapter 8

Locations of maximum and minimum pressure and maximum strain were identified, see Figure 10.1. The optimal sensor lay-out depends on the assessment method used. Three measurement methods were proposed.
The first method aims to numerically predict critical locations using the maximum and minimum pressure in the brain, such that the sensors can be located at those locations in the brain. As the pressure distribution is different in the physical and numerical BI2PED-FE the locations can not be accurately predicted at the moment. Additionally the BI2PED brain is homogeneous unlike the human brain and neuro-pathological knowledge is needed to predict critical locations.
The second is the relation between the external strain and internal pressure. For this method the external strain can be measured at locations of maximum strain and deformation. The internal sensors function as a additional check.
In the third method the maximum load transferred by the skull to the brain is measured. The location of load introduction into the brain can be predicted more reliably.
Besides the chosen method the optimal sensor lay-out depends on fabrication restrictions and instrumentation. It is concluded that the last two methods to improve the sensor lay-out are feasible. For these methods it is proposed to extend the current sensor lay-out with additional sensors, see Figure 10.2.

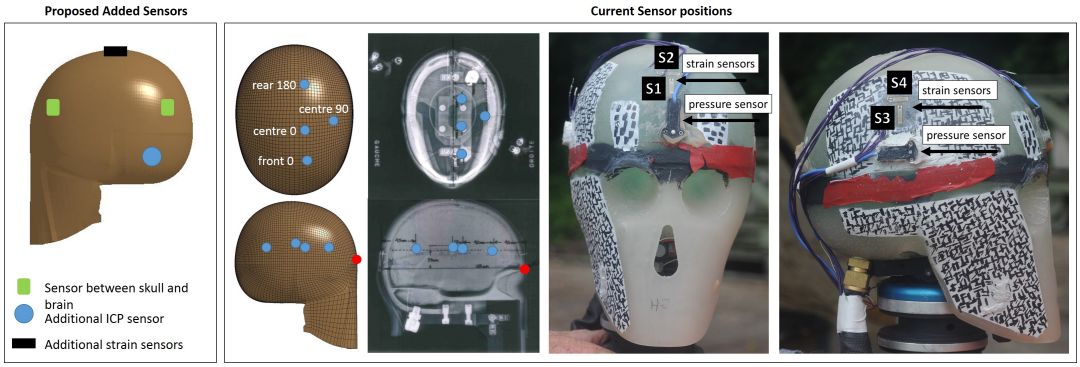

Figure 10.2: Current sensor positions and proposed additional sensors

Feasibility study of a combined numerical/experimental method to predict the protective capabilities of helmets against blast-induced mTBI, using a human head surrogate

A combined method where numerical simulations of the BI2PED-FE are directly used to assess the effect of a helmet on the numerical head response without modelling each helmet in detail is not considered to be feasible at this time. The numerical load applied to the head by the helmet can not be modelled based on pressure or strain measurements obtained during the shock tube experiments. An alternative is provided by using the numerical simulations to improve the measurement of the physical response during shock tube experiments with helmets. This approach is considered feasible. Two main approaches are proposed; Measuring the external skull strain, or measuring the maximum load transferred to the brain to compare the head response for different helmets. The measurement locations are in this case based on the FE analysis simulation results. A combination of the two approaches is considered able to provide a strong indication of the protective capabilities of helmets. The combined approach proposed in this study considers the reduction of internal loads as indicator of protective capabilities, as there is no consent at the time with regard to the damage mechanism responsible for mbTBI. However, research on the damage mechanisms is ongoing.

Recommendations

It is recommended to further study the third response mechanism of the physical BI2PED model in order to improve the BI2PED-FE model for a closer match between internal pressure distribution of both models. As is, the BI2PED-FE model is not yet suitable for validation. Improvement of the interface is considered the first step to incorporate the third response mechanism in the numerical model. Additionally, for a correct bending of the skull at least three solid elements over the skull thickness are advised, while in the BI2PED-FE model only two elements over the skull thickness are used. Because of the non-linearity in the material models even smaller elements would be advised. In order to include the skin in the simulations it is recommended to use the ALE model including the air domain. Use of the ALE model also enables a better approximation of the blast load applied to the head, which is necessary for validation of the simulation results with the shock tube tests.

At the moment it is assumed that the reduction of maximum positive and negative pressure in the brain is a measure of the protective capabilities of the helmet. There is no consensus on the neuropathological damage mechanisms that lead to mbTBI at this time. If more information on the damage indicators or parameters becomes available, the numerical model can be updated with the level of detail necessary to include the local damage effects. The level of detail of the BI2PED model is currently limited to a homogeneous isotropic brain.

After improving the validity of the numerical BI2PED-FE model, it is advised to run simulations with a simple helm model. A generic open face helmet model for the BI2PED-FE model was developed at DRDC[3]. It is recommended to also study the effect of a face shield as it influences the direct impact of the blast. The purpose of the simulations with helmet are to check whether the conclusions with respect to the response and behaviour of the unprotected BI2PED head model are also valid for protected cases. If the location of maximum load transfer to the brain can be accurately predicted, these locations can be used to measure the effect of the helmet on the maximum load to the brain. The

simulations including a helmet should also be used to check whether the location of maximum skull strain can be predicted for protected cases.
When the relation between the strain or pressure measurements during shock tube tests and internal load reduction is quantified, using a set of load cases for the simulation representative for the specific test set-up, a method to quantify the protective capabilities is available.

A

BI2PED shock tube test matrix

Various tests were done with the BI2PED head model at TNO [24]. Table A.1 and Table A.2 show an overview of the shock tube tests. The data of the tests boxed in black are used in this report.

Pre-tests

Test no.	Charge [gr]	Headform	Measured Pressure			
			P1	P2	Pdyn	Pside on
Pre-1	7	Hyb III	x[1)]	x	x	-
Pre-2	7	Hyb III	x	x	x	-
Pre-3	20	Hyb III	x	x	x	
Pre-4	21	Hyb III	x	x	x	x
Pre-5	21	None	x	x	-[2)]	-
Pre-6	7	None	x	x	-	-

Table A.1: Test matrix of the pre-test done for the BI2PED shock tube experiment

BI2PED tests

Test no.	Charge [gr]	Headform		Helmet	Orientation
5	7	H2		No	face on
6	7	H2		No	face on
7	21	H2		No	face on
8	21	H2		No	face on
9	21	H2		Std	face on
10	21	H2	Skin	Std	face on
11	7	H2		Std	face on
12	7	H2		Std	face on
13	7	H2		full face	face on
14	7	H2		full face	face on
15	21	H2		full face	face on
16	21	H2		full face	face on
19	7	H2		No	face on
20	7	H2		No	face on
21	21	H2		No	face on
22	21	H2		No	face on
23	7	H2	Skull only	No	right lateral
24	7	H2		No	right lateral
25	21	H2		No	right lateral
26	21	H2		No	right lateral
27	7	H2		No	left lateral
28	7	H2		No	left lateral
29	21	H2		No	left lateral
30	21	H2		No	left lateral

Table A.2: Test matrix of the BI2PED shock tube tests

B

Fitting Load Blast Enhanced to experimental data

In order to compare the numerical and experimental internal pressures of the BI2PED head model a numerical load was fitted to the experimental load measured in the shock tube. The goal is to obtain a load that is able to qualitatively compare the numerical and physical BIPED head response. First the incident pressure is fitted to measured data obtained from the shock tube sensor data collected during the shock tube experiments. Then the load measured on the physical BI2PED model during the experiments is compared with the numerical load applied to the BI2PED-FE.

Step 1: Fitting the incident pressure wave
By varying the simulation model's distance to the blast origin and the equivalent TNT mass, the peak incident pressure and positive phase duration output is altered. The pressure profile applied and impulse transferred by this load to a reference segment is compared with the experiment's sensor data.
Figure B.1 shows the experimental set-up. Because the decay of the shock wave over time and distance could be different numerically compared to the experiment, P2 is chosen as reference point because this sensor location is closest to the head model.

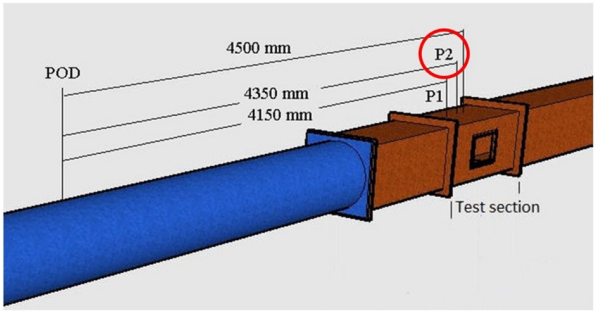

Distance Point Of Detonation – pressure sensor P1:	4150 mm
Distance Point Of Detonation – pressure sensor P2:	4350 mm
Distance pressure sensor P1 – middle test section :	350 mm
Distance pressure sensor P2 – middle test section:	**150 mm**

Figure B.1: Schemtatic of the BI2PED shocktube experiment

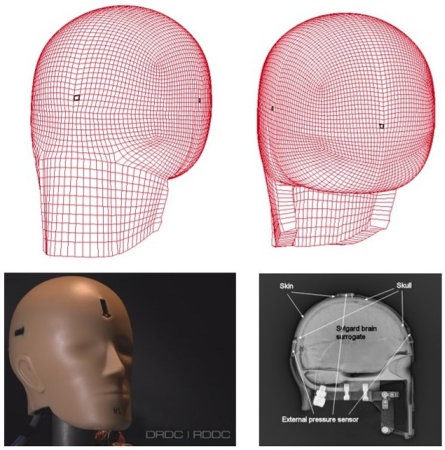

Figure B.2: External BI2PED pressure sensors

To account for disturbances in the air flow due to the presence of the head, both a shock tube test with and without the presence of a head model are included. These are pre-test 3, 4 and 5 from the test matrix table in Appendix A. The experiment's blast profile is characterised by an incident pressure of 160kPa and a positive phase of 17ms.
Figure B.3 contains the incident pressure curve measured at sensor P2 during the experiment and at the numerical reference segment at equal distance to the head model. The numerical peak pressure

has to be lower than 160kPa for the pressure to follow a trend that falls within the sensor data and have a comparable impulse. To obtain a better fit, the numerical positive phase duration is 15ms.
Figure B.4 shows the impulse transferred by the incident pressure curves. The impulse of PreTest 3 is significantly lower because the explosive charge was smaller during that test (20gr instead of 21gr). The chosen numerical blast falls within the range of PreTest 4 and 5.

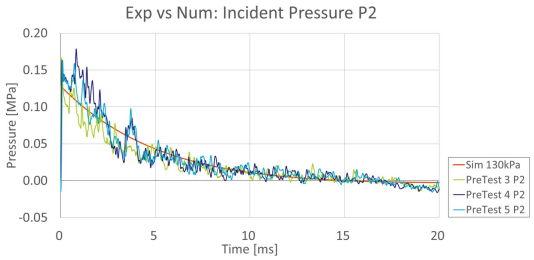

Figure B.3: Numerical and experimental incident pressure wave at a distance respectively 150mm before the head model

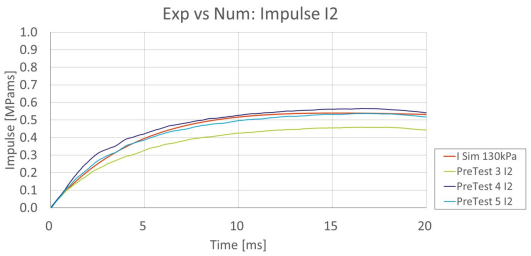

Figure B.4: Numerical and experimental impulse of the incident pressure wave at a distance respectively 150mm before the head model

Step 2: Comparison of the head load

The load applied to the numerical head model by the fitted blast wave is compared with the load measured on the physical head model during the shock tube tests. The numerical positions of the external pressure sensors are estimated using BI2PED pictures, see Figure B.2.
Figure B.5 shows the numerical and experimental load applied to the head at the front, side and back of the head. The pressure profile measured during the experiments decays faster than numerical load. Therefore the load applied to the numerical model is largely overestimated at the front of the BIPED (red line). This is confirmed looking at the impulse plotted in Figure B.6. An option is to lower the incident peak pressure such that the total impulse is a better match. However it is assumed that the peak pressure is a dominant factor for the response of the head model. Analysis of the pressure distribution in Chapter 8 confirms this assumption. The chosen blast profile provides the best match for the peak pressure and impulse in the first 2ms where the highest internal loads occur. This load is considered suitable for a qualitative analysis of the FE models and comparison of the numerical and physical behaviour.

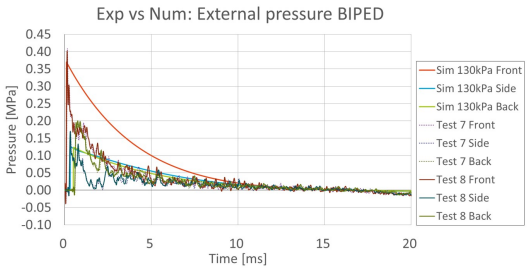

Figure B.5: Numerical and experimental pressure measured on the front, side and rear of the head

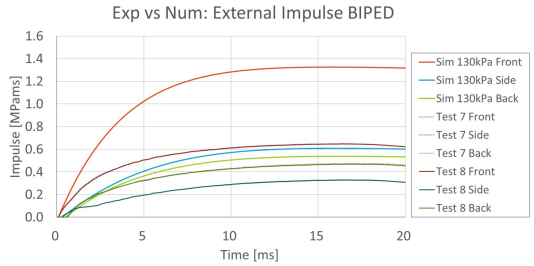

Figure B.6: Numerical and experimental impulse of the pressure measured on the front, side and rear of the head

C

ALE test simulation of the BI2PED-FE including HIII neck

Figure C.1 shows the working connection of the BI2PED-FE head and HIII dummy neck in the ALE simulation environment. It is a test simulation of 4ms duration with one of the load cases provided with the ALE model as received from DRDC. The load used is: 4.5kg 5m ground effect. The head-neck model has not been validated with experimental data. The airflow around the neck does not contribute significantly to the load on the head[17]. Therefore the interaction of the airflow with the neck is not included in the ALE model.

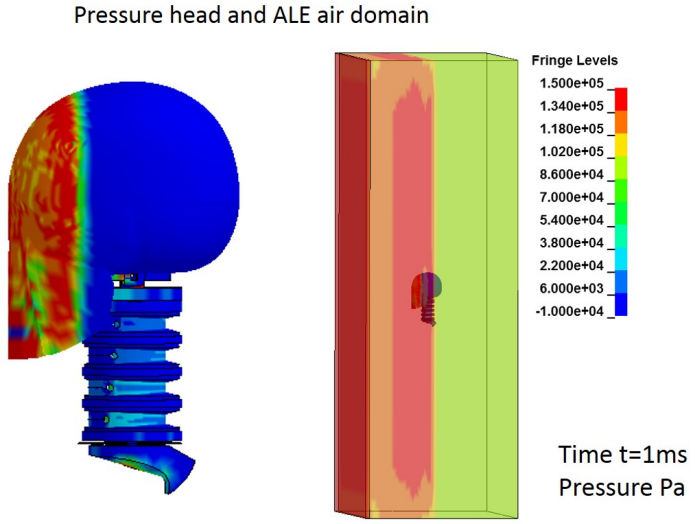

Figure C.1: Test simulation of the connection of the HIII dummy neck and BI2PED-FE in ALE environment

D

The influence of the blast positive phase duration on the internal pressure response

To study the influence of the blast positive phase duration, the response of the reference blast load case (Pi 160kPa, tpos 4ms) is compared with a load with equal peak pressure but significantly longer positive phase duration (Pi 160kPa, tpos 20+ms). The internal pressure response to both load cases is presented in Figures D.1 and D.2. It is seen that the internal peak pressure is similar, and oscillations in pressure exist in both cases. However in the case of a long positive phase an almost uniform pressure is present after impact, which decays over time. In the internal pressures it is seen that this transposes the oscillation around a decaying trend. In the center of the sphere this trend is clearly distinguishable. To conclude, the positive phase duration elongates the transition phase.

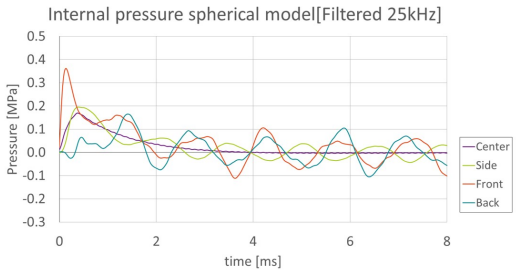

Figure D.1: Internal pressure in the sphere LC:160kPa-4ms

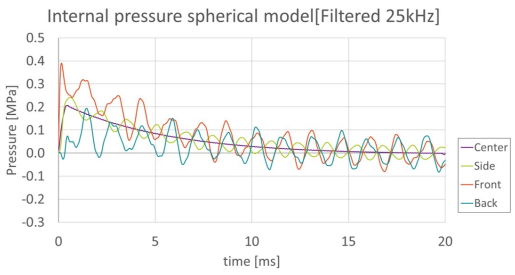

Figure D.2: Internal pressure in the sphere LC:160kPa-20+ms

E

Numerical analysis of a 1D bar

E.1. Parameter studies for a 1D bar

Different load types and material properties are applied to the 1D bar to study the influence on the internal pressure wave propagation and transmission. It is investigated what the relation is between the load type and internal pressure response. The different materials are included to study the relation between the frequency of the internal pressure and the material type. The element size used for the parameter studies is 2.33mm, because this is the element used in the spherical model.

Load type and shape

The mechanism of wave propagation into the head model induced by impact is studied using a variation in a triangular pressure profile, applied to the front of the bar and a variation in blast load amplitude. Figure E.1 shows the pressure in the middle of a 1D bar with element size 2.33mm made out of synbone for different load shapes. The peak load for the three triangular shaped loads is equal, as is the total impulse of the load. It can be seen that the amplitude of the high frequent pressure signal increases when the onset of the load profile is steeper. For a blast the pressure gradient is infinitely steep. The amplitude of the blast peak load influences the amplitude of the pressure signal, as can be seen in Figure E.2.

It is concluded that the high frequent component of the internal pressure is a pressure wave generated by a sudden impact, the amplitude of which depends on the load gradient and amplitude.

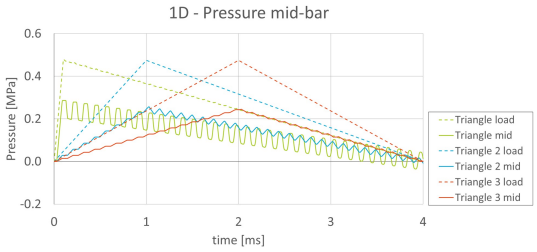

Figure E.1: Pressure in the middle of the bar under different load triangles with constant impulse

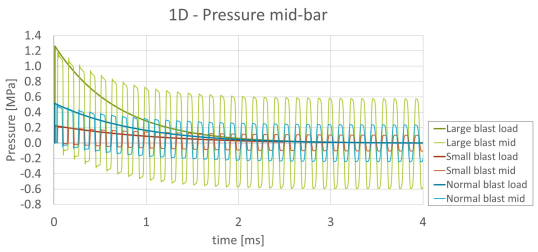

Figure E.2: Pressure in the middle of the bar under different blast load amplitudes

Material properties

The wave propagation through a structure induced by sudden impact occurs with the local materials' speed of sound which depends on the stiffness and density. To study the wave propagation induced by the blast through the skull, brain and skin material, the pressure in the middle of a 1D bar with varying material properties is compared.

In a Synbone bar the speed of sound is 3279m/s. The frequency of a wave travelling back and forth along a 200mm bar is 8330Hz. This corresponds to the frequency of the pressure in the middle of the

200mm bar. For half a bar with length 100mm this frequency is doubled, see Figure E.4.
For materials with a different speed of sound like gelatin, Figure E.5 and skin, Figure E.6 the frequency of the pressure signal is different. Note: the peaks at the maxima and minima of the pressure signal are a numerical artefact, as the 2.33mm element size is slightly too large to describe the pressure gradient smoothly, see Section 5.2.
At a boundary of different materials part of the wave is transmitted and part is reflected according to the impedance mismatch. The reflection coefficient describes the part of the wave that is reflected at the boundary. It is calculated as described in Figure E.3, where □is the material density and V the material acoustic velocity.

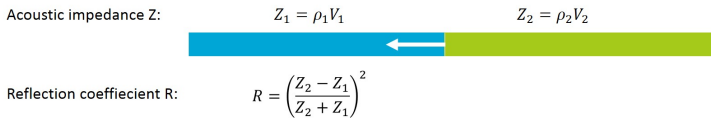

Figure E.3: Calculation of the impedance and reflection coefficient

Figure E.7 shows the pressure at the middle of the 1D bar for a bar that is half Synbone and half Gelatin, with the difference between the two cases being the material on which the blast impacts. In case multiple materials are present multiple frequencies can be distinguished in the pressure signal. Interestingly the amplitude of the internal pressure depends on the order of the materials. This can be explained by the difference of impedance mismatch between the air and the material of impact. It could be an interesting mechanism with which the load transmitted into the head can be reduced.

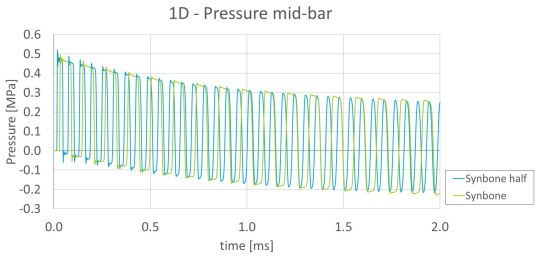

Figure E.4: Pressure in the middle of the reference bar (L=200mm) en a half bar (L=100mm) (LC:160kPa-4ms)

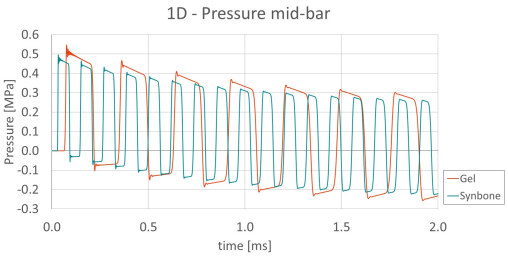

Figure E.5: Pressure in the middle of a fully synbone and fully gelatin material bar (LC:160kPa-4ms)

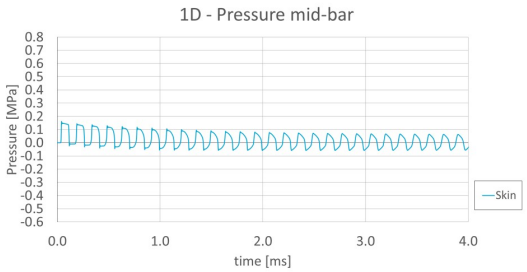

Figure E.6: Pressure in the middle of a fully skin material bar (LC:160kPa-4ms)

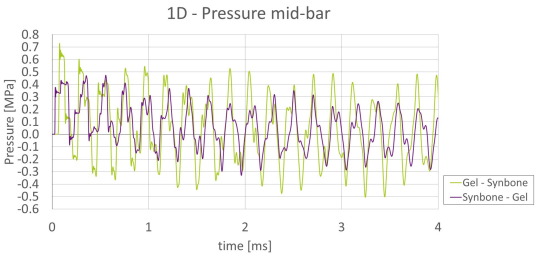

Figure E.7: Pressure in the middle of a half Synbone and half Gelatin material bar (LC:160kPa-4ms)

E.2. Frequency analysis of the response mechanisms of a 1D bar

An oscillating internal pressure is seen in the response to blast of the bar and head models. For the spherical model the oscillation consists of two dominant components of a low and high frequency. Two mechanisms are hypothesized to cause the oscillation:

- The impact of the blast causes a pressure wave propagating through the material and reflecting internally, resulting in a periodic pressure signal
- The blast causes the model to vibrate in its Eigen mode where skull deformation causes an oscillating internal pressure

A frequency analysis is performed in this section on the 1D Synbone bar, in order to identify the two hypothesized mechanisms in the internal pressure. The analysis of the wave propagation in a 1D bar in the Chapter 5 showed that a pressure wave is indeed travelling through a bar after an impact load. This section also includes the analysis of the second vibration mechanism. The Synbone bar model is used to identify the frequencies present in the internal pressure response of the bar to blast using a Fast Fourier Transform. These frequencies are linked to the first mechanism using the speed of sound of the bar material. The frequencies are linked to the second mechanism using a modal analysis of the bar.

Fast Fourier Transform internal pressure: Figure E.8 shows the frequency spectrum of the pressure signal in the middle of the bar. The spectrum is obtained by applying a Fast Fourier Transform to the pressure signal over time. The frequency peaks above 50kHz are negligible. Three peaks can be distinguished of 8.546kHz, 25.64kHz and 42.65kHz.

Wave propagation: If the pressure waves travels back and forth through the bar of 200mm this is equal to 1 cycle. The wave travels with the speed of sound of 3279m/s in Synbone. The frequency of this pressure oscillation is then equal to 8.330kHz.

Modal analysis: An implicit modal analysis provides the Eigen modes of the bar with the corresponding Eigen frequencies. Two types of modes are identified; Symmetric modes with contraction and expansion around the center and asymmetric mode with expansion to one side and contraction on the other side of the bar. The uneven symmetric (n=1,3,5,..) modes have Eigen frequencies of 8.536kHz, 25.59kHz and 42.60kHz.

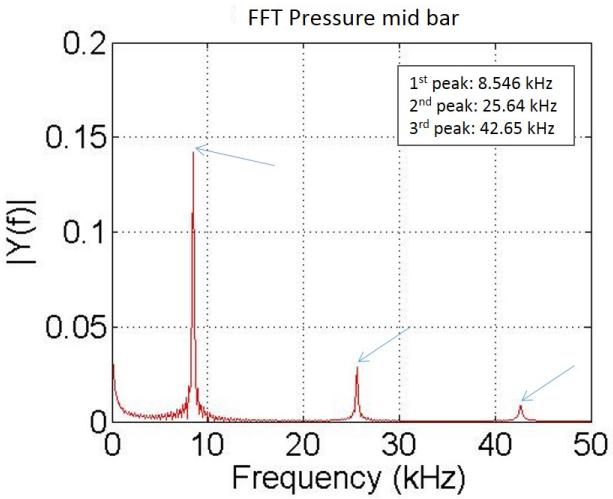

Figure E.8: Single sided frequency spectrum of the pressure in the middle of the bar (LC:160kPa-4ms)

Figure E.9 presents an overview of the frequencies obtained using the three methods. It is seen that the frequencies of the uneven modes correspond to the frequencies found in the spectrum of the pressure in the middle of the bar under blast loading. The frequency of the propagating wave is close to the frequency of the first mode and the first peak in the frequency spectrum.
Using this bar model it is not possible to definitively distinguish between the two mechanisms for the first dominant frequency in the pressure signal. The Eigen mode type of the bar is axial compression. This is similar to a compression wave moving along the bar and could explain the similarity of frequencies.
It is concluded that both wave propagation and vibration in Eigen modes are likely present in the response to blast. A similar analysis is applied to the sphere model in order to be able to separate the two mechanisms, Chapter 7.

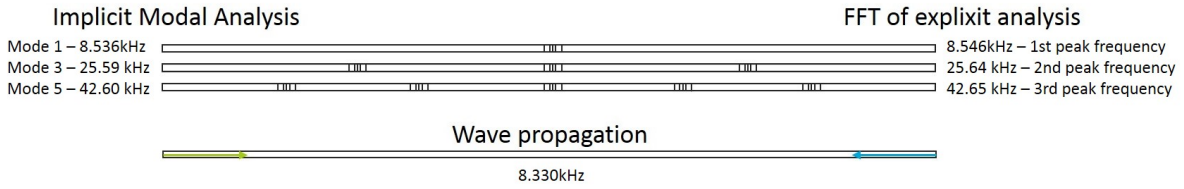

Figure E.9: Dominant modes in the 1D bar with their corresponding frequencies obtained from the implicit numerical -modal- analysis (left) and a Fast Fourier Transform of the response to blast with an explicit numerical analysis (right) and the frequency of wave propagation (lower). The zones of maximum contraction/expansion are indicated with multiple vertical lines in the bar.

F

Interaction of the blast with the shocktube

To reproduce a blast in a shock tube it is recommended that the test subject is limited to block no more than 10% or even 5% percent of the tube cross sectional area[21]. For a headform with protective equipment a shock tube diameter of approximately 0.91m is considered sufficient[17].
The shock tube used for the tests with the BI2PED head form has a cross section of 0.4x0.4m. During the tests of the BI2PED head around 25% of the area was blocked. In the case where the full face helmet was included over 40% of the area was blocked, see Figure F.1. Additionally the head was not positioned in the center of the tube due to the length of the Hybrid III neck. The distance of the model to the shock tube walls is related to the pressure that is reflected back onto the head model. Figures F.3 and F.4 show the pressure measured at the shock tube wall, see Figure F.2, where an increase in reflected peak is seen when a helmet is included. The additional peaks are highlighted by the red oval. Due to these additional peaks, the difference between the unprotected and protected cases is not only the presence of the helmet, but also an alteration of the load due to a reduction of the free flow area and changes in reflected pressures.

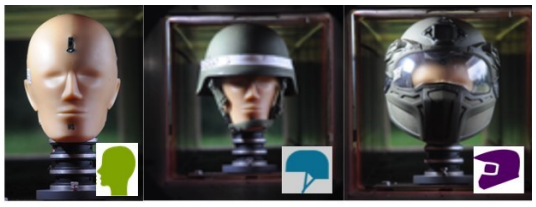

Figure F.1: Shock tube tests of the BI2PED head form with and without protective gear [24]

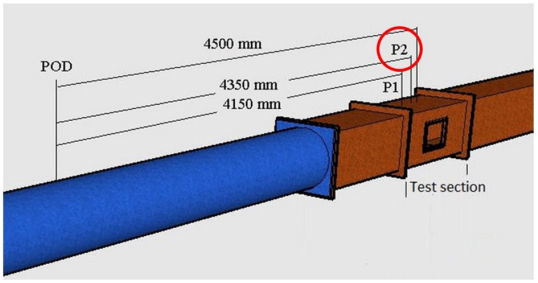

Distance Point Of Detonation – pressure sensor P1:	4150 mm
Distance Point Of Detonation – pressure sensor P2:	4350 mm
Distance pressure sensor P1 – middle test section :	350 mm
Distance pressure sensor P2 – middle test section:	**150 mm**

Figure F.2: Position of pressure sensors on the shock tube wall[24]

The effect of the altered load on the observed internal pressure needs to be identified, because the internal pressure in the transition phase is amplified when a helmet is present. Therefore the contribution of the reflected pressure in the tube to this amplification needs to be studied.

A 2D Multi Material Arbitrary Lagrangian Eulerian (MMALE) simulation is used to study the influence of the free flow area around the spherical head model. It consists of a single mesh: the container is filled with Ale Multi Material Groups (AMMG) for each material type and there is an ambient layer responsive to Load blast Enhanced on the edge of the mesh. It is a 2D axi symmetric sphere in a tube, see Figure

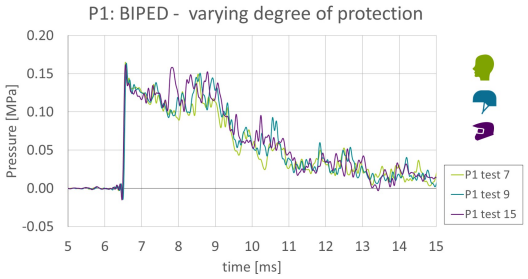

Figure F.3: P1 during BI2PED shock tube experiment; frontal blast (Pi=160kPa tpos=17ms) Test 7: No helmet - Test 9: Combat helmet - Test 15: Full face helmet. [Filtered LP10kHz]

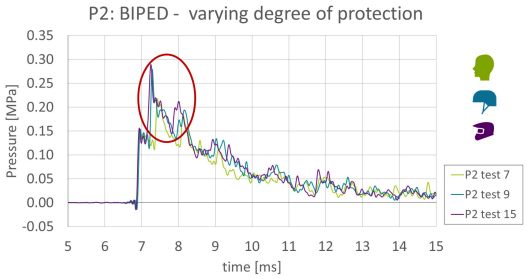

Figure F.4: P2 during BI2PED shock tube experiment; frontal blast (Pi=160kPa tpos=17ms) Test 7: No helmet - Test 9: Combat helmet - Test 15: Full face helmet. [Filtered LP10kHz]

F.5, with a diameter of 0.35m or 0.15m. The red domain consists of air. The yellow edge is a steel wall and the sphere skull is blue filled with green gelatin. The output is studied at the locations specified in Figure F.6.

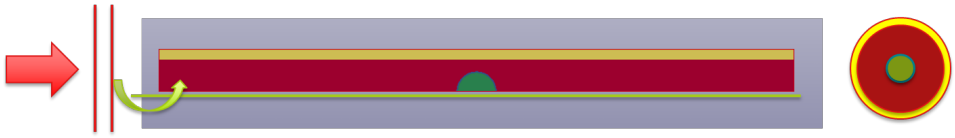

Figure F.5: 2D axi symmteric MMALE model

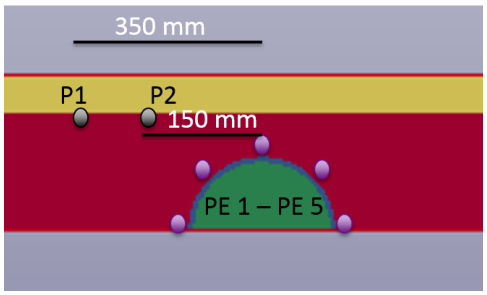

Figure F.6: 2D axi symmteric MMALE model output locations

Qualitatively the results of the pressures P1 and P2, shown in Figure F.7, from the MMALE simulation show additional peaks similar to the ones observed in the BI2PED tests. The pressure directly in front of the sphere, Figure F.8 shows that the load transferred to the sphere model is somewhat higher due to the reflected shock wave. The impulse contained in this additional peak is however small. Therefore it is likely that the effect of this peak is negligible for the internal sphere response.
This simulation did not show reliable internal pressures for the sphere, therefore the effect of the altered load on the internal pressure response remains unknown. The cause of the issue is not yet definitively identified. Possibly the modelling of a solid as a fluid AMMG creates problems for the pressure calculation in the solid. An alternative would be to use a Constrained Lagrange in Solid approach for the sphere. In this ALE type simulation, a Lagrangian mesh of solid elements, the sphere, is positioned as a separate mesh within the Eulerian fluid domain, similar to the set-up of the ALE BI2PED-FE model. As the effect of the load on the internal pressure is expected to be limited and other parts of the research were prioritised the investigation was not continued.

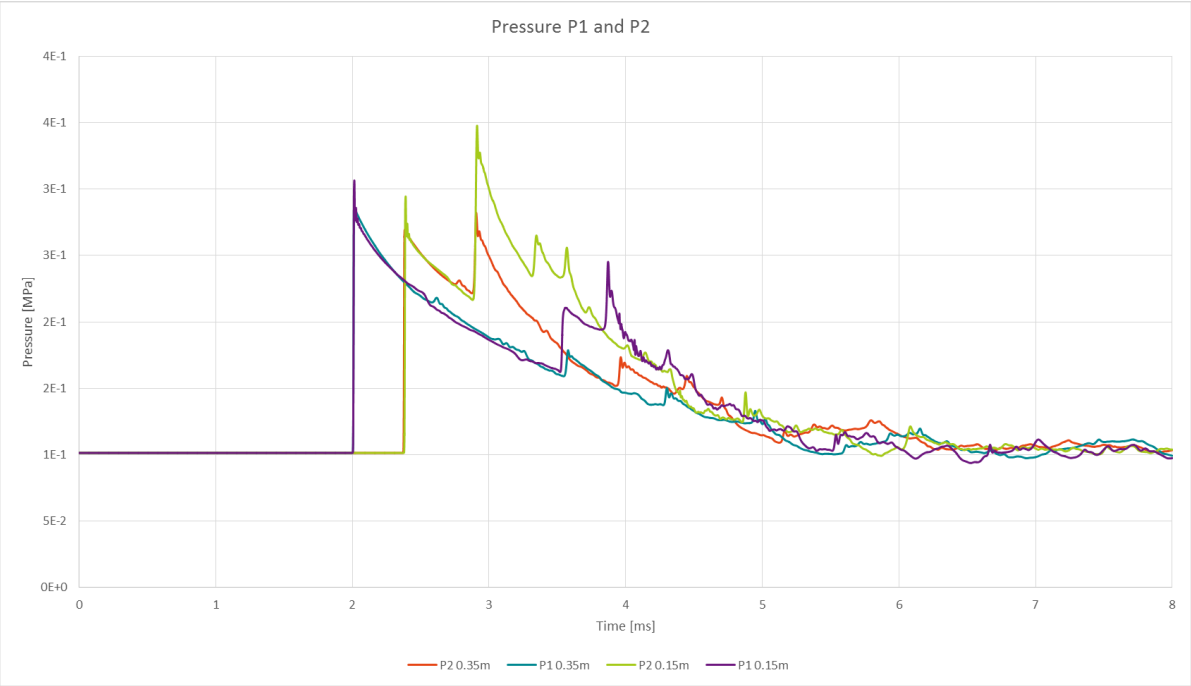

Figure F.7: Pressure at the shock tube wall at the location of sensor P1 and P2

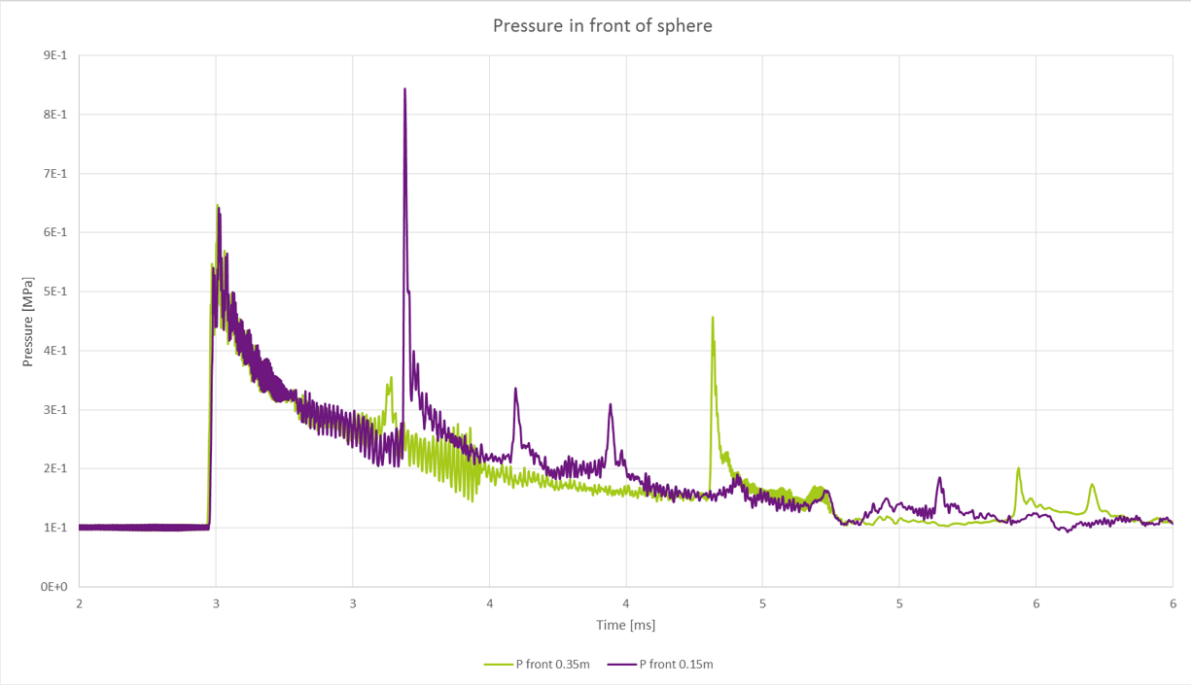

Figure F.8: Pressure directly in the front of the sphere

G

Simulation Overview

The graphic on the next page, Figure G.1, shows the research questions and the simulation models used to investigate them. It gives an indication of the reference models used upon which alterations are done. For example: for the study into the influence on the interface multiple variations on the 2D axi symmetric sphere exist. One where the brain and skull share nodes, one where penalty contact is defined between the brain and skull and one with a solid fluid layer. These variations are discussed in the corresponding sections of the main body of this report.

Part 1: ***Which factors dominate the nature of the head response?***

1.1 Gaining better understanding of the physics involved in the response of a skull brain model to blast.

Pressure wave propagation

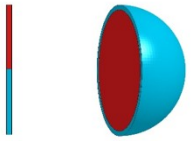

Relating the head vibration to modal deformation

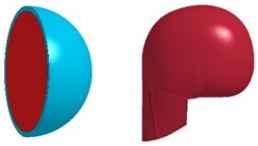

1.2 What is the effect of the head geometry and other model features, properties and boundary conditions on the internal brain pressures?

Neck constraints

Skin layer

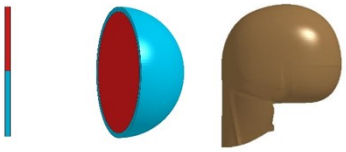

Skull-brain interface

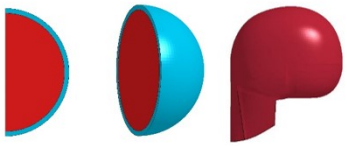

Part 2: ***Can the measurement of the internal response be improved?***

2.1 Can the effect of a helmet be numerically evaluated without modelling the helmet?

2.2 What is the internal pressure distribution and can locations of maximum and minimum pressure be identified?

2.3 Can a relation be defined between external skull strains and internal brain pressure?

2.4 What is the optimal strain and pressure sensor layout in order to effectively combine test and FE data to determine the protective capabilities of helmets?

Figure G.1: (sub)Research questions with the main simulation models used to investigate them

Bibliography

[1] Hiii dummy free download provided by lstc version: Lstc ncac h3 50th detailed 151214 beta k, 2015.

[2] P. Avitabile. Experimental modal analysis a simple non-mathematical presentation. *Sound and Vibration*, 2001.

[3] R. Bouamoul and J. Belanger. Development of a numerical model of a biofidelic head surrogate for blast-induced traumatic brain injury assessment. Technical Report DRDC-RDDC-2014-R137, Defence Research and Development Canada, 2014.

[4] D. W. A. Brands. *Predicting brain mechanics during closed head impact: numerical and constitutive aspects*. PhD thesis, Eindhoven University of Technology, 2002.

[5] M. S. Chafi, V. Dirisala, G. Karami, and M. Ziejewski. A finite element method parametric study of the dynamic response of the human brain with different cerebrospinal fluid constitutive properties. 223(8):1003–1019, 2009. doi: 10.1243/09544119JEIM631. URL http://www.scopus.com/inward/record.url?eid=2-s2.0-70450210410&partnerID=40&md5=440291abad0a90c86aa7bcd0201250e8.

[6] D. V. W. M. de Vries. Mechanisms of blast-induced mtbi a literature survey.

[7] D. V. W. M. de Vries. Mechanisms of blast-induced mild traumatic brain injury. Master's thesis, Eindhoven University of Technology, 2012.

[8] R. H. Eppinger. On the development of a deformation measurement system and its application toward developing mechanically based injury indices. 1989. doi: 10.4271/892426. URL https://www.scopus.com/inward/record.uri?eid=2-s2.0-84881194497&partnerID=40&md5=fa199730fdc3e420fc0cc3dbc0fe16c8.

[9] M. Grujicic, W. C. Bell, B. Pandurangan, and P. S. Glomski. Fluid/structure interaction computational investigation of blast-wave mitigation efficacy of the advanced combat helmet. 20(6):877–893, 2011. doi: 10.1007/s11665-010-9724-z. URL http://www.scopus.com/inward/record.url?eid=2-s2.0-80052605907&partnerID=40&md5=9172bb31daf86bc8c689e1e85072a3ea.

[10] M. Grujicic, A. Arakere, B. Pandurangan, A. Grujicic, A. Littlestone, and R. Barsoum. Computational investigation of shock-mitigation efficacy of polyurea when used in a combat helmet: A core sample analysis. 8(3):297–331, 2012. doi: 10.1108/15736101211269122. URL http://www.scopus.com/inward/record.url?eid=2-s2.0-84866996089&partnerID=40&md5=1cb78f2409f46975d2ccdf28ddd8471a.

[11] L. Gu, M. S. Chafi, S. Ganpule, and N. Chandra. The influence of heterogeneous meninges on the brain mechanics under primary blast loading. 43(8):3160–3166, 2012. doi: 10.1016/j.compositesb.2012.04.014. URL http://www.scopus.com/inward/record.url?eid=2-s2.0-84866734082&partnerID=40&md5=5e2ff9b12ee44fcad6ea867a072764d0.

[12] J. Li, H. N. S. Tan, and K. Y. Seng. A biomechanical computational study of the role of helmet pads in mitigating blast-induced traumatic brain injury. In *6th World Congress of Biomechanics, WCB 2010 - In Conjunction with 14th International Conference on Biomedical Engineering, ICBME and 5th Asia Pacific Conference on Biomechanics, APBiomech*, volume 31 IFMBE, pages 1518–1521, 2010. URL http://www.scopus.com/inward/record.url?eid=2-s2.0-77957976229&partnerID=40&md5=ae0ffea97774822d02774bca54330518.

[13] editor Livermore Software Technology Corporation (LSTC). Ls-dyna keyword user's manual, volume 1. 2016.

[14] editor Livermore Software Technology Corporation (LSTC). Ls-dyna keyword user's manual, volume 2. 2016.

[15] editor Livermore Software Technology Corporation (LSTC). Ls-dyna theory manual. 2016.

[16] P. Lubock and W. Goldsmith. Experimental cavitation studies in a model head-neck system. 13(12):1041–1047,1049–1052, 1980. doi: 10.1016/0021-9290(80)90048-2. URL https://www.scopus.com/inward/record.uri?eid=2-s2.0-0019204991&partnerID=40&md5=f9a9f8c5e3a69cd7994cfdc672ffbb3f.

[17] M. Maffeo, M. Carboni, J. Cyganik, B. Decristofano, C. Carneal, D. Zinn, J. Andrist, J. Clark, V. Alphonse, R. Kumar, and A. Nedungadi. Test method development for the evaluation of head borne equipment with a blast simulator, 2016.

[18] A. C. Merkle, I. D. Wing, and J. C. Roberts. Human surrogate head response to dynamic overpressure loading in protected and unprotected conditions. In *IFMBE Proceedings*, volume 32 IFMBE, pages 22–25, 2010. doi: 10.1007/978-3-642-14998-6{_}6. URL http://www.scopus.com/inward/record.url?eid=2-s2.0-78049405501&partnerID=40&md5=e290e0cb6b98cfbc65d0241ed7c4ae0b.

[19] W. C. Moss, M. J. King, and E. G. Blackman. Skull flexure from blast waves: A mechanism for brain injury with implications for helmet design. 103(10), 2009. doi: 10.1103/PhysRevLett.103.108702. URL https://www.scopus.com/inward/record.uri?eid=2-s2.0-69849096988&partnerID=40&md5=5df821c1af06afc9eb5211639ac43b43.

[20] M. K. Nyein, A. M. Jason, L. Yu, C. M. Pita, J. D. Joannopoulos, D. F. Moore, and R. A. Radovitzky. In silico investigation of intracranial blast mitigation with relevance to military traumatic brain injury. 107(48):20703–20708, 2010. doi: 10.1073/pnas.1014786107. URL http://www.scopus.com/inward/record.url?eid=2-s2.0-78650569546&partnerID=40&md5=39cb9a06c011f8173ccb23bfb6173d65.

[21] S. Oueleet, T. Josey, and S. Bjarnason. Guidelines for reproducing blast exposures in the laboratory (draft). 2016.

[22] S. Ouellet, R. Bouamoul, R. Gauvin, J.S. Binette, K.V. Williams, and L. Martineau. Development of a biofedelic head surrogate for blast-induced traumatic brain injury assessment. 2012.

[23] S. Ouellet, C. Bir, and R. Bouamoul. Direct comparison of the primary blast response of a physical head model with post-mortem human subjects. Technical Report DRDC-RDDC-2014-P113, Defence Research and Development Canada, 2014.

[24] M. M. G. M. Philippens. Blast tbi risk reduction by military helmets: An assessment method to qualify the helmet icp reducing performance. Technical Report TNO 2016 R11454, TNO Explosions Ballistics and Protection, 2016.

[25] G Randers-Pehrson and K. Bannister. Airblast loading model for dyna-2d and dyna-3d. Technical Report ARL-TR-1310, Army Research Laboratory, 1997.

[26] J. C. Roberts, T. P. Harrigan, E. E. Ward, T. M. Taylor, M. S. Annett, and A. C. Merkle. Human head-neck computational model for assessing blast injury. 45(16): 2899–2906, 2012. doi: 10.1016/j.jbiomech.2012.07.027. URL http://www.scopus.com/inward/record.url?eid=2-s2.0-84868383639&partnerID=40&md5=08c13a535f71466e3d92202a26b6afdf.

[27] J. C. Roberts, T. P. Harrigan, E. E. Ward, D. Nicolella, L. Francis, T. Eliason, and A. C. Merkle. The influence of neck kinematics on brain pressures and strains under blast loading. In *ASME International Mechanical Engineering Congress and Exposition, Proceedings (IMECE)*, volume 3 A, 2013. doi: 10.1115/IMECE2013-64821. URL http://www.scopus.com/inward/record.url?eid=2-s2.0-84903469723&partnerID=40&md5=ca46b13edefd284a7a2e3d715b8f65f5.

[28] M. Salimi Jazi, A. Rezaei, G. Karami, F. Azarmi, and M. Ziejewski. Effects of attached body on biomechanical response of the helmeted human head under blast. In *ASME International Mechanical Engineering Congress and Exposition, Proceedings (IMECE)*, volume 3 A, 2013. doi: 10.1115/IMECE2013-65140. URL http://www.scopus.com/inward/record.url?eid=2-s2.0-84903440798&partnerID=40&md5=3999e35fb7626e39d7f4b13c0a35d90e.

[29] H. Sarvghad-Moghaddam, M. S. Jazi, A. Rezaei, G. Karami, and M. Ziejewski. Examination of the protective roles of helmet/faceshield and directionality for human head under blast waves. 18(16):1846–1855, 2015. doi: 10.1080/10255842.2014.977878. URL http://www.scopus.com/inward/record.url?eid=2-s2.0-84923491475&partnerID=40&md5=565aad5024d7f79dd572d291939d0f26.

[30] L. W. Schneider, M. P. Haffner, R. H. Eppinger, M. J. Salloum, M. S. Beebe, S. W. Rouhana, A. I. King, W. H. Hardy, and R. F. Neathery. Development of an advanced atd thorax system for improved injury assessment in frontal crash environments. 1992. doi: 10.4271/922520. URL https://www.scopus.com/inward/record.uri?eid=2-s2.0-79959821404&doi=10.4271%2f922520&partnerID=40&md5=02690df48817878d3b4e28e1862992ae.

[31] A. S. Shah, B. D. Stemper, N. Yoganandan, F. A. Pintar, N. Rangarajan, J. J. Hallman, and B. S. Shender. Methodology to study attenuation of a blast wave through the cranium. In *ASME 2011 International Mechanical Engineering Congress and Exposition, IMECE 2011*, volume 2, pages 17–24, Medical College of Wisconsin, Milwaukee, WI, United States, 11 November 2011 through 17 November 2011 2011. ISBN 9780791854884 (ISBN). URL http://www.scopus.com/inward/record.url?eid=2-s2.0-84869166682&partnerID=40&md5=fe001138c8e313ee2a78873fa9c01856.

[32] A. E. Tschiffely, S. T. Ahlers, and J. N. Norris. Examining the relationship between blast-induced mild traumatic brain injury and posttraumatic stress-related traits. *Journal of Neuroscience Research*, 2015.

[33] A. G. van Erkel. Basics of blast and shock. Powerpoint Presentation Internal Lecture TNO Structural Dynamics, May 17 2016.

[34] J. S. H. M. Wismans, M. Janssen, M. Beusenberg, R. Koppens, R. Happee, and P. H. M. Bovendeerd. Injury boimechanics, chapter 4 - head injury biomechanics. Collegedictaat Eindhoven University of Technology.

[35] J. Zhang and F. A. Pintar. A finite element study of blast overpressure on the skull with and without helmet. In *ASME 2010 Summer Bioengineering Conference, SBC 2010*, number PARTS A AND B, pages 799–800, Department of Neurosurgery, Medical College of Wisconsin, Milwaukee,WI, United States, 16 June 2010 through 19 June 2010 2010. ISBN 9780791844038 (ISBN). doi: 10.1115/SBC2010-19083. URL http://www.scopus.com/inward/record.url?eid=2-s2.0-84893785327&partnerID=40&md5=c2b3f5870174a849e12e6b7d010b2a04.

[36] T. G. Zhang, S. S. Satapathy, A. M. Dagro, and P. J. McKee. Numerical study of head/helmet interaction due to blast loading. In *ASME 2013 International Mechanical Engineering Congress and Exposition, IMECE 2013*, volume 3 A, Bowhead Science and Technology, Belcamp, MD, United States, 15 November 2013 through 21 November 2013 2013. American Society of Mechanical Engineers (ASME). ISBN 9780791856215 (ISBN). doi: 10.1115/IMECE2013-63015. URL http://www.scopus.com/inward/record.url?eid=2-s2.0-84903466784&partnerID=40&md5=b7ceb033313d7a547bbcef7d60904a34.

[37] A. M. Zwanenburg, B. C. de Jong, and W. van den Heuvel. Dummy head and neck response to a small blast - biped head and hiii neck. Technical report, TNO Structural Dynamics, 2016. Powerpoint Report.

[38] A. M. Zwanenburg, B. C. de Jong, and W. van den Heuvel. Analysis bi2ped-fe project phase i, ii, iii, iv. Technical report, TNO Structural Dynamics, 2017. Powerpoint Report.